OPTIMIZATION OF TOOTH ROOT PROFILE AND DRIVE SIDE PRESSURE ANGLE TO MINIMIZE BENDING STRESS AT CRITICAL SECTION OF ASYMMETRIC SPUR GEAR TOOTH

A Thesis submitted to Gujarat Technological University

for the Award of

Doctor of Philosophy

in

Mechanical Engineering

By

VAGHELA PRIYAKANT AATMARAM

(Enrollment No.: 129990919015)

under supervision of

Dr. J M Prajapati

Associate Professor, Department of Mechanical Engineering, Faculty of Technology and Engineering, The Maharaja Sayajirao University of Baroda, Vadodara

GUJARAT TECHNOLOGICAL UNIVERSITY
AHMEDABAD

NOVEMBER – 2019

DECLARATION

I declare that the thesis entitled **Optimization of tooth root profile and drive side pressure angle to minimize bending stress at critical section of asymmetric spur gear tooth** submitted by me for the degree of Doctor of Philosophy is the record of research work carried out by me during the period from November 2012 to 2018 under the supervision of **Dr. J M Prajapati** and this has not formed the basis for the award of any degree, diploma, associateship, fellowship, titles in this or any other University or other institution of higher learning.

I further declare that the material obtained from other sources has been duly acknowledged in the thesis. I shall be solely responsible for any plagiarism or other irregularities, if noticed in the thesis.

Signature of the Research Scholar: Date:

Name of Research Scholar: **Vaghela Priyakant Aatmaram**

Place: Ahmedabad

CERTIFICATE

I certify that the work incorporated in the thesis **Optimization of tooth root profile and drive side pressure angle to minimize bending stress at critical section of asymmetric spur gear tooth** submitted by **Shri Vaghela Priyakant Aatmaram** was carried out by the candidate under my supervision/guidance. To the best of my knowledge: (i) the candidate has not submitted the same research work to any other institution for any degree/diploma, Associateship, Fellowship or other similar titles (ii) the thesis submitted is a record of original research work done by the Research Scholar during the period of study under my supervision, and (iii) the thesis represents independent research work on the part of the Research Scholar.

Signature of Supervisor: Date:

Name of Supervisor: **Dr. J M Prajapati**

Place: Ahmedabad

Course-work Completion Certificate

This is to certify that **Shri Vaghela Priyakant Aatmaram** enrolment no. **129990919015** is a PhD scholar enrolled for PhD program in the branch **Mechanical Engineering** of Gujarat Technological University, Ahmedabad.

(Please tick the relevant option(s))

☐ He has been exempted from the course-work (successfully completed during M.Phil Course)

☐ He has been exempted from Research Methodology Course only (successfully completed during M.Phil Course)

☐ He has successfully completed the PhD course work for the partial requirement for the award of PhD Degree. His performance in the course work is as follows

Grade Obtained in Research Methodology (PH001)	Grade Obtained in Self Study Course (Core Subject) (PH002)
BB	BB

Supervisor's Sign

Dr. J M Prajapati

Originality Report Certificate

It is certified that PhD Thesis titled **Optimization of tooth root profile and drive side pressure angle to minimize bending stress at critical section of asymmetric spur gear tooth** has been examined by us. We undertake the following:

a. Thesis has significant new work / knowledge as compared already published or are under consideration to be published elsewhere. No sentence, equation, diagram, table, paragraph or section has been copied verbatim from previous work unless it is placed under quotation marks and duly referenced.

b. The work presented is original and own work of the author (i.e. there is no plagiarism). No ideas, processes, results or words of others have been presented as Author own work.

c. There is no fabrication of data or results which have been compiled / analysed.

d. There is no falsification by manipulating research materials, equipment or processes, or changing or omitting data or results such that the research is not accurately represented in the research record.

e. The thesis has been checked using **turnitin** (copy of originality report attached) and found within limits as per GTU Plagiarism Policy and instructions issued from time to time (i.e. permitted similarity index <=25%).

Signature of the Research Scholar: Date:

Name of Research Scholar: **Vaghela Priyakant Aatmaram**

Place: Ahmedabad

Signature of Supervisor: Date:

Name of Supervisor: **Dr. J M Prajapati**

Place: Ahmedabad

Thesis

ORIGINALITY REPORT

7%	4%	10%	2%
SIMILARITY INDEX	INTERNET SOURCES	PUBLICATIONS	STUDENT PAPERS

PRIMARY SOURCES

1	www.matec-conferences.org Internet Source	3%
2	P.A. Vaghela, J.M. Prajapati. "Hybridization of Taguchi and Genetic Algorithm to minimize iteration for optimization of solution", MethodsX, 2019 Publication	3%

Exclude quotes	On	Exclude matches	< 2%
Exclude bibliography	On		

PhD THESIS Non-Exclusive License to GUJARAT TECHNOLOGICAL UNIVERSITY

a) In consideration of being a PhD Research Scholar at GTU and in the interests of the facilitation of research at GTU and elsewhere, I, **Vaghela Priyakant Aatmaram** having Enrollment No.**129990919015** Hereby grant a non-exclusive, royalty free and perpetual license to GTU on the following terms:

b) GTU is permitted to archive, reproduce and distribute my thesis, in whole or in part, and/or my abstract, in whole or in part (referred to collectively as the "Work") anywhere in the world, for non-commercial purposes, in all forms of media;

c) GTU is permitted to authorize, sub-lease, sub-contract or procure any of the acts mentioned in paragraph (a);

d) GTU is authorized to submit the Work at any National / International Library, under the authority of their "Thesis Non-Exclusive License";

e) The Universal Copyright Notice (©) shall appear on all copies made under the authority of this license;

f) I undertake to submit my thesis, through my University, to any Library and Archives. Any abstract submitted with the thesis will be considered to form part of the thesis.

g) I represent that my thesis is my original work, does not infringe any rights of others, including privacy rights, and that I have the right to make the grant conferred by this non-exclusive license.

h) If third party copyrighted material was included in my thesis for which, under the terms of the Copyright Act, written permission from the copyright owners is required, I have

Obtained such permission from the copyright owners to do the acts mentioned in paragraph (a) above for the full term of copyright protection.

i) I retain copyright ownership and moral rights in my thesis, and may deal with the copyright in my thesis, in any way consistent with rights granted by me to my University in this non-exclusive license.

j) I further promise to inform any person to whom I may hereafter assign or license my copyright in my thesis of the rights granted by me to my University in this non-exclusive license.

k) I am aware of and agree to accept the conditions and regulations of PhD including all policy matters related to authorship and plagiarism.

Signature of the Research Scholar:

Name of Research Scholar: **Vaghela Priyakant Aatmaram**

Date:

Place: Ahmedabad

Signature of Supervisor:

Name of Supervisor: **Dr. J M Prajapati**

Date:

Place: Ahmedabad

Seal:

Thesis Approval Form

The viva-voce of the PhD Thesis submitted by **Shri Vaghela Priyakant Aatmaram** Enrollment No. **129990919015** entitled **Optimization of tooth root profile and drive side pressure angle to minimize bending stress at critical section of asymmetric spur gear tooth** was conducted on / / 2018 at Gujarat Technological University.

(Please tick any one of the following option)

☐ The performance of the candidate was satisfactory. We recommend that he/she be awarded the PhD degree.

☐ Any further modifications in research work recommended by the panel after 3 months from the date of first viva-voce upon request of the Supervisor or request of Independent Research Scholar after which viva-voce can be re-conducted by the same panel again.

☐ The performance of the candidate was unsatisfactory. We recommend that he/she should not be awarded the PhD degree.

Name and Signature of Supervisor with Seal

---
1) (External Examiner 1) Name and Signature

---
2) (External Examiner 2) Name and Signature

---
3) (External Examiner 3) Name and Signature

ABSTRACT

Gear design is an extremely difficult art. High load-carrying capacity, less expensive, quieter running, lighter weight, and longer life are the primary goal of the present industry for making gears. The gear tooth-root is exposed to a combination of both shearing and bending. Due to repeated excessive stresses a bending fatigue often occurs at the root of tooth. The first crack initiates at the regions with the highest stress concentrations and propagates until failure occurs. The fatigue of gear tooth due to bending is always a challenge to designers.

At the critical section of tooth, concentration occurs due to curvature discontinuity. Such discontinuities cause a drastic jump in stress values, thereby making these regions prone to mechanical failure. Hence, the optimization of the gear tooth-root profile plays a significant role in reducing the stress concentration and improving the gear tooth strength. This research focuses on the minimization of stress concentration by optimizing root profile at critical section of asymmetric gear. For asymmetric gear bending stress at critical section is always lower then symmetric gear. Combined effect of asymmetric gear and optimized root profile gives better reduction in bending stress at critical section. It will reduce stress concentration. Geometric continuity of order 2 at connection point of involute profile and root profile plays a very important role in reducing stress concentration. A Bezier curve is used with geometric continuity of order 2 at the critical section of an asymmetric spur gear tooth to reduce curvature discontinuity. It will reduce bending fatigue which is challenge of designers.

In asymmetric gear higher pressure angel on drive side as compare to coast side gives higher reduction in bending stress at critical section but value of higher pressure angel on drive side constrained by contact ratio and tip thickness of tooth. Modification in the drive side pressure angle will change involute profile of drive side of gear tooth which affects gear geometry. Strength of gear is affected by gear tooth geometry. Hence it is most important for improve strength. The parametric analysis helps to understand the effect of drive side pressure angle on tooth geometry of symmetric and asymmetric spur gear. Developed equations of “bending stress equation parameters” have been used to calculate various parameters. Parametric analysis has been explained with consideration of gear parameter. Application of parametric analysis is also discussed.

Objective function to minimize a bending stress at critical section of asymmetric involute spur gear with circular fillet has been developed in terms of drive side pressure angle. Application of objective function is also discussed.

To minimize stress at critical section, a mathematical model of asymmetric involute spur gear has been developed and established Bezier curve with geometric continuity of order 2 at critical section. To create exact geometric of CAD model in CAD software, an algorithm has been presented. Three CAD model has been created in AutoCAD using algorithm. These three models are symmetric spur gear with standard fillet, asymmetric spur gear with standard fillet and asymmetric spur gear with the modified root.

Using FEA simulation software, for developed models FEA analysis has been carried out. von-Mises stress of asymmetric with normal fillet is compared with normal filleted symmetric gear and found that, it is reducing by 17.50 %. von-Mises stress of optimized root profile with asymmetric is compared with normal filleted symmetric gear and found that, it is reducing by 31.27%. It is observed that modified tooth and root profile was reduced stress concentration.

It is very difficult to obtain desire root profile using a conventional manufacturing technique. CNC machine capable of manufacturing gear as per desire parameter but require G code to manufacture gear. To develop G code, CAD model and G code generation software are required. To eliminate this, an algorithm has been presented to generate G code without using a G code generation software and CAD model**.** To manufacture modified gear, G code generation algorithm has been presented which is essential for develop a software. It also allows Direct Gear Manufacturing.

In this work, an integrated approach for design, modeling, and manufacturing of symmetric and asymmetric involute spur gear has been developed. All equations and algorithms are in generalizing form for given input to design gear. So, it is applicable for all type of input data.

Acknowledgement

It is a pleasant aspect that I have now the opportunity to express my gratitude for many people who accompanied and supported me during the journey of my work. Firstly, I offer my adoration to almighty who created me, gave me the strength and courage to complete my research work. I would like to express my deep gratitude to my supervisor **Dr. J M Prajapati**, Associate Professor, Department of Mechanical Engineering, Faculty of Technology and Engineering, The Maharaja Sayajirao University of Baroda, Vadodara for his guidance and whole hearted cooperation. His helping nature, valuable moral support and appreciation have inspired me and will continue to inspire for the rest of my career.

I would like to thank my doctoral progress committee: **Prof. & Dr. Hetal Shah**, Principal, Gandhinagar Institute of Technology, Gujarat & **Dr. Bhavesh Patel** Associate Professor, Mechanical Engineering Department, U V Patel College of engineering, Ganpat University, Kherva, Mahesana, Gujarat for their insightful comments and encouragement during entire period of research work.

I express my profound gratitude to Principal, RCTI, Ahmedabad, Head of Mechanical Engineering Department, RCTI, Ahmedabad, my colleague Smt. A N Mahajan and entire staff of mechanical engineering department for their untiring consistent cooperation.

I am short of words for my family members being grateful to them for all the sacrifices they have made for me. I owe deepest gratitude to my mother, sister and brother their mental support. My heartiest thank to my wife and true inspiration, **Pallavi Vaghela** for her care and all the sacrifices. This work would not have been completed without her unconditional love and support during entire period of my work. I am short of words to express my loving gratitude to my adorable daughter **Diya** and son **Jal**, whose innocent smile and love has given me mental support during the entire work.

VAGHELA PRIYAKANT AATMARAM
Enroll. No. 129990919015

Table of Content

List of Abbreviation

Symbol	Parameter
FEA	Finite Element Analysis
HPSTC	Highest Point of Single Tooth of Contact

List of Symbols

α_{Fen}	Load angle	deg
α	Standard normal pressure angle for symmetric gear	deg
α_c	Pressure angle on coast side	deg
α_d	Pressure angle on drive side	deg
ε	Overlap ratio, axial contact ratio	-
ρ_F	Fillet radius	mm
σ_F	Stress	MPa
σ_{F0}	Nominal stress	MPa
b	Effective face width	mm
d_p, d_g	Standard pitch diameter, pinion and gear	mm
r_p, r_g	Standard pitch radii, pinion and gear	mm
$r_b/r_{bp}/r_{bg}$	Base circle radius, pinion, gear	mm
r_a/r_t	Addendum / tip circle radius	mm
r_d	Dedendum circle radius	mm
r_{bc}	Base circle radius at coast side	mm
r_{bd}	Base circle radius at drive side	mm
r_{HPSTC}	Radius at HPSTC	mm
r_{tp}, r_{tg}	Tip circle radius, pinion and gear	mm
r_{pp}, r_{pg}	Pitch circle radius, pinion and gear	mm
r	Any radius	mm
F_t	Load	N
i	Speed ratio	-
k	Asymmetric factor	-
h_{Fe}	Bending moment arm	mm
S_{pd}	Tooth thickness at pitch circle on drive side	mm
S_{pc}	Tooth thickness at pitch circle on coast side	mm
S_c	Tooth thickness at any radius r on coast side	mm
S_d	Tooth thickness at any radius r on drive side	mm
S_{td}	Tooth thickness at tip circle on drive side	mm
S_{tc}	Tooth thickness at tip circle on coast side	mm
S_t	Total tip thickness at tip circle	mm
S_{Fn}	Total thickness at critical section	mm

S_{Fnd}	Tooth thickness at critical section on drive side	mm
S_{Fnc}	Tooth thickness at critical section on coast side	mm
θ / θ_r / θ_I	Angle at radius r w.r.t y-axis	rad
δ	Angle at pitch circle radius w.r.t y-axis	rad
φ	Involutes of pressure angle	rad
Φ	Correspondence angle of involute of Φ at any radius r	rad
θ_{tc}	Angle at tip circle radius w.r.t y-axis on coast side	rad
θ_t	Angle at tip circle radius w.r.t y-axis	rad
θ_{td}	Angle at tip circle radius w.r.t y-axis on drive side	rad
θ_b	Angle at base circle radius w.r.t y-axis	rad
$\theta_{bc}d$/ θ_{Fnd}	Angle at coast side base circle radius w.r.t y-axis on drive side	rad
$\theta_{bc}c$/ θ_{Fnc}	Angle at coast side base circle radius w.r.t y-axis on coast side	rad
θ_{HPSTC}	Angle at HPSTC radius w.r.t y-axis	rad
$\theta_{A,B,C,D,E}$	Angle at A, B, C, D, E points w.r.t y-axis	rad
K_A	Application factor	–
$K_{F\alpha}$	Transverse load factor	–
$K_{F\beta}$	Face load factor	–
K_v	Dynamic factor	–
m/m_n	Module / Normal module	mm
s_{Fn}	Tooth thickness at critical section	mm
T_1, T_2	Torque on the pinion (1), gear (2)	Nm
Y_β	Helix angle factor	-
Y_F	Tooth form factor	-
Y_S	Stress correction factor	-
z_p	Number of tooth of pinion	-
z_g	Number of tooth of gear	-
t ,I, J	Variables	-
a	Addendum height to module ratio	

List of Figures

List of Tables

CHAPTER – 1

INTRODUCTION

1.1 History of gear

Gears are machine elements used to transmit power from one shaft to other shaft. Gears are existed from around 2600 BC. Chinese used gears to measure the speeds of chariots as per early records. Around 250 BC, Archimedes used a screw to drive toothed wheels which were used in engines of war. In four-century BC, Aristotle used gears to simulate astronomical ratios. Greek and Roman literature mention the use of gears in clocks of cathedrals and ecclesiastic buildings [1, 3].

In early centuries, wood or stone teeth set in wood base are used to develop gears. Then in metal age, Iron or bronze or tin was used instead of stone. Until 1835, there were no standard methods or procedures to manufacture a gear. Whitworth patented the first hobbing process to manufacture a gear [2, 3]. In 1897, Pfauter patented the first gear hobbing machine which is capable to cutting both spur and helical gear, they introduced the first NC hobbing machine in 1975 and that they introduced the basic all six-axis gear hobbing machine in 1982. Until 1892, the failure of gear due to bending stress and contact stress still remained a challenge for both designers and manufacturers. In 1892 the City of Brotherly Love Engineers club 1st recognized, Wilfred Lewis presentation of stresses on the gear tooth and it still is the idea to see the gear stress [3].

1.2 Gear profile

Gear profile follows the fundamental law of gearing. It states that the angular velocity ratio between the gears of a gear set must remain constant throughout the mesh [3]. Involute, cycloidal and circular arc or Novikov profiles satisfy the law of gearing. Among these, cycloidal was the first to be evolved [3]. This is followed by the invention of an involute profile which replaced many of the other profiles due to several technological advantages. Circular arc or Novikov profile has some advantages over the other profiles. But due to manufacturing difficulties, it did not become popular [3].

Among all profile, the involute profile becomes more popular due to easy to manufacturing, variation in center distance does not affect the velocity ratio and pressure angle remains constant throughout the engagements which result in smooth running [3].

Involute profile is depends on a pressure angle. Among pressure angle 14.5^0, 20^0 and 25^0 , a 20^0 pressure angle becomes more popular [1].

1.3 Gear manufacturing

Gear manufacturing can be divided into two main categories 1) forming and 2) machining [1].

Forming consist of casting, drawing, forging, preforming, injection molding, etc. Machining is sub-categories into two main processes [1] a) roughing and b) finishing. The roughing process consists of forming, generation, shaping and hobbing processes [1]. By this method, gears are made to an accuracy which is more than adequate for the slow speed operations. Finishing process consists of shaving, grinding, burnishing, lapping and honing [1].

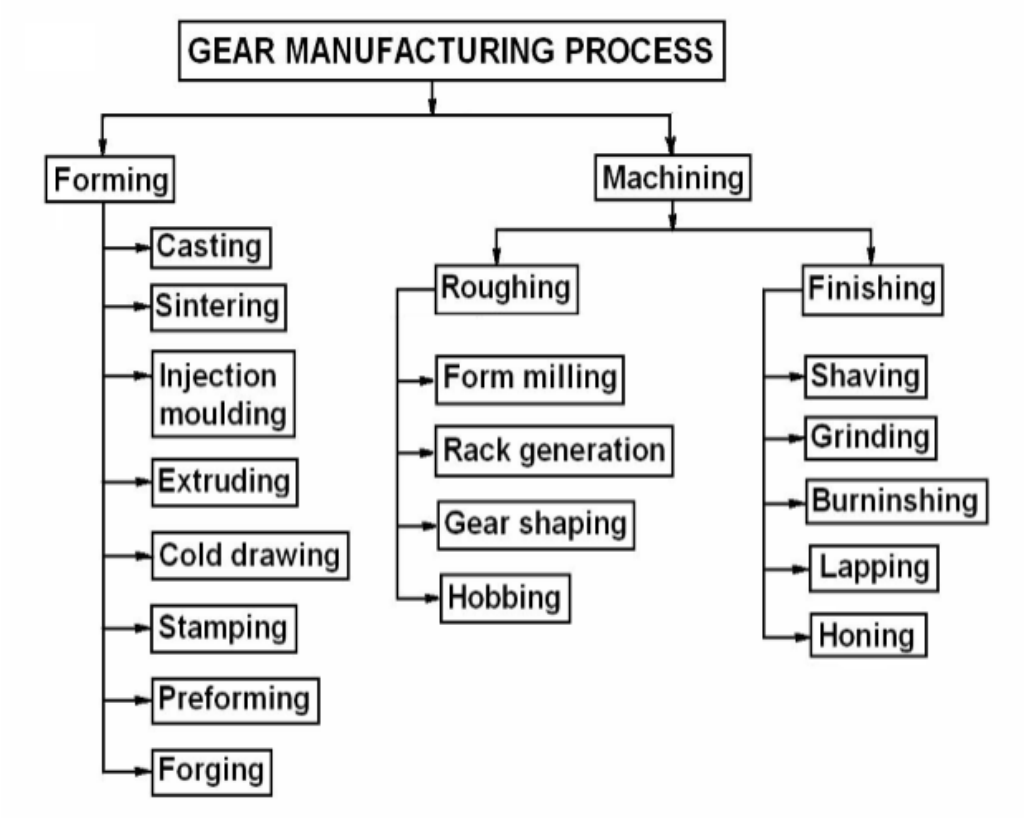

FIGURE 1.1: Gear manufacturing process

There are many types of error encountered in conventional gear manufacturing [1]. These include:

Profile Shifting: as per standard cutting procedure, gear cutting done by hobbling, a single cutter is used to cut a range of a number of teeth per gear like from 35 to 54 numbers of teeth. Due to this, error may occur in tooth profile. It is found that in one of the tooth there is a tendency for the thickness to reduce at the tip. This is because the involute curve tends to shift inwards as the number of teeth reduces, thus reducing the base circle.

Undercutting at root surface: In cutting operation, when the number of gear teeth on gear is less, the hobbing tool sweeps out its path and remove some of the profile so, produces an undercut tooth form.

Runout error of gear teeth: Runout error defines the runout of pitch circle.

Lead error of gear: It occurs due to deviation of actual advancement of tooth profile from its ideal position.

Tooth profile error: It is a summation of deviation between actual tooth profile and correct involute curve.

1.4 Gear tooth Interference, undercut and profile shift

Spur gear teeth are manufactured by either involute profile or cycloidal profile [1]. Most of the gears are manufactured by involute profile with 20° pressure angle [1]. When two gears are in mesh at one instant there is a chance to mate involute portion with a non-involute portion of the mating gear. This phenomenon is known as interference [1, 2]. It occurs when the number of teeth on the smaller of the two meshing gears is less than a required minimum. To avoid interference we can have undercutting, but this is not a suitable solution as undercutting leads to weakening of tooth at its base. In this situation, corrected gears are used. In corrected gears cutter rack is shifted upwards or downwards. Undercutting is removing some material from the base of the gear tooth to avoid interference [1, 2].

Various methods are available to eliminate the gear tooth interface. Mainly using stub teeth, increasing the number of teeth on the mating pinion, increasing the pressure angle, tooth profile modification or profile shifting and increasing the center distance, etc, [1, 2].

Equation 1.1 gives the condition of minimum No. of Teeth on the pinion to avoid interference [2].

$$Z_p^2 + 2 \cdot Z_p \cdot Z_g = \frac{4 \cdot a \cdot (Z_g + a)}{\sin \alpha^2} \quad (1.1)$$

Profile shift: When the number of gear teeth to be cut becomes small, the generating tool will sweep out its path, removing some of the profile, and producing an undercut tooth form. To prevent undercut, some correction must be introduced, and it is called a profile shift [3]. Profile shift can not only prevent undercut but also can adjust the center distance between two gears [3].

1.5 Gear failure

Gear failure can occur in various modes. If care is taken during the design stage, it prevents failures given in figure 1.2.

In running condition, cyclic load acts on tooth of gear. So, cyclic stress occurs. Due to this tooth failures occurs [1]. Tooth flank and root fillet are main two regions found in research where gear tooth failures occurs. Various modes of failures are presented in figure 1.2.

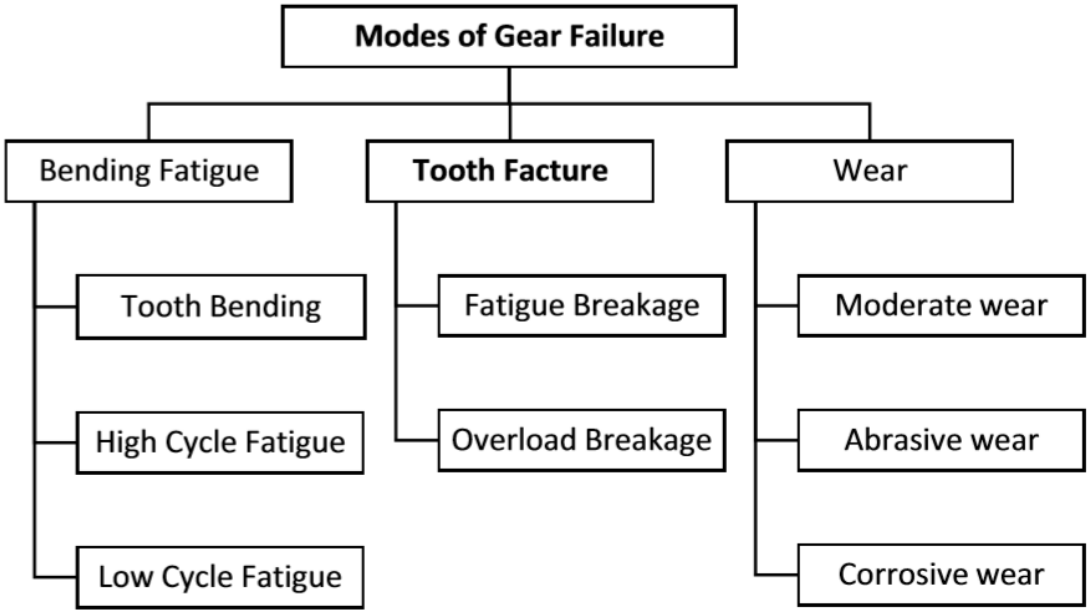

FIGURE 1.2: Mode of gear failure

Tooth breakage occurs due to overload and fatigue failure. Tooth failure from bending fatigue mostly appears at a root of tooth where crack initiation starts [4]. Other main reason of bending fatigue failures are too much load and cyclic loading, so stress at the tooth of gear increases beyond the endurance limits of the material.

Tooth failure from bending fatigue occurs due to the crack propagation at root of gear tooth. This happen based on rotational motion and load carry by tooth [5]. Failure occurs under load less than 10,000 cycles are considered as low cycle fatigue. When failure occurs after more than 10,000 cycles are considered as high cycle fatigue. Level of stress in low cycle fatigue is normally higher then yield strength of material.

During power transmission, contact occurs between teeth. It tends to wear out. Common type of wear failure is moderate wear. It happens due to lack of lubricant of fine dirt in the contact. Abrasive wear occurs due to presents of metal particles in the contact of gear tooth. Corrosive wear occurs due to corrosion action takes place between two gear teeth.

CHAPTER – 2

LITERATURE REVIEW

2.1 Literature Survey

Gears are used in most types of machinery, like nuts and bolts, they are a common machine element which will be needed from time to time by almost all machine designers. Current trends of industry are to improve fatigue life and load carrying [1]. There are lots of ways to achieve that, namely using novel materials, heat-treatment or novel gear geometries [6]. In the past several decades, more accurate manufacturing capabilities have allowed engineers to design and manufacture gears to much more stringent specifications. In addition, better computational methods and sophisticated gear system analysis packages have been developed that allow designers to explore solutions far beyond the conventional design practices. This research investigates the impact of two such unconventional methods, namely alternate root fillet geometries and asymmetric tooth profiles, on gear durability.

Gear development phase focus on tooth strength [6], standards [7, 8] and manufacturing technical. Researchers are focus on development of hob or cutter and how fillet radius affects strength of gear. Simultaneously, Researchers also focus on root fillet [24-26] for improve tooth strength.

In 1926, Timoshenko et al. worked on strength of gear teeth [9] and found, fillet radius greatly affect gear strength [9]. Kelley et al. also worked on beam strength of modern gear design [10]. In 1962, Aida et al. worked on bending stress of spur gear [11]. Wilcox et al. applied finite elements to analysis gear tooth stress [12].

In 1975, Francavilla et al. characterized the optimal shape defined by a set of geometric design parameters upon minimizing the stress concentration factors [13]. Drago et al. explore current limitation in tooth root stress analysis [14]. Winter et al. investigated effect of notches at root fillet of tooth for endurance strength of gear [15].

In 1977 Oda conducted an iterative procedure in which a pre defined fundamental shape is modified based on the stresses obtained by carrying out a finite element analysis in each iteration [16].In 1981, Drago et al. experimentally investigate effect of pitch diameter and rim thickness on spur gear tooth root and fillet stress [17].

In 1983, Angeles showed how periodic splines can be used to synthesize curves that meet the local geometric properties of a finite set of points located through the interval of interest [18].In 1987, Andrews et al. investigated procedure to minimize fillet bending stresses in involute spur gears by automatic design optimization [19]. Duraisamy conducted fatigue testing of spur gear to obtain optimal root geometry [20]. Der Hovanesian et al. optimized gear root stress using photoelastic optimization techniques [21].

In 1990, Rogers et al. designed non standard spur gear cut by a hob [22] and generated it with pinion cutters [23]. Clapper gives prediction of gear root stress. Also made comparisons of experimental and FEM results [24].In 1998, Tsai, M et al. investigated design of high contact ratio spur gears using quadratic parametric tooth profiles [25]. In 2000, Pulley FT et al. filed patent on method for producing and controlling a fillet on a gear [26].

During the power transmission in gear pair, a several effects works, like stress concentration, tooth error and misalignment etc, [28]. During the transmitting load, each gear tooth behaves like a cantilever beam and subjected bending [29]. It is found that maximum bending stress occurs at root fillet of tooth [30].Repeated excessive stresses cause bending fatigue often at the tooth-root [27]. The first crack initiates at the regions with the highest stress concentrations and propagates until failure occurs [31]. Failure due to crack is always challenge to designer.

In 1982, Buenneke et al. conducted single gear tooth bending fatigue test [32].In 1992, Wheitner investigated fatigue crack detection methods in gear teeth [33]. In 1996-97, Lewicki D et al. found effects of rim thickness on gear crack propagation path [34]. Blarasin A et al. found fatigue crack growth prediction in specimens similar to spur gear teeth [35]. Fernandes P worked on tooth bending fatigue analysis in gears [36]. In 1998-99, Daniewicz, S.R et al. increasing the bending fatigue resistance of spur gear teeth using a presetting process [37]. Ciavarella, M et al. developed a numerical methods for the optimization of specific sliding, stress concentration and fatigue life of gears [38]. In 2002, Glodez et al. developed computational model for determination of service life of

gears [39]. In 2007, Jelaska et al. worked on gear tooth root fatigue behaviour [40]. Pehan et al. investigate crack propagation occurs at the root of the gear tooth [41]. Ananda et al. worked on crack propagation path analysis using finite element method for spur gear [42].

Asymmetric gear tooth design concepts have also been introduced around 1983s, as a method to reduce bending stresses [43]. However, they were not strongly pursued due to few practical applications and limited capabilities in cutting asymmetric profiles accurately.

In 1997, DiFrancesco et al. worked on concept of asymmetric profile of gear and structural analysis of teeth with asymmetric profiles [44]. In a standard symmetric gear, pressure angle on both drive and coast sides of a gear tooth profile is same. But in asymmetric gear pressure angle on both sides are different, so, standard symmetric gear becomes asymmetric spur gear.

In 2000, Kapelevich et al. has also developed involute gears with asymmetric tooth profiles for gear applications where opposite flanks of the gear tooth are functionally different [45]. Also developed geometry model of asymmetric involute spur gear teeth [46] and modified asymmetric spur gear drives [46]. Deng, G et al. also found that using asymmetric tooth profile, bending tooth root stress is decreases [47] and Enhanced bending load capacity [48] which increase service life. Karpat et al. conducted computer aided analysis of involute spur gears with asymmetric teeth [49]. And also conducted dynamic analysis of involute spur gears with asymmetric teeth [50]. V. Senthil Kumar et al. improved the fillet capacity in bending [51].

Th. Costopoulos et al. reduced fillet stresses of the asymmetric one-sided -involute gear teeth [52]. Kapelevich et al. optimize the fillet profile which reduces the maximum bending stress in the gear tooth root area by 10-30% [53] and optimized fillet form for potential application in helicopter main drives [54]. Niels L. Pedersen has suggested that higher reduction in the bending stress can be obtain when the drive side pressure angle is greater than the coast side pressure angle [55]. Alipiev developed a geometric design of involute spur gear drives with symmetric and asymmetric teeth using the realized potential method [56]. Muthuveerappan et al estimated the tooth form factor for normal contact ratio asymmetric spur gear tooth [57].

Direct Gear Design® is a concept of focus on parameter of gear instead of method to manufacture it [58-60]. Conventional gear design is generally based on standard tools, the gears provided are usually not optimum. The author separated gear-geometry definition

from tool selection; hence, the gear tooth profiles did not depend on the standard set of parameters of the generating rack and its location relative to a standard pitch diameter of the gear. The foregoing approach allowed gear designers to explore more gear combinations, which could provide better performance for a particular product or application. The next step is defining unique tool geometry to generate the designed gear set; therefore, the cost of a custom cutting tool had to be added.

Kapelevich et al. developed Direct Gear Design® results in 15-30% reduction in stress level when compared to traditionally designed gears. Direct Gear Design® for asymmetric tooth profiles provides additional opportunity for improvement of gear drives with single directional load cycles. [61, 62].

Muthuveerappan et al. In 2007, optimized asymmetric spur gear drives to improve bending strength using direct gear design method [63]. In 2014, estimated optimum profile shift for direct design asymmetric normal and high contact ratio spur gears based on load sharing and worked on fillet stress analysis of asymmetric helical gears through direct design [64, 65]. In 2016, designed asymmetric normal contact ratio spur gear drive to enhance the load carrying capacity through direct design [66].

Spitas et al. develop new concept in numerical modelling and calculation of the maximum root stress in spur gears versus standard methods [67]. Also found novel circular root fillet which increase strength of standard involute gear [68]. So, conventional gears are designed with a circular-filleted tooth-root [68]. A circular fillet avoids stress concentrations that would arise due to an infinite curvature at the corner between the tooth flank and the root circle. However, at the connection point of involute profile of tooth and circular fillet at root, stress concentration occurs due to curvature discontinuity. Such discontinuities cause a sudden rise in stress values, so it is necessary to making these regions prone to mechanical failure. Hence, stress concentration plays a important role to reduce or avoid mechanical failure. Reduction in stress concentration will improve the gear tooth strength. Optimize gear tooth geometry for minimum fillet stresses using bem and experimental verification with photo elasticity [69] and also maximum bending strength and equivalent pitting resistance [70] and show that bending strength of gear affected by circular and trochoidal fillet [71,72].

Pedersen has been reduced bending stress of spur gear by redesign a standard cutting tool [73]. Cuneyt Fetvaci have developed mathematical model of spur gears with asymmetric involute teeth according to the gearing theory and also investigated trochoidal

envelope traced by cutter during the generating process [74]. Sanders conducted experiment and investigate, an elliptical profile can be used to create larger fillet curvatures that can yield lower stresses than the corresponding best design practice using the largest possible circular root fillet. Each gear size (pitch diameter, diametral pitch, etc.) will have a unique, optimum elliptical shape [75]. Zhao X optimizes cutting tool profile, to increases bending strength of spur gear [76].

Andrzej Kawalec et al. presented a comparative analysis using ISO and AGMA standards of tooth root strength for spur and helical Gears with consideration of FEM verification [77]. Xiao et al. optimized fillet shape of gear tooth using B-splines curve. A genetic algorithm (GA) was taken as the optimizer. The control points of the B-splines were defined as design variables, as opposed to discrete nodes as in the former approach [78]. Yeh et al. designed new tooth profile for high load carrying capacity [79]. Senthilvelan et al. found effect of fillet radius on performance of injection molded nylon 6/6 gears [80]. Flodin et al. talk about how powder metal manufacturing technology can be used to manufacture gears with optimized fillets in mass production [81]. It may be less efficient to use conventional methods of gear manufacturing in this case.

Sankar et al. modified profile to increase tooth strength of spur gear using CAD [82]. Wang et al. analysis the influence of fillet curves on gear bending strength [83]. T. Zou et al worked to increase load carrying capacity by modifying root profile of spur gear. To modify root profile, FEA with APDL-ANSYS Parametric Design Language is implemented in Matlab [84].

Finite Element Analysis (FEA) is also known as Finite Element Method (FEM).It is a numerical method [85] to solve complex elastic and structural problems. This method is developed by Alexander Hrennikoff and Richard Courant [86].

Gear design is very complex procedure [1]. Good gear design will give high durability and consistency in power transmission [1]. Gear design as per ISO [8] and AGMA [7] published many numerical standards used to design gear. It required FEA analysis to check gear failure and predicts gears life in service [87] which is necessary for good gear design [88]. then result will checked by experimental test [88].

In research, many researcher works on same design of gear with different parameters to obtain optimize design parameters. Researcher develops various CAD model for FEA. For example in asymmetric gear to optimize pressure angle, different pressure angle drive side CAD model is required. Then all CAD model are analyzed in FEA simulator to

predict bending stress at root of tooth. In such situation, researchers need to develop each CAD model and also need to create virtual environment in FEA simulator. It required lots of time and work. To avoid such situation, in this research author developed method to calculate multiplication factor (MF) for given material and gear design parameters (module, number of tooth on gear and pinion). Multiplication factor is eliminates multiple FEA analysis to calculate bending stress at root of symmetric and asymmetric gear.

Current researchers are works on the optimization of tooth root fillet which improve load carrying capacity and life [26-27, 29, 65, 67-68, 78-79, 84]. Roughing processes generates trochoidal at the root of the tooth [72, 74]. So, roughing processes are unable to obtain desire root profile as per design [72]. This thing will reduce the performance of gear in terms of load caring capacity and longer life [72]. So, an alternative manufacturing technique is required. Some researchers have developed a form tool for desire root profile [89]. It makes a very costly manufacturing technique. Another approach is CNC wire cut machine to manufacture a gear as per the design parameter [90].

CNC (computer numerical control) works on a set of instruction in which the process is controlled by numbers, letters, and symbols. In CNC, the numbers, symbols form an instruction based program designed for a gear [90]. These instructions are called G-code. CNC works as per instruction given by G codes in the form of program to perform a task. Writing a program using G-code is very much complicated task and it requires high knowledge of the machine. Written codes may have faults which without performing the operations is very difficult to find. Trial and error method is needed to identify the problems and make a successful product [90]. So, CAM software is required CAD model of gear to generate G-code [91]. CAD model requires modeling software.

CNC wire cut machine capable of manufacturing gear as per desire parameter [89] but require G code generation software and modeling software to create a CAD model [91,92].Optimize profile developed by a researcher is on equation-based and it is very difficult to create in CAD model [92]. So, Use of CNC wire cut depend on complicated CAD model [92] and G code generation software which is also complicated [91]. An alternative is required in this situation. In this research, authors generate G code without using a G code generation software and CAD model.

Reducing bending stresses in gears is widely investigated in the literature with the aim of increasing the load-carrying capacity and extending the gear life. When reviewing the vast literature published, approaches in achieving the foregoing goal have been

directed towards either identifying and selecting the optimum combination of gear geometrical parameters or optimizing the tooth-root fillet profile shape.

Most of the work reviewed above in regards to optimizing the root geometries and/or using asymmetric tooth shapes. Work done with little or no consideration of G2 continuity using Bezier curve at root of tooth is reported in literature survey. Lizheng Lu et al found that, In order to reduce concentration of stress , an important condition or criterion is geometric continuity of order 2(G2 continuity) [93]. G2 continuity gives connection between two curves with equal tangent and equal curvature [93]. G2 continuity is very important to decrease stress concentration at the root of tooth. G2 continuity at the connection points of tooth profile and root profile of gear plays very important role in reducing stress concentration. Bezier curve mimics the shape of its control polygon. A Bezier curve passes through its first and last control points, and is tangent to the control polygon at those endpoints [94].

In this analysis to reduce stress concentration, a Bezier curve is used with G2 continuity at blending point of involute tooth profile and root profile of asymmetric spur gear tooth and also introduced concept of multiplication factor which eliminate multiple FEA. Method to create exact involute and developed root profile in CAD software is presented. Method to generate G code without using a G code generation software and CAD model also presented which solve problem to manufacture desire profile of gear. In short integrated module of design, modelling and manufacturing of symmetric and asymmetric involutes spur gear has been presented.

2.2 Graphical interpretation of literature survey

Due to lots of combination development in gear root and tooth profile, it is very difficult to develop graphical interpretation of literature survey. But author try to explain overall idea about research in development in gear root and tooth profile, in terms of graphical interpretation of literature survey.

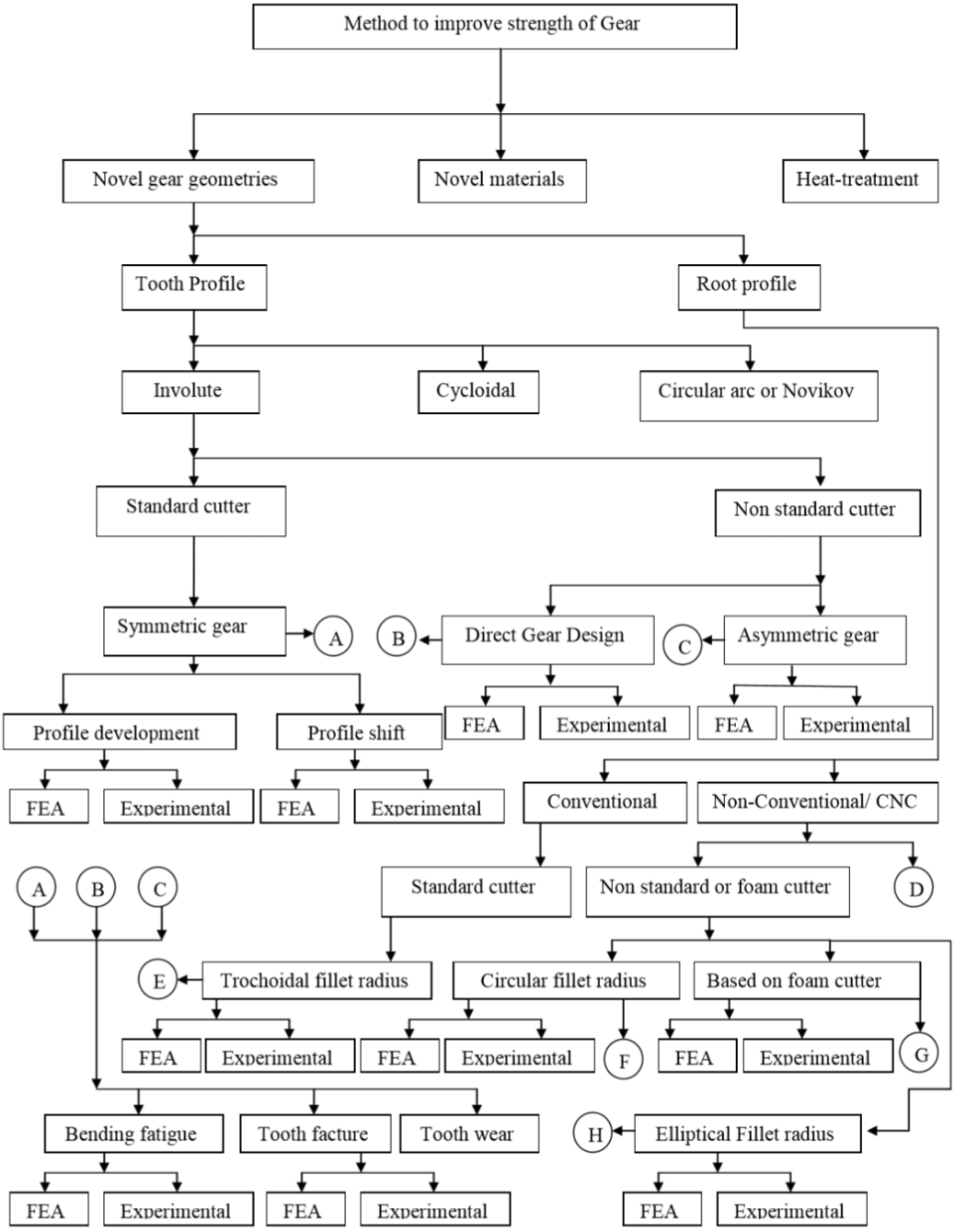

FIGURE 2.1: Graphical interpretation of literature survey- part 1

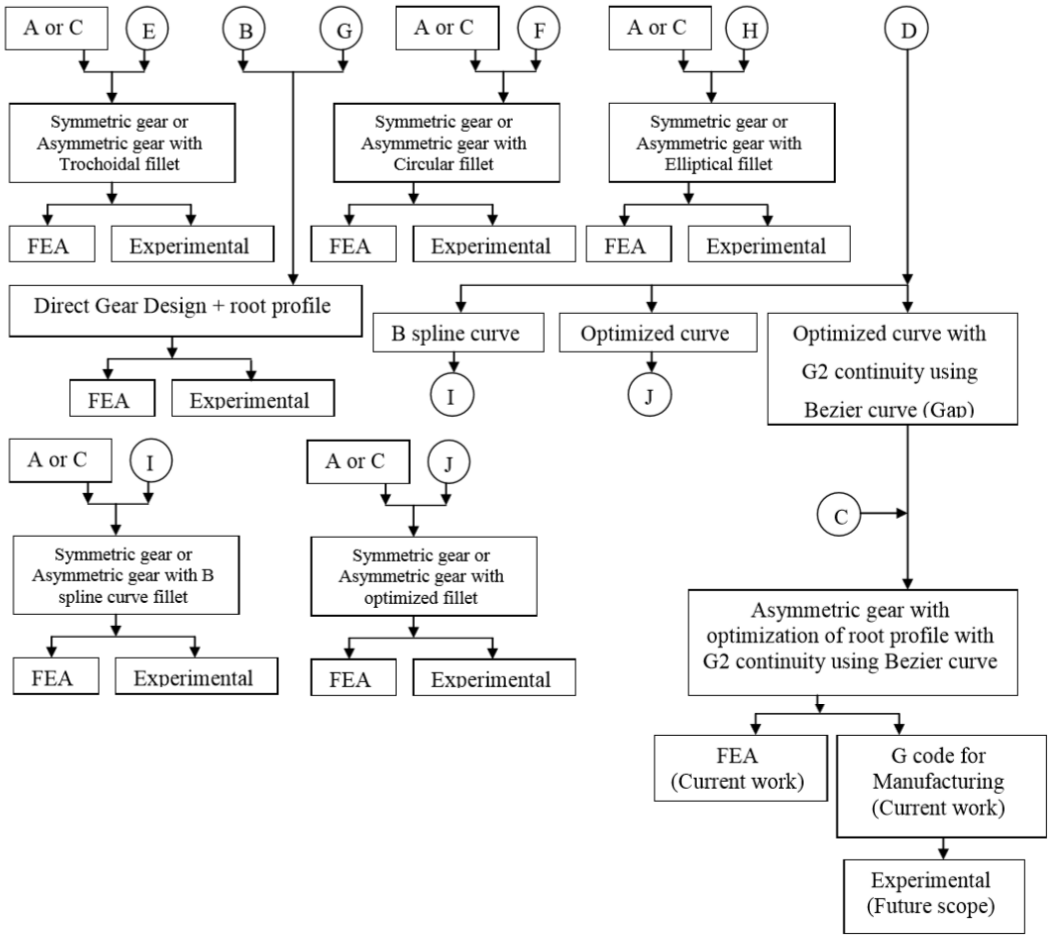

FIGURE 2.2: Graphical interpretation of literature survey- part 2

2.3 Thesis objectives and scope

The specific objectives of this study are as follows:

1) To generate a mathematical model of symmetric and asymmetric involute spur gear.

2) To identify constraints which affect higher value of drive side pressure angle.

3) To develop equations to calculate “bending stress equation parameters” of symmetric and asymmetric involute spur gear.

4) To develop objective function to select input parameters for desire output in terms of bending stress.

5) To investigate effect of pressure angle on tooth geometry, parametric analysis of asymmetric spur gear tooth is required.

6) To optimize drive side pressure angle.

7) To optimize tooth root profile using G2 continuity with Bezier curve.

8) To develop algorithm and code for CAD model of symmetric and asymmetric involute spur gear.

9) To generate G Code for manufacture symmetric and asymmetric involute spur gear without using CAD model and G code generation software.

To develop an intergraded module which is capable to design, modeling and manufacture of a symmetric and asymmetric involute spur gear.

2.4 Layout of Thesis

In this section a chapter wise brief introduction is given below.

Chapter 1 presents a general introduction spur gear. It includes history of gear, various profile of gear, gear manufacturing techniques, error occurs in gear, profile shift, interference, undercuts and various mode of failure.

Chapter 2 focuses on a literature review. State of art literature has been carryout. Reducing bending stresses in gears is widely investigated in the literature with the aim of increasing the load-carrying capacity and extending the gear life. When reviewing the vast literature published, approaches in achieving the foregoing goal have been directed towards either identifying and selecting the optimum combination of gear geometrical parameters or optimizing the tooth-root fillet profile shape. At the end of chapter research objectives and layout of the thesis are described.

Chapter 3 presents a mathematical model of symmetric and asymmetric spur gear. Equations to calculate “bending stress equation parameters” of symmetric and asymmetric of involute spur gear has been derived.

Chapter 4 presents standard bending stress equation as per BS ISO 6336 part 3. Based on standard bending stress equation and developed equations of “bending stress equation parameters” an objective function has been created to reduce bending stress at the critical section of tooth.

Chapter 5 explains parametric analysis of asymmetric spur gear tooth. In asymmetric gear a higher pressure angle on drive side within the constraints is required to minimize bending stress at root of tooth. So, higher pressure angle on drive side effect on tooth

geometry. The parametric analysis helps to understand the effect of drive side pressure angle on tooth geometry of asymmetric spur gear. Developed equations of "bending stress equation parameters" have been used to calculate various parameters. Parametric analysis has been explained with consideration of gear parameter. Application of parametric analysis is given in result and discussion section.

Chapter 6 focus on optimization of drive side pressure angle. Constraints which affect drive side pressure angle to minimize bending stress at critical section of asymmetric spur gear tooth are also described. Optimize drive side pressure angle has been calculated for given parameter.

Chapter 7 explains method to optimize root profile in generalize foam. It explains basics of G2 continuity and Bezier curve. A curve synthesis approached has been established to minimize stress concentration or bending stress using Bezier curve with G2 continuity at critical section of tooth.

Chapter 8 is divided in two parts. In First part algorithm has been developed to create a CAD model of symmetric spur gear with standard fillet, asymmetric spur gear with standard fillet and asymmetric spur gear with the modified root. Second part presents a developed CAD models in AutoCAD software using algorithm presented in first part.

Chapter 9 focus on finite element analysis of symmetric spur gear with standard fillet, asymmetric spur gear with standard fillet and asymmetric spur gear with the modified root for given virtual environment. von-Mises stress has been calculated for above mention models.

Chapter 10 explains algorithm to create G Code for Symmetric and Asymmetric involute spur gear without using CAD model and G code generation software.

Current focus of works is on the optimization of tooth root fillet which improve load carrying capacity and life. It is very difficult to manufacturing a gear using convectional technique. So, an alternative manufacturing technique is required. Some researchers have developed a form tool for desire root profile. It makes a very costly manufacturing technique. Another approach is CNC wire cut machine to manufacture a gear as per the design parameter. CNC (computer numerical control) works on a set of instruction in which known as a G-code. Writing a program using G-code is very much complicated task and it requires high knowledge of the machine. Written codes may have faults which without performing the operations is very difficult to find. Trial and error method is needed to identify the problems and make a successful product. So, CAM software is alternate for

same. CAM software is required CAD model of gear to generate G-code. CAD model requires modeling software. An alternative is required in this situation. In this research, authors generate G code without using a G code generation software and CAD model.

Chapter 11 presents a result, discussion and application of parametric analysis, optimization drive side pressure angle, optimization of root profile and G code to manufacture gear.

At last conclusions has been made for of parametric analysis, optimization drive side pressure angle, optimization of root profile and G code to manufacture gear.

Appendix I present a various codes

CHAPTER – 3

MATHEMATICAL MODEL OF INVOLUTE SPUR GEAR

This chapter presents a mathematical model of symmetric and asymmetric spur gear. Equations to calculate “bending stress equation parameters” of symmetric and asymmetric of involute spur gear has been derived.

3.1 Involute profile

The involute of a circle is the spiraling curve traced by the end of an imaginary taut string unwinding itself from that stationary circle called the base circle [3]. Figure 3.1[3] shows an involute geometry. T is point on involute profile.

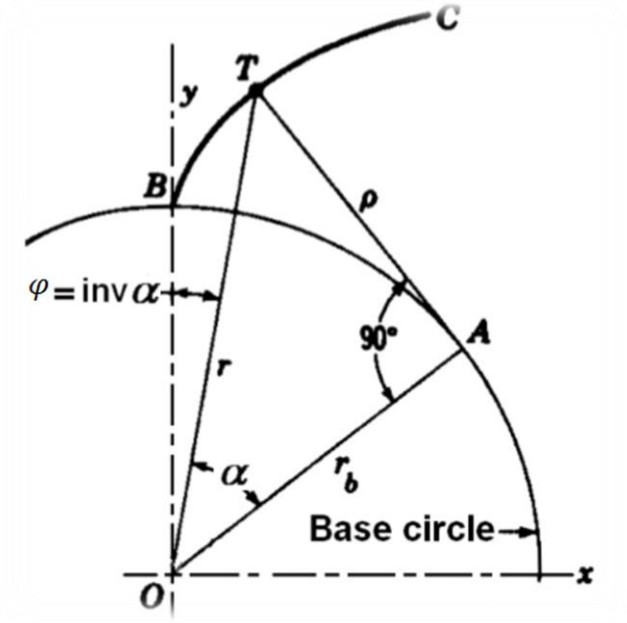

FIGURE 3.1: Involute profile

From figure 3.1, value of ρ is given by

$$\rho = r_b \tan\alpha \tag{3.1}$$

$$\rho = r_b(\alpha + \varphi) \tag{3.2}$$

From equation 3.1 and 3.2,

$$\varphi = \tan\alpha + \alpha \tag{3.3}$$

Equation 3.3 also writes as,

$$inv\alpha = \tan\alpha + \alpha \tag{3.4}$$

Equation 3.3 is mathematical foam of involute profile. It show that involute profile is depends on angle α which is known as a pressure angle [1].Involute profile becomes more popular due to easy to manufacturing, variation in centre distance does not affect the velocity ratio and pressure angle remains constant throughout the engagements which results in smooth running [3].

3.2 Mathematical model of symmetric involute spur gear

In a standard symmetric gear tooth, pressure angle on both sides of involute profile is same [1-2].

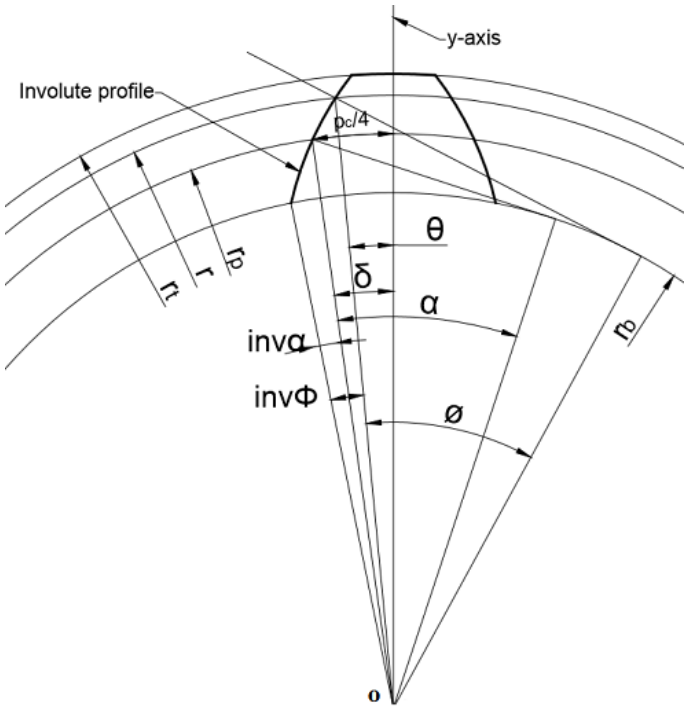

FIGURE 3.2: Geometric model of involute symmetric gear tooth profile

From fig. 3.2 shows geometric model of gear tooth. It is observe that,

$$inv\phi - inv\alpha = \delta - \theta \tag{3.5}$$

Hear, $\delta = \frac{p_c / 4}{r_p}$, $p_c = \pi \cdot m$ and $r_p = \frac{m \cdot z}{2}$

$$\delta = \frac{\pi}{2 \cdot z}$$

So,

$$\theta = \frac{\pi}{2 \cdot z} + inv\alpha - inv\phi \tag{3.6}$$

From fig. 3.2, we obtain

$$r_{bc} = r_p \cdot \cos\alpha \text{ and } r_{bc} = r \cdot \cos\phi$$

$$\phi = \cos^{-1}\left(\frac{r_p}{r} \cdot \cos\alpha\right) \tag{3.7}$$

Due to this,

$$\theta = \frac{\pi}{2 \cdot z} + inv\alpha - inv\left(\cos^{-1}\left(\frac{r_p}{r} \cdot \cos\alpha\right)\right) \tag{3.8}$$

But as per definition of involute profile,

$$inv\alpha = \tan\alpha - \alpha$$

$$\theta = \frac{\pi}{2 \cdot z} + \tan\alpha - \alpha - \left(\tan\left(\cos^{-1}\left(\frac{r_p}{r} \cdot \cos\alpha\right)\right) - \left(\cos^{-1}\left(\frac{r_p}{r} \cdot \cos\alpha\right)\right)\right) \tag{3.9}$$

Equation 3.9 shows angle θ at given radius r. Radius r is varies between base circle radius to addendum circle radius. It defines location of points on the involute profile as shown in figure 3.3.

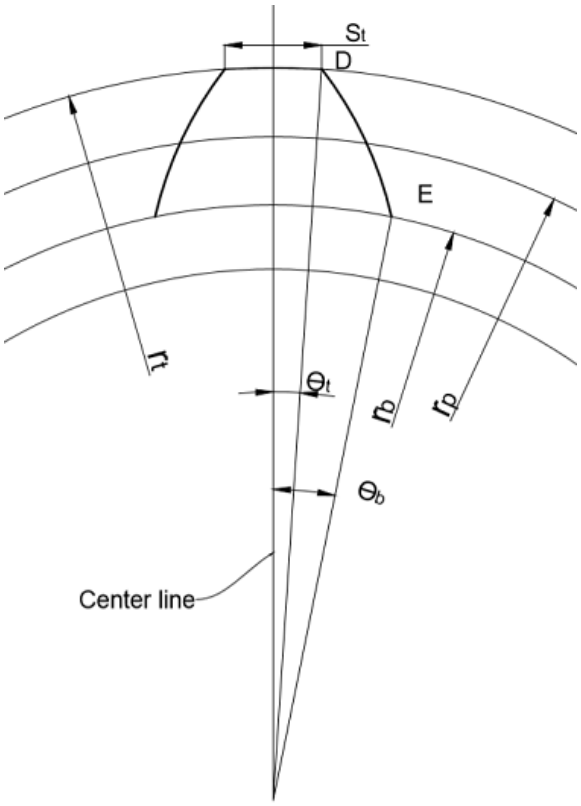

FIGURE 3.3: Involute profile of symmetric spur gear tooth

To develop both involute profiles, θ is varied between $\theta_b \le \theta \le \theta_t$ and $-\theta_b \le \theta \le -\theta_t$ respectively.

Involute profile coordinate (x_i , y_i) given by:

$$x_i = r_i \cdot \cos\theta_i$$

$$y_i = r_i \cdot \sin\theta_i$$

$$\theta_i = \frac{\pi}{2.z} + \tan\alpha - \alpha - \left(\tan\left(\cos^{-1}\left(\frac{r_p}{r_i}.\cos\alpha \right) \right) - \left(\cos^{-1}\left(\frac{r_p}{r_i}.\cos\alpha \right) \right) \right) \quad (3.10)$$

Where design parameter θ_i is varied

$\theta_b \le \theta \le \theta_t$ for drive side profile

$-\theta_b \le \theta \le -\theta_t$ for coast side profile

3.3 Mathematical model of asymmetric involute spur gear

3.3.1 Introduction of asymmetric involute spur gear

In design of gear, most important thing is bending stress must be low at critical section. So it is necessary to minimize bending stress of tooth at critical section. To minimize bending stress one way is optimize geometrical shape of standard symmetric

gear [1-2]. To minimize bending stress, pressure angle on drive side must be higher than coast side profile within constraint [45-57]. In a standard symmetric gear, on both side of tooth profile pressure angle remains same [1-2]. But due to higher pressure angle on drive side, standard symmetric gear becomes asymmetric spur gear [45-57] as shown in figure 3.4. In asymmetric spur gear, at root of tooth the bending stress decreases as the pressure angle on drive side is higher than coast side [45-57]. Contact ratio and tip thickness are limiting factor for higher drive side pressure angle.

Gear standard procedures recommend that, the contact ratio should be higher or equal to 1.1 [1-2]. Below this contact ratio tooth loading period increases and it is undesirable condition for cyclic loading. Gear standard procedures recommend that, the tip thickness should be $\geq$ *0.4m* for hardened gears. In exceptional cases, tip thickness decreases to *0.25m* [1-2]. Below this tip thickness it becomes more pointed.

Main advantages of asymmetric spur gear are high load carrying capacity and longer fatigue life as compare to standard symmetric spur gear [45]. It gives better performance in one direction, is main disadvantage of asymmetric spur gear [45]. Main application of asymmetric spur gear is in aerospace [45].

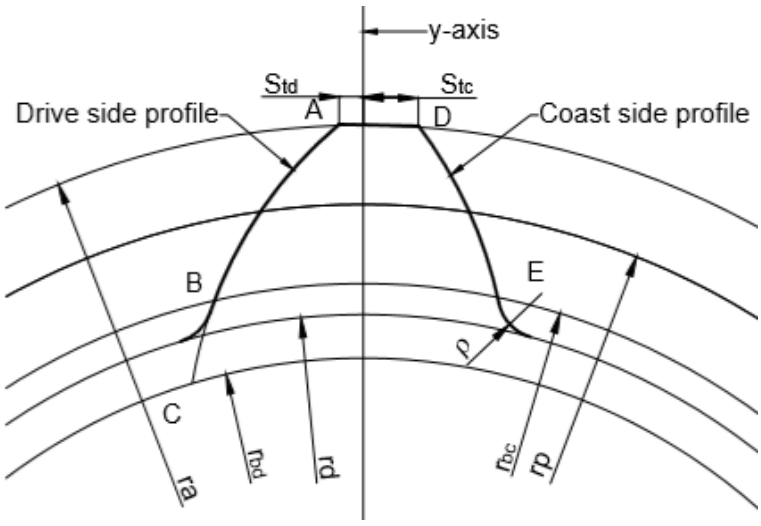

FIGURE 3.4: Asymmetric involute spur gear tooth

3.3.2 Mathematical model of asymmetric spur gear

Asymmetric spur gear tooth means both sides of gear tooth profile are with different pressure angles. As shown in fig. 3.5, as pressure angle on drive side increases, base circle radius decreases and so, longer involute profile is available on drive side from tip point A

to base circle radius point C. While on coast side involute profile is available from tip point D to base circle radius point E developed by pressure angle on coast side.

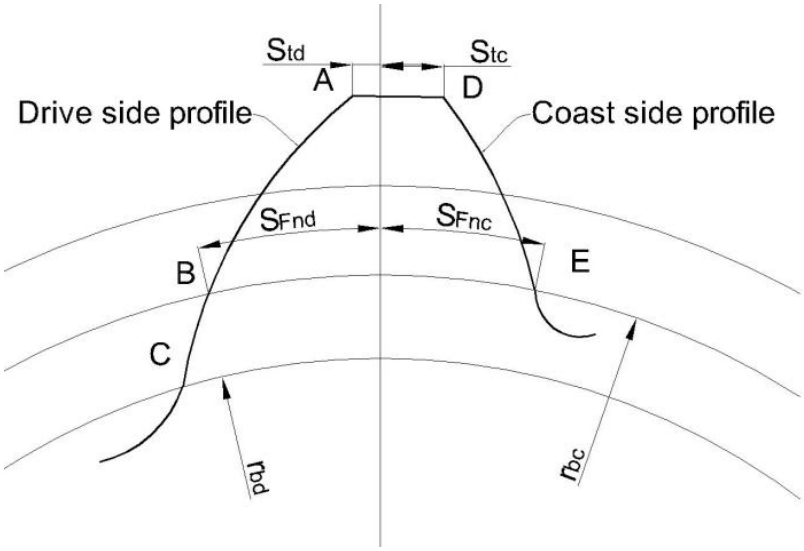

FIGURE 3.5: Asymmetric involute spur gear tooth

So on drive side the available involute profile is from tip (point A) to base circle radius (point B at same radius as point E) developed by pressure angle on coast side but at pressure angle on drive side profile.

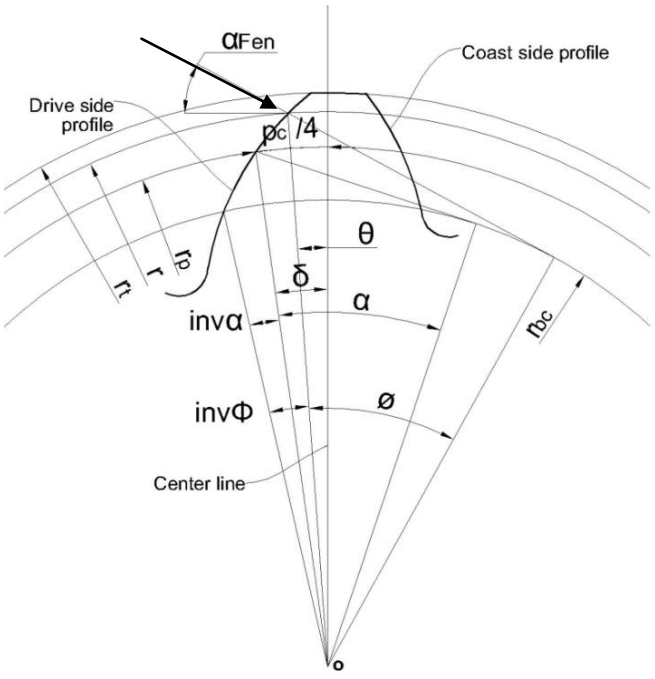

FIGURE 3.6: Geometric model of asymmetric gear tooth

From fig. 3.6 shows geometric model of gear tooth. It is observe that,

$$inv\phi - inv\alpha = \delta - \theta \tag{3.11}$$

$$\delta = \frac{S_{pd}}{r_p} \tag{3.12}$$

$$\theta = \frac{S_d}{r} \tag{3.13}$$

$$S_d = r \cdot \left(\frac{S_{pd}}{r_p} - \left(inv\phi - inv\alpha \right) \right) \tag{3.14}$$

Above equation gives tip thickness on drive side at any radius *r*. Thickness at pitch circle radius, ϕ becomes equal to α and so $inv\phi - inv\alpha$ becomes 0. It means thickness at pitch circle radius does not depend on pressure angle and it is constant at any pressure angle at pitch circle radius.

Hear, $S_{pd} = \frac{p_c}{4}$, $p_c = \pi \cdot m$ and $r_p = \frac{m \cdot z}{2}$

$$\delta = \frac{\pi}{2 \cdot z}$$

$$\theta = \frac{\pi}{2 \cdot z} + inv\alpha - inv\phi \tag{31.5}$$

From fig. 3.6, we obtain

$r_{bc} = r_p \cdot \cos\alpha$ and $r_{bc} = r \cdot \cos\phi$

$$\phi = \cos^{-1}\left(\frac{r_p}{r} \cdot \cos\alpha \right) \tag{3.16}$$

Due to this,

$$\theta = \frac{\pi}{2 \cdot z} + inv\alpha - inv\left(\cos^{-1}\left(\frac{r_p}{r} \cdot \cos\alpha \right) \right) \tag{3.17}$$

But as per definition of involute profile,

$inv\alpha = \tan\alpha - \alpha$

$$\theta = \frac{\pi}{2 \cdot z} + \tan\alpha - \alpha - \left(\tan\left(\cos^{-1}\left(\frac{r_p}{r} \cdot \cos\alpha \right) \right) - \left(\cos^{-1}\left(\frac{r_p}{r} \cdot \cos\alpha \right) \right) \right) \tag{3.18}$$

Equation 3.18 gives angle θ. Angle θ is angle with respect to axis y at any radius on involute profile for given pressure angle.

Fig. 3.7 shows involute profile of asymmetric spur gear tooth, which is represented by three, curves. 1. Drive side involute profile 2. Coast side involute profile and 3. Circular arc at tip circle radius and it is further divided in two parts,i) circular arc at tip for drive side (S_{td}) and ii)circular arc at tip for coast side (S_{tc}).

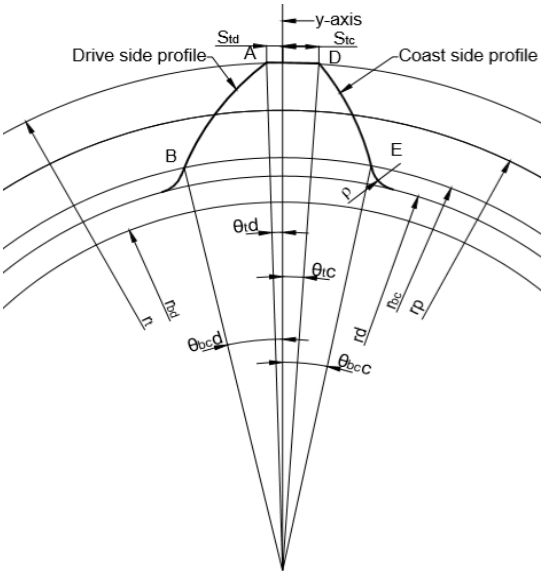

FIGURE 3.7: Involute profile of asymmetric spur gear tooth

Figure 3.7 shows angle θ is varied between $\theta_{bc}d \le \theta_i \le \theta_t d$ and $-\theta_{bc}c \le \theta_i \le -\theta_t c$.

Coordinate points (x_i , y_i) of nnvolute profile given by:

$$x_i = r_i \cdot \cos\theta_i$$

$$y_i = r_i \cdot \sin\theta_i$$

$$\theta_i = \frac{\pi}{2.z} + \tan\alpha - \alpha - \left(\tan\left(\cos^{-1}\left(\frac{r_p}{r_i}.\cos\alpha \right) \right) - \left(\cos^{-1}\left(\frac{r_p}{r_i}.\cos\alpha \right) \right) \right) \quad (3.19)$$

$\theta_{bc}d \le \theta_i \le \theta_t d$ and $\alpha = \alpha_d$ for drive side profile

$-\theta_{bc}c \le \theta_i \le -\theta_t c$ and $\alpha = \alpha_c$ for coast side profile

3.4 Gear tooth parameters

Figure 3.8 (a) and (b) shows representation of various parameters of symmetric and asymmetric involute spur gear. Bending stress is affected by various parameters of gear tooth [8]. It is observed that nominal bending stress at the root of the tooth depends on tooth thickness at the root of the tooth (S_{Fn}), load angle (α_{Fen}), root fillet (ρ_F) and

height of bending moment arm (h_{Fe}) [8]. Tip thickness (S_t) is limiting parameters for higher pressure angle of drive side of asymmetric spur gear.

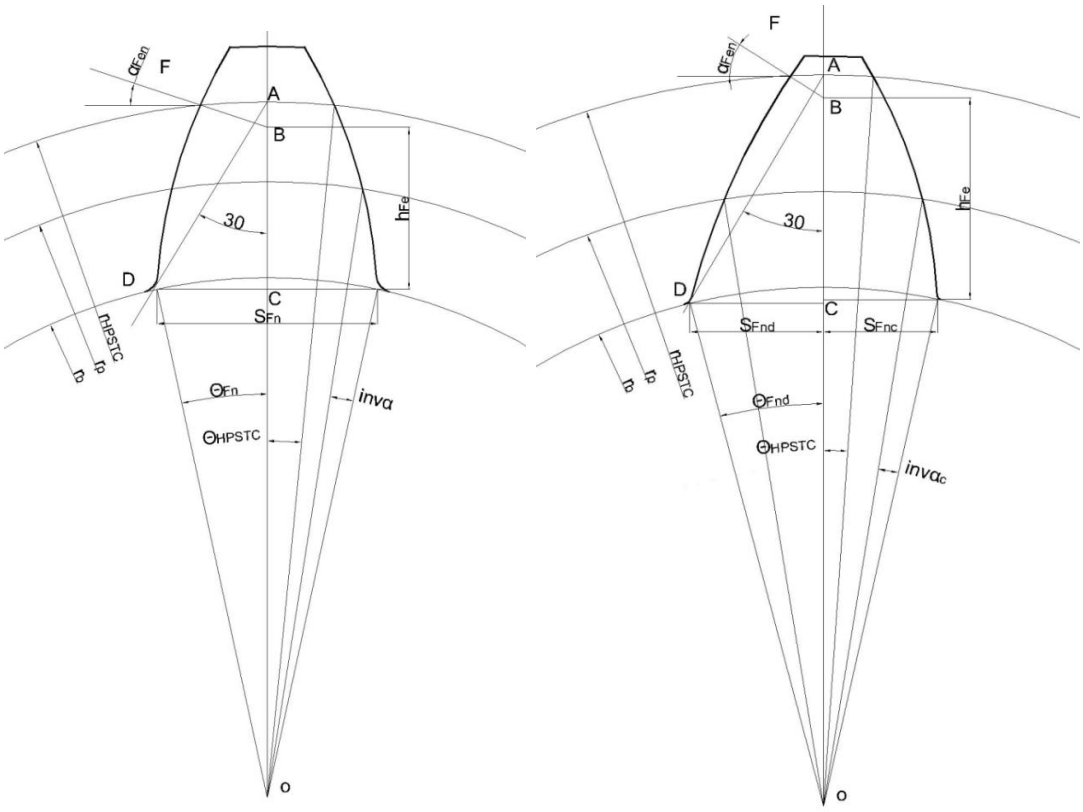

FIGURE 3.8 (a): Symmetric involute spur gear tooth (b) Asymmetric involute spur gear tooth

To understand basic phenomena of tooth geometry of symmetric and asymmetric spur gear, value of these parameters are required. Equation 3.9 and 3.18 gives location any point on involute curve at given pressure angle for symmetric and asymmetric spur gear respectively. To obtain value of these parameters an Equation has been developed.

3.4.1 Tip Thickness (S_t)

Tip thickness is main constraints for higher value of drive side pressure angle. Small thickness makes tooth very sharp and pointed. The formula for calculating tip thickness of tooth is:

a) Tip Thickness for symmetric spur gear tooth

$$S_t = 2 \cdot r_t \cdot \theta_t \tag{3.20}$$

$$\theta_t = \frac{\pi}{2.z} + \tan\alpha - \alpha - \left(\tan\left(\cos^{-1}\left(\frac{r_p}{r_t}.\cos\alpha \right) \right) - \left(\cos^{-1}\left(\frac{r_p}{r_t}.\cos\alpha \right) \right) \right)$$

b) Tip Thickness of asymmetric spur gear tooth

$$S_t = r_t\theta_{tc} + r_t\theta_{td} \tag{3.21}$$

$$\theta_{td} = \frac{\pi}{2.z} + \tan\alpha_d - \alpha_d - \left(\tan\left(\cos^{-1}\left(\frac{r_p}{r_t}.\cos\alpha_d\right)\right) - \left(\cos^{-1}\left(\frac{r_p}{r_t}.\cos\alpha_d\right)\right)\right)$$

$$\theta_{tc} = \frac{\pi}{2.z} + \tan\alpha_c - \alpha_c - \left(\tan\left(\cos^{-1}\left(\frac{r_p}{r_t}.\cos\alpha_c\right)\right) - \left(\cos^{-1}\left(\frac{r_p}{r_t}.\cos\alpha_c\right)\right)\right)$$

3.4.2 Tooth thickness at critical section S_{Fn}

Critical section is most affected by load. It must be high. Higher critical section means stronger tooth. In most of cases failures stats at critical section.

a) Tooth thickness at critical section S_{Fn} for symmetric spur gear tooth

The formula for calculating Tooth Thickness at critical section of symmetric tooth is:

$$S_{Fn} = 2 \cdot r_b.\sin\theta_{Fn} \tag{3.22}$$

Where,

$$\theta_{Fn} = \frac{\pi}{2.z} + \tan\alpha - \alpha - \left(\tan\left(\cos^{-1}\left(\frac{r_p}{r_b}.\cos\alpha\right)\right) - \left(\cos^{-1}\left(\frac{r_p}{r_b}.\cos\alpha\right)\right)\right)$$

b) Tooth thickness at critical section S_{Fn} for asymmetric spur gear

The formula for calculating tooth thickness at critical section of asymmetric tooth is:

$$S_{Fn} = S_{Fnd} + S_{Fnc} \tag{3.23}$$

Where,

$$S_{Fnd} = r_{bc}.\sin\theta_{Fnd}$$

$$S_{Fnc} = r_{bc}.\sin\theta_{Fnc}$$

$$\theta_{Fnd} = \frac{\pi}{2.z} + \tan\alpha_d - \alpha_d - \left(\tan\left(\cos^{-1}\left(\frac{r_p}{r_{bc}}.\cos\alpha_d\right)\right) - \left(\cos^{-1}\left(\frac{r_p}{r_{bc}}.\cos\alpha_d\right)\right)\right)$$

$$\theta_{Fnc} = \frac{\pi}{2.z} + \tan\alpha_c - \alpha_c - \left(\tan\left(\cos^{-1}\left(\frac{r_p}{r_{bc}}.\cos\alpha_c\right)\right) - \left(\cos^{-1}\left(\frac{r_p}{r_{bc}}.\cos\alpha_c\right)\right)\right)$$

3.4.3 Load angle

From fig. 3.6, it is observed that;

$$\alpha_{Fen} = \phi - \theta$$

From equation (3.16) and (3.18)

$$\phi = \cos^{-1}\left(\frac{r_p}{r}\cdot\cos\alpha\right)$$

$$\theta = \frac{\pi}{2\cdot z} + \tan\alpha - \alpha - \tan\left(\cos^{-1}\left(\frac{r_p}{r}\cdot\cos\alpha\right)\right) + \left(\cos^{-1}\left(\frac{r_p}{r}\cdot\cos\alpha\right)\right)$$

So, Load angle is given by

$$\alpha_{Fen} = \tan\left(\cos^{-1}\left(\frac{r_p}{r}\cdot\cos\alpha\right)\right) - \frac{\pi}{2\cdot z} - \tan\alpha + \alpha \qquad (3.24)$$

3.4.4 Bending moment arm h_{Fe}

a) Bending moment arm h_{Fe} for symmetrical gear tooth

For symmetric gear tooth, pressure angle on both sides is same. Fig 3.8 (a) shows representation of bending moment arm h_{Fe} for symmetric gear tooth.

The bending moment arm h_{Fe} for symmetric gear tooth is:

$$h_{Fe} = OA - (OC + AB) \qquad (3.25)$$

Where,

$$OA = r_{HPSTC}\cdot\cos\theta_{HPSTC}$$

$$OC = r_b\cos\theta_{Fn}$$

$$AB = r_{HPSTC}\cdot\sin\theta_{HPSTC}\cdot\tan\alpha_{Fen}$$

$$\theta_{HPSTC} = \frac{\pi}{2.z} + \tan\alpha - \alpha - \left(\tan\left(\cos^{-1}\left(\frac{r_p}{r_{HPSTC}}.\cos\alpha\right)\right) - \left(\cos^{-1}\left(\frac{r_p}{r_{HPSTC}}.\cos\alpha\right)\right)\right)$$

$$\theta_{Fn} = \frac{\pi}{2.z} + \tan\alpha - \alpha - \left(\tan\left(\cos^{-1}\left(\frac{r_p}{r_b}.\cos\alpha\right)\right) - \left(\cos^{-1}\left(\frac{r_p}{r_b}.\cos\alpha\right)\right)\right)$$

b) Bending moment arm h_{Fe} for asymmetrical gear tooth

The bending moment arm h_{Fe} for asymmetrical gear tooth is:

$$h_{Fe} = OA - (OC + AB) \tag{3.26}$$

Where,

$$OA = r_{HPSTC} \cdot \cos\theta_{HPSTC}$$

$$OC = r_{bc} \cos\theta_{Fnd}$$

$$AB = r_{HPSTC} \cdot \sin\theta_{HPSTC} \cdot \tan\alpha_{Fen}$$

$$\theta_{HPSTC} = \frac{\pi}{2.z} + \tan\alpha_d - \alpha_d - \left(\tan\left(\cos^{-1}\left(\frac{r_p}{r_{HPSTC}}.\cos\alpha_d \right) \right) - \left(\cos^{-1}\left(\frac{r_p}{r_{HPSTC}}.\cos\alpha_d \right) \right) \right)$$

$$\theta_{Fnd} = \frac{\pi}{2.z} + \tan\alpha_d - \alpha_d - \left(\tan\left(\cos^{-1}\left(\frac{r_p}{r_{bc}}.\cos\alpha_d \right) \right) - \left(\cos^{-1}\left(\frac{r_p}{r_{bc}}.\cos\alpha_d \right) \right) \right)$$

c) Radius of HPSTC

HPSTC radius is maximum radius at which single tooth is in line contact [68, 95]. It is location of load. Konstandinos G. Raptis et al. shows how to calculate highest point of single tooth contact [68, 95].

$$r_{HPSTC} = \sqrt{r_t^2 + (\varepsilon - 1)\cdot t_g \cdot \left((\varepsilon - 1)\cdot t_g - 2 \cdot \sqrt{r_t^2 - r_b^2} \right)} \tag{3.27}$$

Where,

$$t_g = \pi \cdot m \cdot \cos\alpha,$$

$$\varepsilon = \frac{\sqrt{r_{tp}^2 - r_{bp}^2} + \sqrt{r_{tg}^2 - r_{bg}^2} - C \cdot \sin\alpha}{p \cdot \cos\alpha} \tag{3.28}$$

CHAPTER – 4

STRESS CALCULATION AS PER ISO

This Chapter presents standard bending stress equation as per BS ISO 6336 part 3. Based on standard bending stress equation and developed equations of "bending stress equation parameters" an objective function has been created to minimize bending stress of tooth at critical section.

The maximum stress at the tooth root (in the direction of the tooth height), which may not exceed the permissible bending stress for the material, is the basis for rating the bending strength of gear teeth. The stress occurs in the "tension fillets" of the working tooth flanks. If load-induced cracks are formed, the first of these often appears in the fillets. When the tooth loading is unidirectional and the teeth are of conventional shape, these cracks seldom propagate to failure. Crack propagation ending in failure is most likely to stem from cracks initiated in tension fillets.

When gear rims are thin and tooth spaces adjacent to the root surface narrow (conditions which can particularly apply to some internal gears), initial cracks commonly occur in the fillet. Since, in such circumstances, gear rims themselves can suffer fatigue breakage, special studies are necessary.

Several methods for calculating the critical tooth root stress and evaluating some of the relevant factors have been approved [8].

4.1 Bending Stress as per BS ISO 6336 part 3

Nominal tooth root stress (Method B) as per BS International Standards Organization (ISO) 6336 part 3[8] given by:

Nominal tooth root stress σ

$$\sigma_{F0} = \frac{F_t}{b \cdot m_n} Y_s \cdot Y_F \cdot Y_\beta \qquad \text{(When load acts at HPSTC)} \qquad (4.1)$$

Local tooth root stress σ

$$\sigma_F = \sigma_{F0} \cdot K_A \cdot K_v \cdot K_{F\alpha} \cdot K_{F\beta} \qquad \text{(When load acts at HPSTC)} \tag{4.2}$$

Tooth form factor (Y_F): This factor considers influence of shape of tooth at the tooth-root stress. This shape is defined in computational procedure by the parameters of the critical section.

$$Y_F = \frac{6 \cdot (h_{Fe}/m_n)\cos\alpha_{Fen}}{(S_{Fn}/m_n)^2 \cos\alpha_n} \tag{4.3}$$

Helix angle factor (Y_B): It is applicable for helical gear**.**

$$Y_\beta = 1 - \varepsilon_\beta \frac{\beta}{120} \tag{4.4}$$

Stress correction factor (Y_S): This factor is considered for stress concentration at tooth root.

$$Y_S = (1.2 + 0.13L)q_s^a \tag{4.5}$$

$$L = S_{Fn}/h_{Fe} \tag{4.6}$$

$$q_s = S_{Fn}/(2\rho_F) \tag{4.7}$$

$$a = [1.21 + 2.3/L]^{-1} \tag{4.8}$$

Application factor (K_A): It is a factor for acting loads on tooth compare to the nominal load.

Dynamic factor (K_V): It is a factor which considered caused by vibrations of pinion and gear as internal dynamic loads.

Face load factor ($K_{F\beta}$): It is a factor which considered due to non-uniform distribution of load along contact line.

Transverse load factor ($K_{F\alpha}$): It is a factor which considered due to non-uniform distribution of load along path of contact.

It is observed that nominal bending stress at critical section of tooth depends on 'bending stress equation parameters' like:

S_{Fn} Tooth thickness at critical section

α_{Fen} Load angle

ρ_F Fillet Radius at the critical point

h_{Fe} Bending moment arm

4.2 Objective functions

The objective function is a mathematical term that describes how different variables contribute to a certain value that is being sought to be optimized.

From equation of banding stress, It is observed that nominal bending stress at the root of the tooth depends on tooth thickness at the root of the tooth (S_{Fn}), load angle (α_{Fen}), root fillet (ρ_F) and height of bending moment arm (h_{Fe}) are affects bending stress. These parameters are depends on drive side pressure angle for asymmetric spur gear. Higher pressure angle on drive side desirable for low bending stress and it is constrained by tip thickness and contact ratio. Higher drive side pressure angle as compare to coast side pressure angle gives low bending stress result [45-57].

Objective function to minimize bending stress at critical section with considering of constraint:

$$f(\sigma_{F0})_{min} = \begin{cases} \dfrac{F_t}{b \cdot m_n} Y_s \cdot Y_F \cdot Y_\beta \\ \alpha_d > \alpha_c \\ \varepsilon \geq 1.1 \\ S_t \geq 0.25m \end{cases} \tag{5.9}$$

$$Y_F = \frac{6 \cdot (h_{Fe} / m_n) \cos\alpha_{Fen}}{(S_{Fn} / m_n)^2 \cos\alpha_n}$$

$$\alpha_{Fen} = \tan\left(\cos^{-1}\left(\frac{r_p}{r} \cdot \cos\alpha \right)\right) - \frac{\pi}{2 \cdot z} - \tan\alpha + \alpha$$

$$S_{Fn} = r_{bc}.\sin\theta_{Fnd} + r_{bc}.\sin\theta_{Fnc}$$

Where,

$$\theta_{Fnd} = \frac{\pi}{2.z} + \tan\alpha_d - \alpha_d - \left(\tan\left(\cos^{-1}\left(\frac{r_p}{r_{bc}}.\cos\alpha_d \right)\right) - \left(\cos^{-1}\left(\frac{r_p}{r_{bc}}.\cos\alpha_d \right)\right)\right)$$

$$\theta_{Fnc} = \frac{\pi}{2.z} + \tan\alpha_c - \alpha_c - \left(\tan\left(\cos^{-1}\left(\frac{r_p}{r_{bc}}.\cos\alpha_c \right) \right) - \left(\cos^{-1}\left(\frac{r_p}{r_{bc}}.\cos\alpha_c \right) \right) \right)$$

$$h_{Fe} = r_{HPSTC} \cdot \cos\theta_{HPSTC} - \left(r_{bc}\cos\theta_{Fnd} + r_{HPSTC} \cdot \sin\theta_{HPSTC} \cdot \tan\alpha_{Fen} \right)$$

Where,

$$\theta_{HPSTC} = \frac{\pi}{2.z} + \tan\alpha_d - \alpha_d - \left(\tan\left(\cos^{-1}\left(\frac{r_p}{r_{HPSTC}}.\cos\alpha_d \right) \right) - \left(\cos^{-1}\left(\frac{r_p}{r_{HPSTC}}.\cos\alpha_d \right) \right) \right)$$

$$\theta_{Fnd} = \frac{\pi}{2.z} + \tan\alpha_d - \alpha_d - \left(\tan\left(\cos^{-1}\left(\frac{r_p}{r_{bc}}.\cos\alpha_d \right) \right) - \left(\cos^{-1}\left(\frac{r_p}{r_{bc}}.\cos\alpha_d \right) \right) \right)$$

$$Y_\beta = 1 - \varepsilon_\beta \frac{\beta}{120}$$

$$Y_S = (1.2 + 0.13L)q_s^a$$

$$L = S_{Fn} / h_{Fe},\ q_s = S_{Fn} / (2\rho_F),\ a = [1.21 + 2.3/L]^{-1}$$

Main aim to develop an objective functions are given below:

- It is helpful to calculate nominal bending stress for given input data of gear.
- It is help to predict or select input parameter of gear for desire output.
- It helps to calculate % reduction in bending stress for different pressure angle of drive side.
- It helps us to found effect of fillet radius to predict % change in bending stress

CHAPTER – 5

PARAMETRIC ANALYSIS OF ASYMMETRIC SPUR GEAR TOOTH

The current focus of gear design in an industry is on failure occurs at critical section/root of the tooth [1]. One major cause of gear failure is a fracture at the root of the gear tooth due to bending fatigue [1]. Failure at the root of the tooth can be reduced by optimizing the geometrical shape of standard symmetric gear tooth [1].In order to achieve this goal, it is necessary to increase the drive side pressure angle as compared to the coast side of a gear tooth. A past study shows that higher pressure angle on the drive side within constraint is desirable to reduce bending stress at the root [2]. Due to both profiles on the tooth are different, gear tooth becomes asymmetric gear tooth and known as an asymmetric tooth. A degree of asymmetry is denoted by an asymmetric factor (AF) and it is a ratio of pressure angle on the drive side to coast side. Higher pressure angle on drive side within constraint is desirable to reduce bending stress at root [2, 3] which improves load carrying capacity.

In asymmetric gear higher pressure angel on drive side as compare to coast side gives higher reduction in bending stress at critical section but value of higher pressure angel on drive side constrained by contact ratio and tip thickness of tooth. Modification in the drive side pressure angle will change involute profile of drive side of gear tooth which affects gear geometry. Strength of gear is affected by gear tooth geometry. Hence it is most important for improve strength. The parametric analysis helps to understand the effect of drive side pressure angle on tooth geometry of symmetric and asymmetric spur gear.

Parametric analysis helps to obtain optimize drive side pressure angle. In addition, it is also helpful to predict % reduction in bending stress without FEA, due to modified drive side pressure angle.

Selection of parameters

Pressure angle: 20^0 pressure angle is standards pressure angle and most popular [1, 2].

Minimum number of teeth on pinion: The minimum number of teeth on a pinion to avoid interference and undercutting for 20^0 pressure angle is 17.09 (eq. 1.1) [1, 2].

For illustration the parameters presented in table 5.1 [96] with above consideration. With help of developed equations presented in chapter 4 and as per gear parameters presented in table 5.1, a code has been developed to calculate various parameters. Developed codes are available in APENDIX-I. A graph has been developed in terms of parametric analysis.

TABLE 5.1: Design parameters [96]

Design Parameters	**Value**	**Unit**
Pressure angle, Coast side	20^0	Degree
Number of teeth on pinion	25	-
Number of teeth on pinion	25	-
Module	4	mm
Power	18	KW
Rotation	1600	RPM

5.1 Effect of drive side pressure angle on contact ratio

Contact ratio is a very important parameter in gear design to transmit power. If the contact ratio is lower than 1.1 then loading period on a single tooth is an increase which is an undesirable condition for power transmission [1]. Equation 3.28, gives a contact ratio for a given drive pair. Contact ratio has been calculated with different pressure angle on the drive side for different speed ratio and values are presented in table 5.2. A graphical representation is shown in figure 5.1.

TABLE 5.2: Effect of drive side pressure angle on the contact ratio for different speed ratio

Pressure angle on drive side	Contact ratio				
	Speed ratio = 1.0	Speed ratio = 1.2	Speed ratio = 1.4	Speed ratio = 1.6	Speed ratio = 1.8
20^0	1.612	1.633	1.650	1.663	1.675
22^0	1.539	1.556	1.570	1.581	1.590
24^0	1.475	1.490	1.502	1.511	1.518
26^0	1.421	1.433	1.44	1.451	1.457
28^0	1.375	1.385	1.393	1.400	1.405
30^0	1.335	1.345	1.3510	1.357	1.361

32^0	1.303	1.311	1.317	1.321	1.325
34^0	1.277	1.283	1.289	1.293	1.296
36^0	1.256	1.262	1.266	1.270	1.273
38^0	**1.241**	1.246	1.250	1.253	1.255
40^0	1.231	1.236	1.239	1.242	1.244
42^0	1.227	1.231	1.233	1.236	1.238

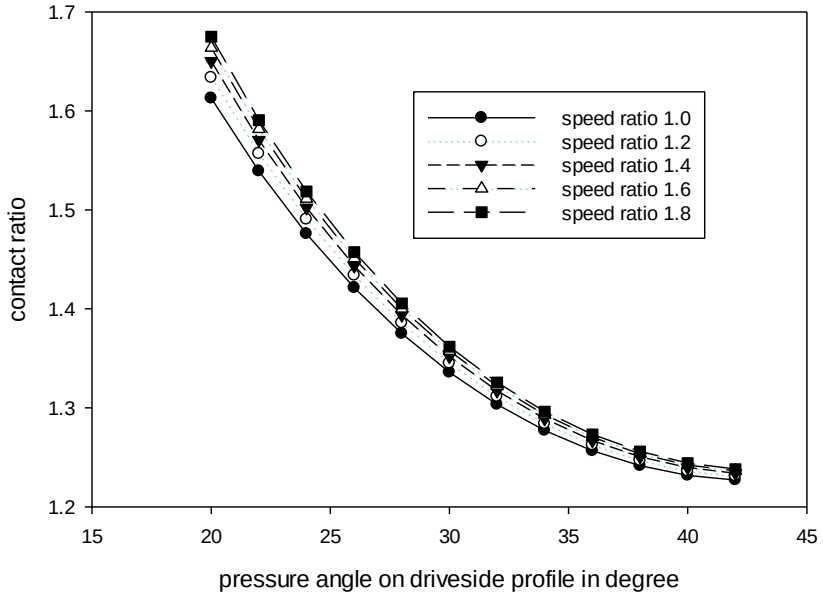

FIGURE 5.1: Effect of drive side pressure angle on the contact ratio for the different speed ratio

As shown in figure 5.2, the pressure angle on the drive side increases contact ratio decreases for different speed ratio (speed ratio is the ratio of the number of teeth on the gear to pinion). An asymmetric factor is the ratio of pressure angle on the drive side to pressure angle on the coast side (AF = $\alpha_{d\,/\,}\alpha_c$). AF is proportional to α_d , increase in α_d also increases AF.

Contact ratio has been calculated with a different number of teeth on pinion for a different asymmetric factor with speed ratio = 1 and values are presented in table 5.3 and it is presented in form of graph as shown in figure 5.2.

TABLE 5.3: Effect of number of teeth (Z_p) on contact ratio of drive side for different AF

Number of teeth on pinion	Contact ratio		
	SR = 1.0	SR = 1.0	SR = 1.0
	AF = 1.0	AF = 1.5	AF = 2.0
25	1.612	1.335	1.231

35	1.687	1.367	1.247
50	1.756	1.394	1.260
65	1.798	1.410	1.267
80	1.827	1.421	1.272
100	1.854	1.430	1.276

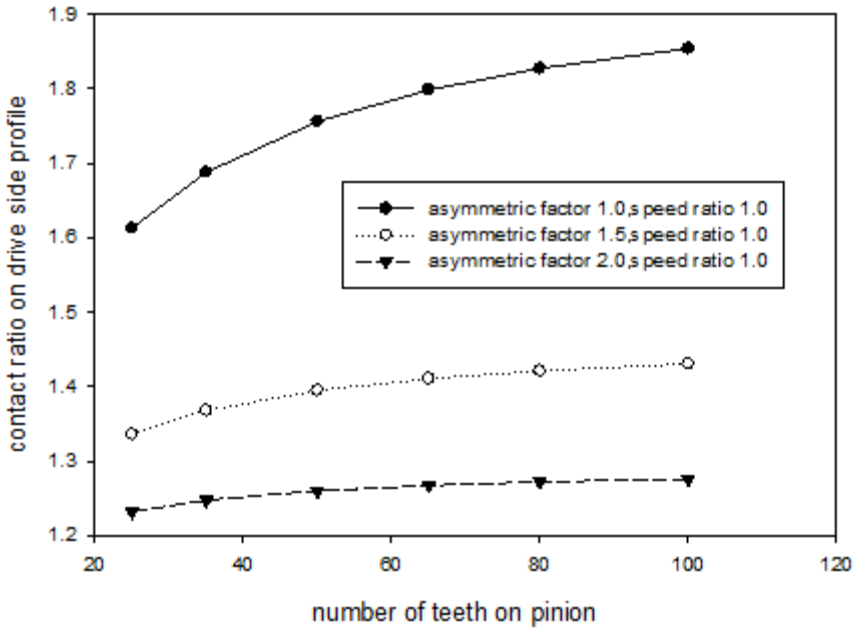

FIGURE 5.2: Effect of number of teeth (Z_p) on contact ratio of drive side for different AF (asymmetric factor)

As shown in figure 5.2 for different value of AF, the number of teeth (Zp) increases contact ratio increases. But for greater AF, contact ratio decreases.

Contact ratio has been calculated with a different number of teeth on pinion for different module and values are presented in table 5.4 and it is presented in form of graph as shown in figure 5.3.

TABLE 5.4: Effect of module on contact ratio for various numbers of teeth on pinion

Number of teeth on pinion	Contact ratio				
	Module = 04	Module = 05	Module = 06	Module = 10	Module = 15
25	1.612	1.612	1.612	1.612	1.612
35	1.687	1.687	1.687	1.687	1.687
50	1.756	1.756	1.756	1.756	1.756

65	1.798	1.798	1.798	1.798	1.798
80	1.827	1.827	1.827	1.827	1.827
100	1.854	1.8541	1.854	1.854	1.8541

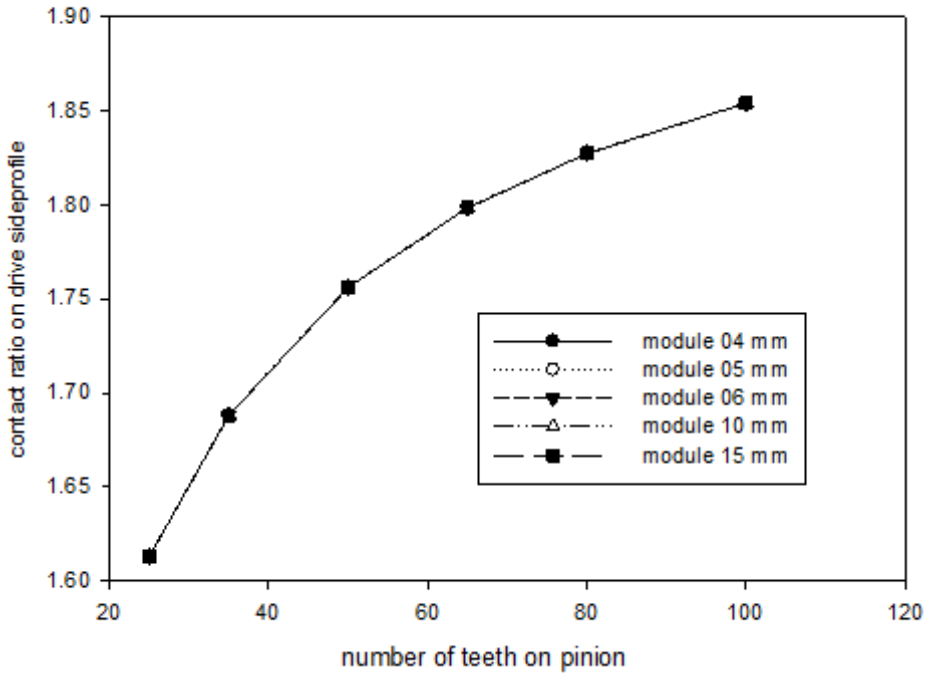

FIGURE 5.3 Effect of a module on contact ratio for various number of teeth on the pinion

As shown in figure 5.3, an effect of the module on the contact ratio can be checked by changing various modules. It shows that change of module has no effect on contact ratio. It remains the same for different module and number of teeth.

5.2 Effect of drive side pressure angle on HSPTC

HPSTC radius is a maximum radius at which a single tooth is in line contact. This is a critical location to apply a load in the design of a gear tooth. Equation 3.27 [68, 95] gives HPSTC radius for gear tooth. HPSTC radius has been calculated with different pressure angle on the drive side for different module and values are presented in table 5.5 and it is presented in form of graph as shown in figure 5.4.

TABLE 5.5: Effect of drive side pressure angle on HPSTC radius for different module

Pressure angle on drive side	HPSTC radius in mm		
	Module = 04	Module = 05	Module = 06
20^0	50.533	63.931	75.800
22^0	50.801	64.228	76.201

24^0	51.060	64.507	76.590
26^0	51.305	64.767	76.958
28^0	51.531	65.004	77.297
30^0	51.735	65.215	77.603
32^0	51.915	65.401	77.873
34^0	52.070	65.558	78.105
36^0	52.196	65.688	78.295
38^0	52.295	65.788	78.443
40^0	52.365	65.859	78.547
42^0	52.441	65.937	78.662
44^0	52.524	66.020	78.786
46^0	52.611	66.109	78.917
48^0	52.703	66.201	79.055
50^0	52.798	66.297	79.198
52^0	52.896	66.395	79.344

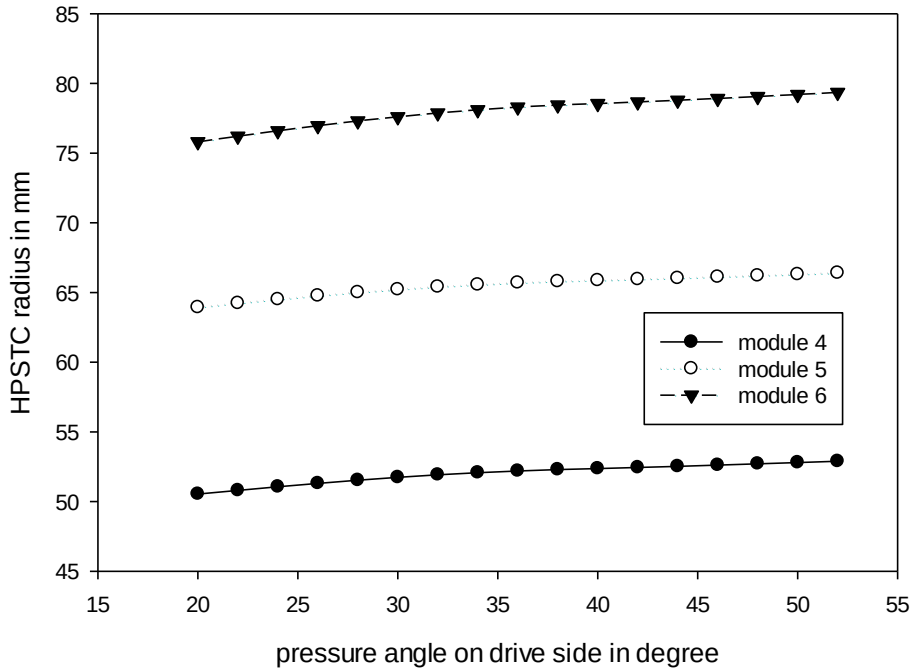

FIGURE 5.4 Effect of drive side pressure angle on HPSTC radius for different module

As shown in figure 5.4, for a different module, as a pressure angle on drive side increases, a HPSTC radius increases. But for greater module HPSTC radius also get increases.

HPSTC radius has been calculated with a different number of teeth on pinion for different module and values are presented in table 5.6 and it is presented in form of graph as shown in figure 5.5.

TABLE 5.6: Effect of the number of teeth on HPSTC radius for different module

Number of teeth on pinion	HPSTC radius in mm		
	Module = 04	Module = 05	Module = 06
25	50.533	49.831	49.200
35	70.689	69.980	69.322
50	100.827	100.118	99.445
65	130.911	130.204	129.525
80	160.967	160.263	159.581
100	201.019	200.317	199.633

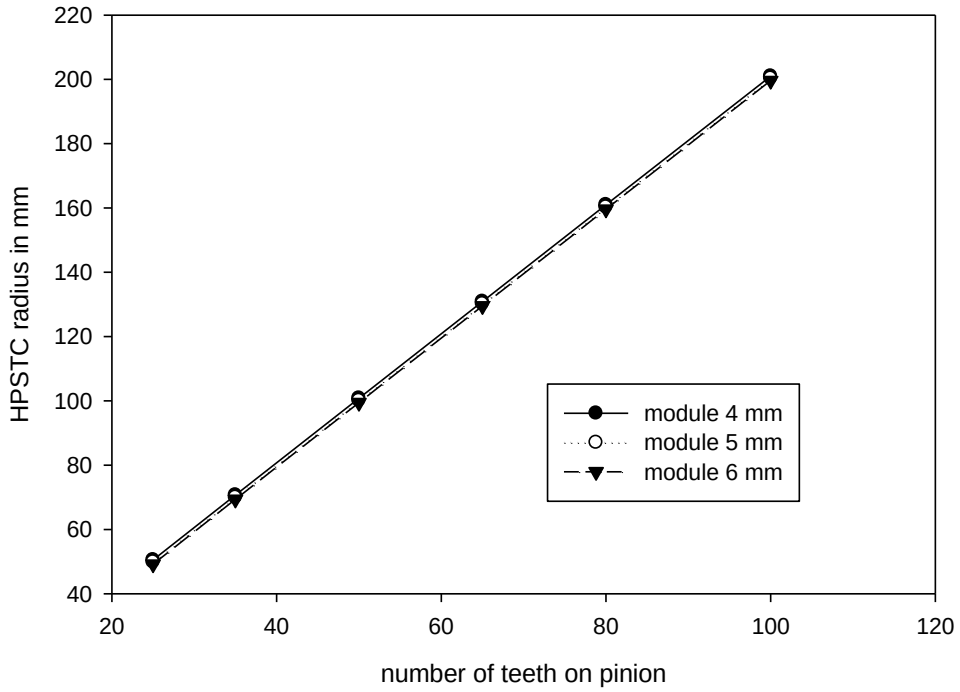

FIGURE 5.5: Effect of the number of teeth on HPSTC radius for different module

As shown in figure 5.5, as a number of teeth increase, a HPSTC radius increases for a different module.

5.3 Effect of drive side pressure angle on load angle

Load angle depends on the pressure angle of the gear tooth profile. Equation 3.24 gives a load angle on the gear tooth. Load angle has been calculated with different pressure angle on the drive side for different module and values are presented in table 5.7 and it is presented in form of graph as shown in figure 5.6.

TABLE 5.7: Effect of variation of drive side pressure angle on load angle

Pressure angle on drive side	Load angle in degree		
	Speed ratio = 1.0	Speed ratio = 1.4	Speed ratio = 1.8
	Module = 04	Module = 04	Module = 04
20^0	18.234	18.234	18.234
22^0	20.929	20.929	20.929
24^0	23.517	23.517	23.517
26^0	26.015	26.015	26.015
28^0	28.435	28.435	28.435
30^0	30.7866	30.7866	30.7866
32^0	33.077	33.077	33.077
34^0	35.314	35.314	35.314
36^0	37.501	37.501	37.501
38^0	39.642	39.642	39.642
40^0	41.741	41.741	41.741
42^0	43.876	43.876	43.876
44^0	46.049	46.049	46.049
46^0	48.259	48.259	48.259
48^0	50.508	50.508	50.508
50^0	52.798	52.798	52.798
52^0	55.132	55.132	55.132

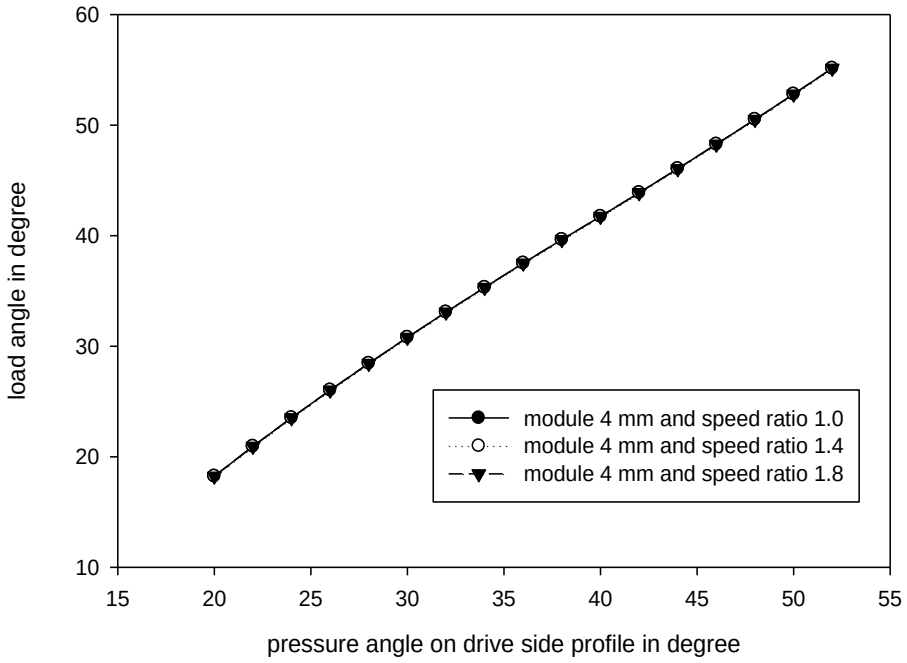

FIGURE 5.6: Effect of variation of drive side pressure angle on load angle

As shown in figure 5.6, as the drive side pressure angle increases, a load angle increases.

5.4 Effect of drive side pressure angle on tip thickness

Tip thickness is a very important parameter in gear design to transmit power. If tip thickness is lower than *0.25m* then tip becomes too sharp which is undesirable for power transmission [1]. Equation 3.20 and 3.21, gives tip thickness for gear tooth. Tip thickness has been calculated with different pressure angle on the drive side for different speed ratio and module. Values are presented in table 5.8 and it is presented in form of graph as shown in figure 5.7.

TABLE 5.8: Effect of drive side pressure angle on tip thickness for different module and speed ratio

Pressure angle on drive side	Tip thickness of pinion in mm								
	SR = 1.0	S R = 1.4	S R = 1.8	S R = 1.0	S R = 1.4	S R = 1.8	S R = 1.0	S R = 1.4	S R = 1.8
	Module = 04			Module = 05			Module = 06		
20^0	2.876	2.876	2.876	3.596	3.596	3.596	4.315	4.315	4.315
22^0	2.733	2.733	2.733	3.417	3.417	3.417	4.100	4.100	4.100
24^0	2.582	2.582	2.582	3.228	3.228	3.228	3.874	3.874	3.874
26^0	2.423	2.423	2.423	3.028	3.028	3.028	3.634	3.634	3.634

28^0	2.254	2.254	2.254	2.818	2.818	2.818	3.382	3.382	3.382
30^0	2.077	2.077	2.077	2.596	2.596	2.596	3.115	3.115	3.115
32^0	1.889	1.889	1.889	2.362	2.362	2.362	2.834	2.834	2.834
34^0	1.691	1.691	1.691	2.114	2.114	2.114	2.537	2.537	2.537
36^0	1.481	1.481	1.481	1.852	1.852	1.852	2.222	2.222	2.222
38^0	1.259	1.259	1.259	1.574	1.574	1.574	1.889	1.889	1.889
40^0	**1.022**	1.022	1.022	1.278	1.278	1.278	1.533	1.533	1.533
42^0	0.769	0.769	0.769	0.962	0.962	0.962	1.154	1.154	1.154
44^0	0.499	0.499	0.499	0.624	0.624	0.624	0.749	0.749	0.749
46^0	0.208	0.208	0.208	0.260	0.260	0.260	0.312	0.312	0.312

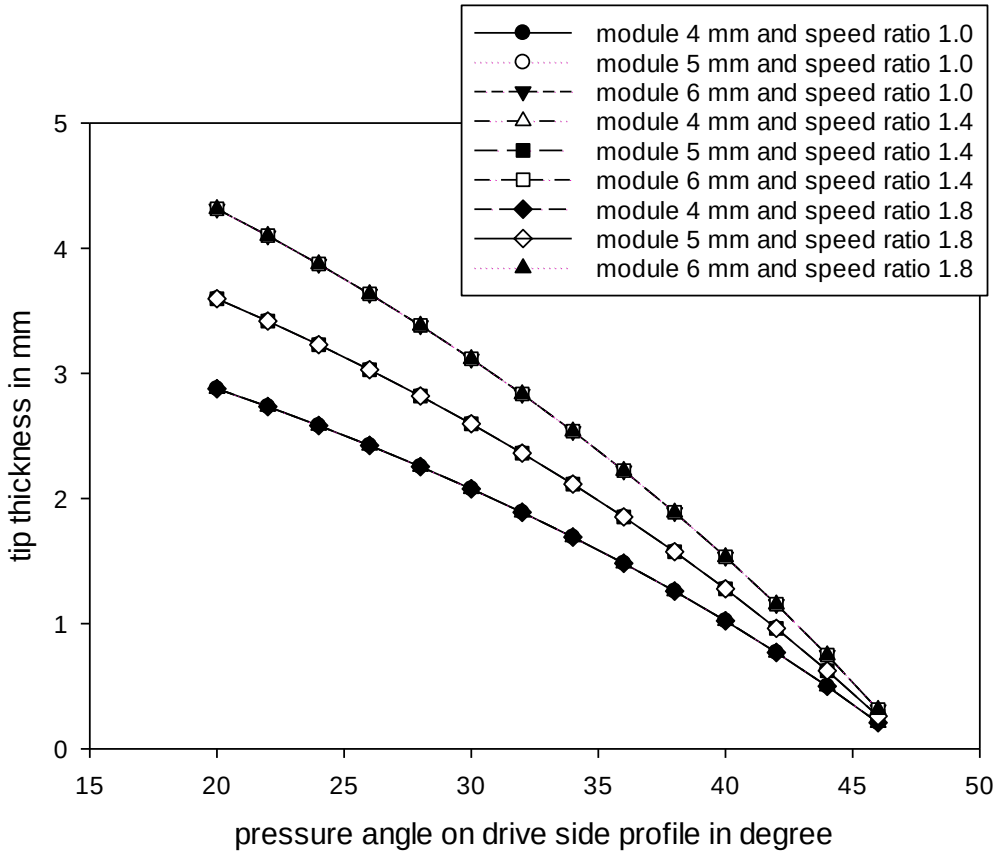

FIGURE 5.7: Effect of drive side pressure angle on tip thickness for different module and speed ratio

As shown in figure 5.7, for a different module, as a pressure angle on drive side increases, a tip thickness of tooth decreases.

Tip thickness has been calculated with a different number of teeth on pinion for a different module and asymmetric factor for speed ratio = 1.0. Values are presented in table 5.9 and it is presented in form of graph as shown in figure 5.8.

TABLE 5.9: Effect of the number of teeth on tip thickness for a different module and AF

Number of teeth on pinion	Tip thickness in mm								
	Module = 04 & Speed ratio=1.0			Module = 05 & Speed ratio=1.0			Module = 06 & Speed ratio=1.0		
	A F = 1.0	A F = 1.5	A F = 2.0	A F = 1.0	A F = 1.5	A F = 2.0	A F = 1.0	A F = 1.5	A F = 2.0
25	2.876	2.077	1.022	3.596	2.596	1.278	4.315	3.115	1.533
35	2.999	2.190	1.140	3.749	2.738	1.425	4.499	3.286	1.711
50	3.099	2.281	1.233	3.874	2.851	1.541	4.649	3.422	1.850
65	3.156	2.332	1.285	3.946	2.915	1.606	4.735	3.498	1.928
80	3.193	2.365	1.318	3.992	2.956	1.648	4.790	3.547	1.978
100	3.227	2.394	1.347	4.033	2.992	1.684	4.840	3.591	2.021

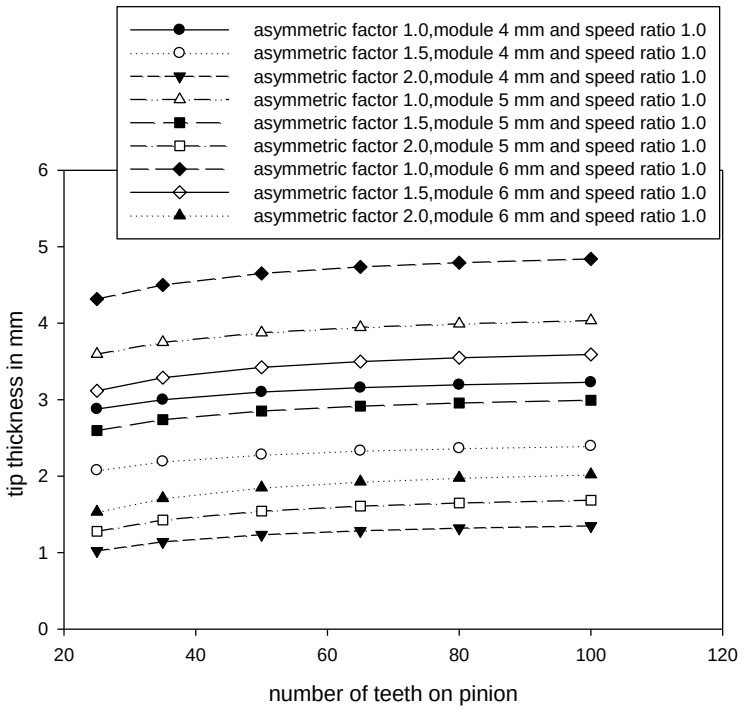

FIGURE 5.8: Effect of number of teeth on tip thickness for different module and AF (asymmetric factor)

As shown in figure 5.8, for different value of AF, as number of teeth increased, tip thickness also gets increased. But for greater AF, tip thickness decreases.

5.5 Effect of drive side pressure angle on thickness of tooth at pitch circle

Equation 5.1 gives a thickness of tooth at the pitch circle of a gear tooth. A thickness of tooth at pitch circle has been calculated with different pressure angle on the drive side for a different module. Values are presented in table 5.10 and it is presented in foam of graph as shown in figure 5.9.

$$S_p = r_p \cdot \theta_{pd} + r_p \cdot \theta_{pc} \tag{5.1}$$

$$\theta_{pd} = \frac{\pi}{2.z}$$

$$\theta_{pc} = \frac{\pi}{2.z}$$

TABLE 5.10: Effect of drive side pressure angle on tooth thickness at pitch circle for different module

Pressure angle on drive side	Thickness of tooth at pitch circle of pinion in mm								
	Module = 04			Module = 05			Module = 06		
	S R = 1.0	S R = 1.4	S R = 1.8	S R = 1.0	S R = 1.4	S R = 1.8	S R = 1.0	S R = 1.4	S R = 1.8
20^0	6.275	6.275	6.275	7.844	7.844	7.844	9.413	9.413	9.413
22^0	6.275	6.275	6.275	7.844	7.844	7.844	9.413	9.413	9.413
24^0	6.275	6.275	6.275	7.844	7.844	7.844	9.413	9.413	9.413
26^0	6.275	6.275	6.275	7.844	7.844	7.844	9.413	9.413	9.413
28^0	6.275	6.275	6.275	7.844	7.844	7.844	9.413	9.413	9.413
30^0	6.275	6.275	6.275	7.844	7.844	7.844	9.413	9.413	9.413
32^0	6.275	6.275	6.275	7.844	7.844	7.844	9.413	9.413	9.413
34^0	6.275	6.275	6.275	7.844	7.844	7.844	9.413	9.413	9.413
36^0	6.275	6.275	6.275	7.844	7.844	7.844	9.413	9.413	9.413
38^0	6.275	6.275	6.275	7.844	7.844	7.844	9.413	9.413	9.413
40^0	6.275	6.275	6.275	7.844	7.844	7.844	9.413	9.413	9.413
42^0	6.275	6.275	6.275	7.844	7.844	7.844	9.413	9.413	9.413

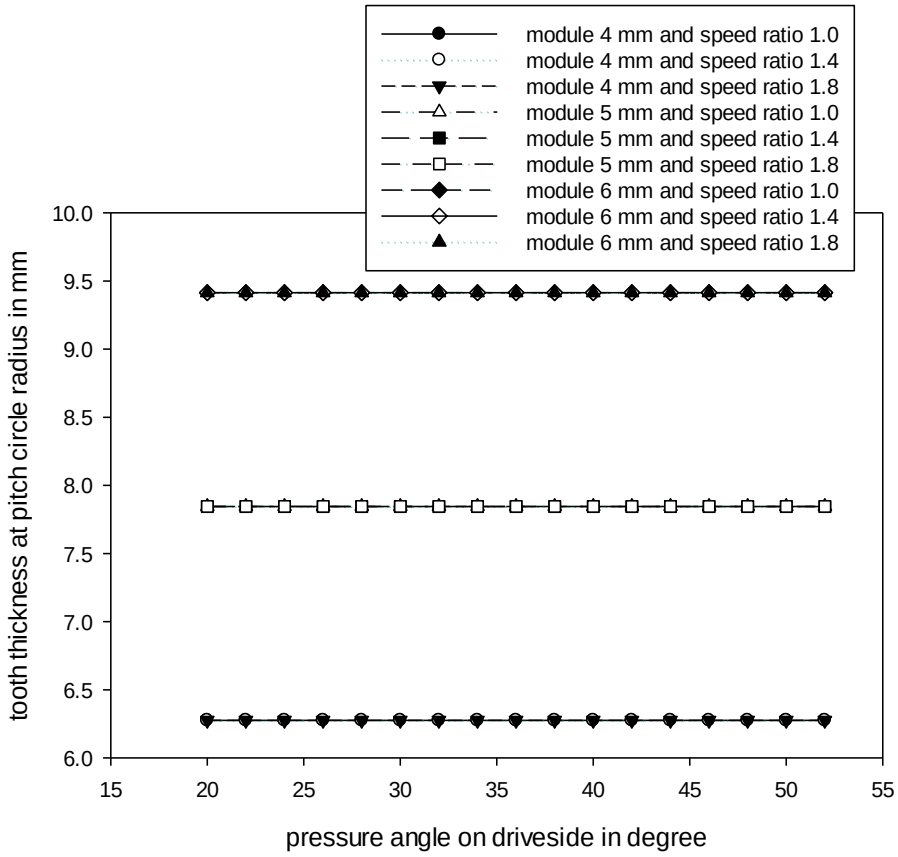

FIGURE 5.9 Effect of drive side pressure angle on tooth thickness at pitch circle for different module (m=4, 5, 6)

As shown in figure 5.9, for the same module, as pressure angle on drive side increases, tooth thickness at pitch circle remain the same. But, with an increase in a module, tooth thickness at pitch circle increases and remain the same for all value of pressure angle on the drive side.

A thickness of tooth at pitch circle has been calculated with a different number of teeth on pinion for a different module and asymmetric factor for speed ratio = 1.0. Values are presented in table 5.11 and it is presented in form of graph as shown in figure 5.10.

TABLE 5.11: Effect of the number of teeth on tooth thickness at pitch circle with a different module and AF

Number of teeth on pinion	Thickness of tooth at pitch circle in mm								
	Module = 04 & Speed ratio=1.0			Module = 05 & Speed ratio=1.0			Module = 06 & Speed ratio=1.0		
	A F = 1.0	A F = 1.5	A F = 2.0	A F = 1.0	A F = 1.5	A F = 2.0	A F = 1.0	A F = 1.5	A F = 2.0
25	6.275	6.275	6.275	7.844	7.844	7.844	9.413	9.413	9.413
35	6.277	6.277	6.277	7.847	7.847	7.847	9.416	9.416	9.416

50	6.278	6.278	6.278	7.848	7.848	7.848	9.418	9.418	9.418
65	6.279	6.279	6.279	7.849	7.849	7.849	9.419	9.419	9.419
80	6.279	6.279	6.279	7.849	7.849	7.849	9.419	9.419	9.419
100	6.279	6.279	6.279	7.844	7.844	7.844	9.419	9.419	9.419

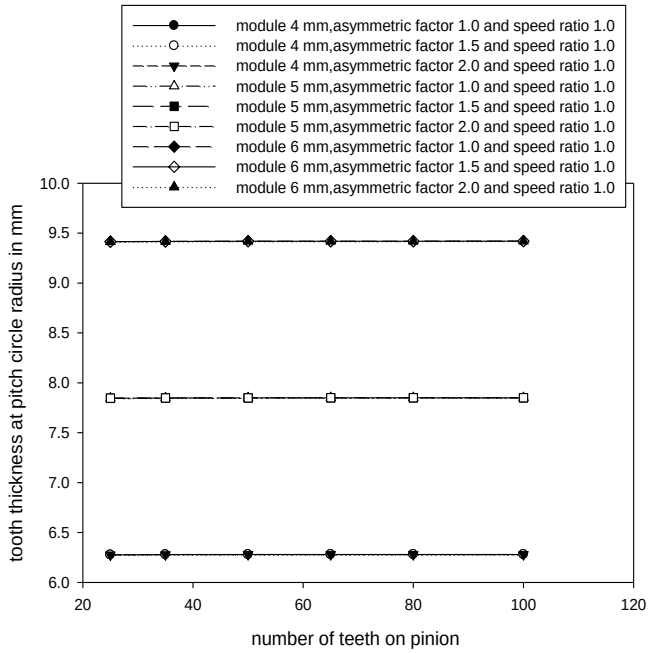

FIGURE 5.10: Effect of number of teeth on tooth thickness at pitch circle with different module and AF (asymmetric factor)

As shown in figure 5.10, for the same module and increasing asymmetric factor with a varying number of teeth, tooth thickness at pitch circle remains the same.

5.6 Effect of drive side pressure angle on tooth thickness at the critical section

Equation 3.22 and 3.23, gives tooth thickness at the critical section of a gear tooth. Tooth thickness at critical section has been calculated with different pressure angle on the drive side for different module and speed ratio. Values are presented in table 5.12 and it is presented in form of graph as shown in figure 5.11.

TABLE 5.12: Effect of drive side pressure angle on critical section thickness for different module and speed ratio

Pressure angle on drive side	Tooth thickness at the critical section of pinion in mm								
	SR = 1.0	S R = 1.4	S R = 1.8	S R = 1.0	S R = 1.4	S R = 1.8	S R = 1.0	S R = 1.4	S R = 1.8
	Module = 04			Module = 05			Module = 06		
20^0	7.292	7.292	7.292	9.115	9.115	9.115	10.939	10.939	10.939
22^0	7.464	7.464	7.464	9.331	9.331	9.331	11.197	11.197	11.197
24^0	7.617	7.617	7.617	9.521	9.521	9.521	11.425	11.425	11.425
26^0	7.763	7.763	7.763	9.704	9.704	9.704	11.645	11.645	11.645
28^0	7.908	7.908	7.908	9.885	9.885	9.885	11.863	11.863	11.863
30^0	8.054	8.054	8.054	10.068	10.068	10.068	12.082	12.082	12.082
32^0	8.203	8.203	8.203	10.253	10.253	10.253	12.304	12.304	12.304
34^0	8.355	8.355	8.355	10.444	10.444	10.444	12.533	12.533	12.533
36^0	8.513	8.513	8.513	10.641	10.641	10.641	12.769	12.769	12.769
38^0	8.676	8.676	8.676	10.846	10.846	10.846	13.015	13.015	13.015
40^0	8.848	8.848	8.848	11.060	11.060	11.060	13.272	13.272	13.272
42^0	9.028	9.028	9.028	11.285	11.285	11.285	13.542	13.542	13.542
44^0	9.219	9.219	9.219	11.524	11.524	11.524	13.828	13.828	13.828
46^0	9.422	9.422	9.422	11.777	11.777	11.777	14.133	14.133	14.133
48^0	9.638	9.638	9.638	12.048	12.048	12.048	14.458	14.458	14.458
50^0	9.872	9.872	9.872	12.340	12.340	12.340	14.808	14.808	14.808
52^0	10.124	10.124	10.124	12.655	12.655	12.655	15.186	15.186	15.186

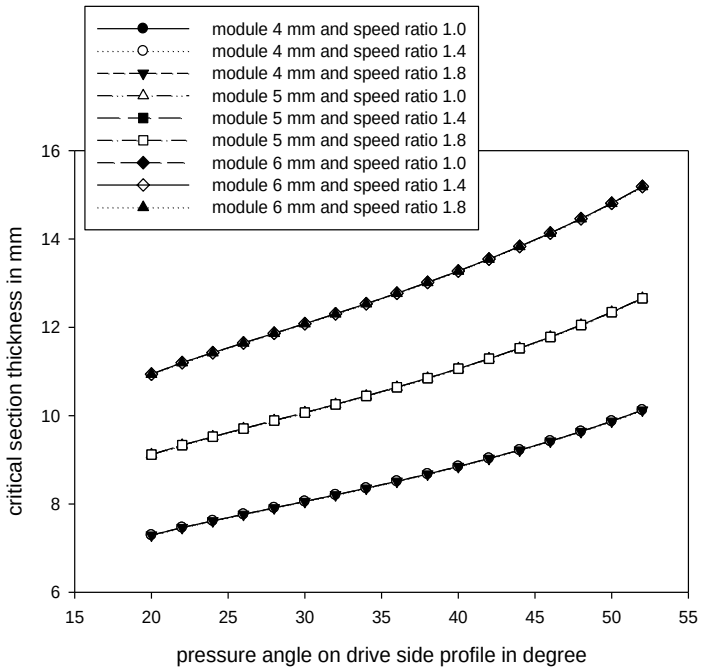

FIGURE 5.11 Effect of drive side pressure angle on critical section thickness for a different module and speed ratio

As shown in figure 5.11, for the same module and varying speed ratio, as pressure angle on drive side increases, critical section thickness increases. But, with an increase in a module, critical section thickness increases and it is further increased by increasing drive side pressure angle for various speed ratio.

Tooth thickness at critical section has been calculated with a different number of teeth on pinion for a different module and asymmetric factor for speed ratio = 1.0. Values are presented in table 5.13 and it is presented in form of graph as shown in figure 5.12.

TABLE 5.13: Effect of the number of teeth on critical section thickness with a different module and AF

Number of teeth on pinion	Tooth thickness at the critical section in mm								
	Module = 04 & Speed ratio=1.0			Module = 05 & Speed ratio=1.0			Module = 06 & Speed ratio=1.0		
	AF=1.0	AF=1.5	AF=2.0	AF=1.0	AF=1.5	AF=2.0	AF=1.0	AF=1.5	AF=2.0
25	7.292	8.054	8.848	9.115	10.068	11.060	10.939	12.082	13.272
35	7.910	9.009	10.154	9.818	11.153	12.544	11.866	13.514	15.231
50	8.695	10.222	11.814	10.869	12.778	14.767	13.043	15.333	17.721
65	9.535	11.521	13.591	11.918	14.401	17.577	14.302	17.281	20.387
80	10.374	12.819	15.368	12.968	16.024	19.210	15.561	19.229	23.052
100	11.493	14.550	17.7368	14.367	18.187	21.310	17.240	21.825	26.605

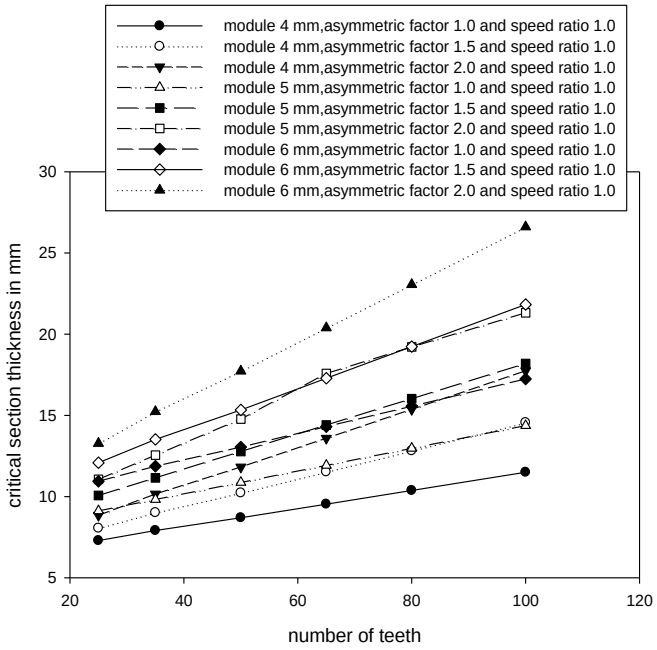

FIGURE 5.12 Effect of the number of teeth on critical section thickness with different module and AF (asymmetric factor)

As shown in figure 5.12, for an increasing module and asymmetric factor with an increasing number of teeth, critical section thickness increases.

5.7 Effect of drive side pressure angle on bending moment arm height

Equation 3.25 and 3.26, gives the bending moment arm height of the gear tooth. Bending moment arm height has been calculated with different pressure angle on the drive side for different speed ratio and module = 4. Values are presented in table 5.14 and it is presented in form of graph as shown in figure 5.13.

TABLE 5.14: Effect of the drive side pressure angle on bending moment arm height

Pressure angle on drive side	Bending moment arm height on pinion in mm		
	Speed ratio = 1.0	Speed ratio = 1.4	Speed ratio = 1.8
	Module = 04	Module = 04	Module = 04
20^0	2.623	2.623	2.623
22^0	2.802	2.802	2.802
24^0	2.995	2.995	2.995
26^0	3.199	3.199	3.199
28^0	3.410	3.410	3.410
30^0	3.623	3.623	3.623
32^0	3.836	3.836	3.836

34^0	4.047	4.047	4.047
36^0	4.251	4.251	4.251
38^0	4.448	4.448	4.448
40^0	4.632	4.632	4.632
42^0	4.867	4.867	4.867
44^0	5.164	5.164	5.164
46^0	5.536	5.536	5.536
48^0	5.999	5.999	5.999
50^0	6.578	6.578	6.578
52^0	7.302	7.302	7.302

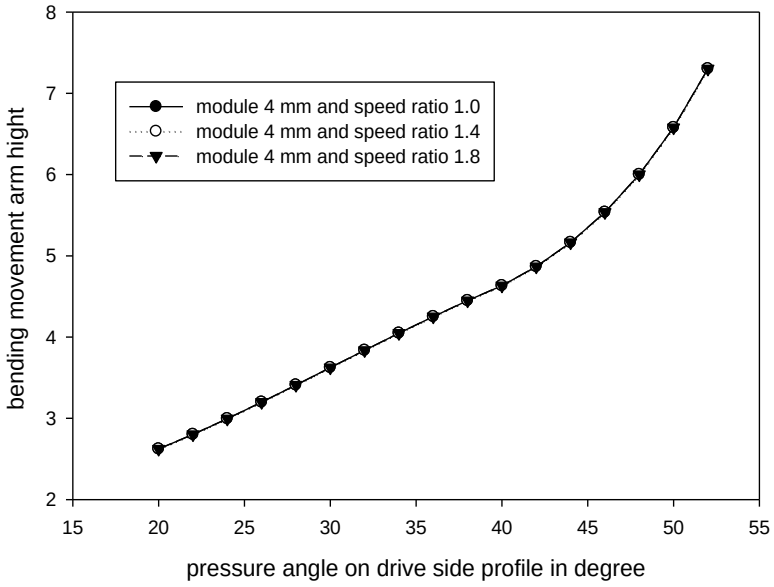

FIGURE 5.13: Effect of the drive side pressure angle on bending moment arm height

As shown in fig. 5.13, as pressure angle on drive side increases, a bending moment arm height increases for different speed ratio.

Bending moment arm height has been calculated with a different number of teeth on pinion for different speed ratio and asymmetric factor for module = 4. Values are presented in table 5.15 and it is presented in form of graph as shown in figure 5.14.

TABLE 5.15: Effect of the number of teeth on bending moment arm height with different module

Number of teeth on pinion	Bending moment arm height in mm								
	Module = 04 & Speed ratio=1.0			Module = 04 & Speed ratio=1.4			Module = 04 & Speed ratio=1.8		
	AF=1.0	AF=1.5	AF=2.0	AF=1.0	AF=1.5	AF=2.0	AF=1.0	AF=1.5	AF=2.0
25	2.623	3.623	4.632	2.623	3.623	4.632	2.623	3.623	4.632
35	4.087	5.056	6.029	4.087	5.056	6.029	4.087	5.056	6.029
50	5.895	6.827	7.779	5.895	6.827	7.779	5.895	6.827	7.779
65	7.789	8.694	9.640	7.789	8.694	9.640	7.789	8.694	9.640
80	9.658	10.545	11.493	9.658	10.545	11.493	9.658	10.545	11.493
100	12.128	13.000	13.958	12.128	13.000	13.958	12.128	13.000	13.958

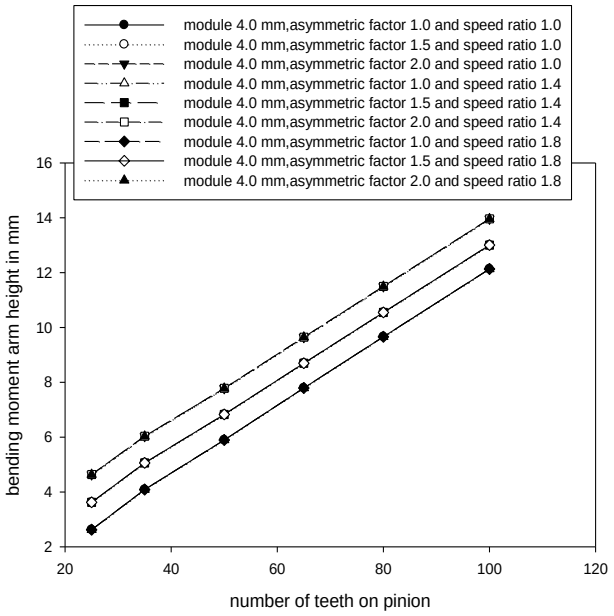

FIGURE 5.14: Effect of the number of teeth on bending moment arm height with a different module

As shown in figure 5.14, for the same asymmetric factor with an increasing number of teeth, a bending moment arm height increases. But, with an increase in asymmetric factor, a bending moment arm height also increases.

5.8 Effect of drive side pressure angle on nominal bending stress

Equation 4.1, gives nominal bending stress of asymmetric tooth. Nominal bending stress has been calculated with different pressure angle on the drive side for different fillet radius. Values are presented in table 5.16 and it is presented in form of graph as shown in figure 5.15.

TABLE 5.16: Effect of the drive side pressure angle on nominal tooth root stress

Pressure angle on drive side	Nominal bending stress		
	fillet radius(ρ_F) = *0.4m*	fillet radius(ρ_F) = *0.3m*	fillet radius(ρ_F) = *0.2m*
	Module = 04	Module = 04	Module = 04
20^0	209.057	**240.762**	293.777
22^0	206.123	236.802	287.951
24^0	203.608	233.281	282.590
26^0	200.972	229.633	277.100
28^0	198.012	225.651	271.280
30^0	194.623	221.235	265.035
32^0	190.751	216.335	258.325
34^0	186.370	210.929	251.134
36^0	181.471	205.011	243.462
38^0	176.056	**198.586**	235.319
40^0	170.131	191.663	226.717
42^0	164.467	184.959	218.248
44^0	159.030	178.438	209.880
46^0	153.784	172.064	201.575
48^0	148.687	165.794	193.298
50^0	143.692	159.584	185.010
52^0	138.752	153.388	176.674

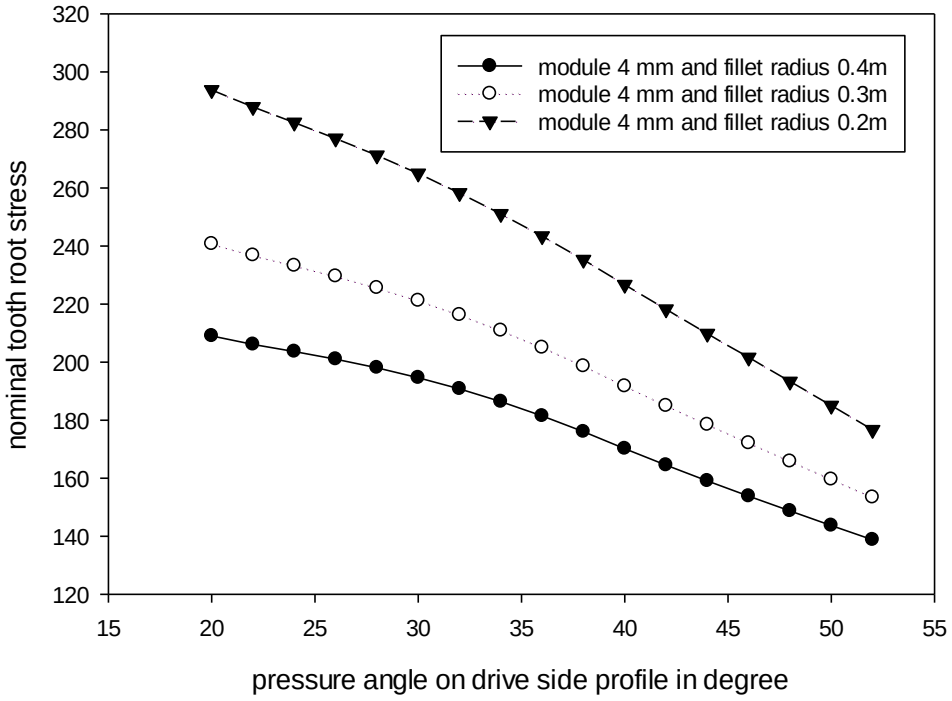

FIGURE 5.15: Effect of the drive side pressure angle on nominal tooth root stress

As pressure angle on drive side increases, nominal bending stress decreases but simultaneously fillets radius increases this effect also increases as shown in fig. 5.15.

Nominal bending stress has been calculated with a different number of teeth on pinion for different fillet radius and asymmetric factor for module = 4. Values are presented in table 5.17 and it is presented in form of graph as shown in figure 5.16.

TABLE 5.17: Effect of number of teeth on bending stress with different fillet radius and asymmetric factor for $m = 4$

Number of teeth on pinion	Nominal bending stress								
	Module = 04 & fillet radius(ρ_F) = *0.4m*			Module = 04 & fillet radius(ρ_F) = *0.3m*			Module = 04 & fillet radius(ρ_F) = *0.2m*		
	AF=1.0	AF=1.5	AF=2.0	AF=1.0	AF=1.5	AF=2.0	AF=1.0	AF=1.5	AF=2.0
25	209.057	194.623	170.131	240.762	221.235	191.663	293.777	265.035	226.717
35	164.515	142.218	117.807	185.480	159.556	131.728	219.643	219.643	154.187
50	128.126	103.765	82.059	142.152	115.225	91.198	164.567	133.558	105.832
65	102.289	78.723	60.140	112.274	86.800	66.548	128.022	99.609	76.756
80	84.128	62.259	46.378	91.669	68.309	51.162	103.459	77.848	58.755
100	66.991	47.617	34.613	72.505	52.003	38.072	81.056	58.879	43.543

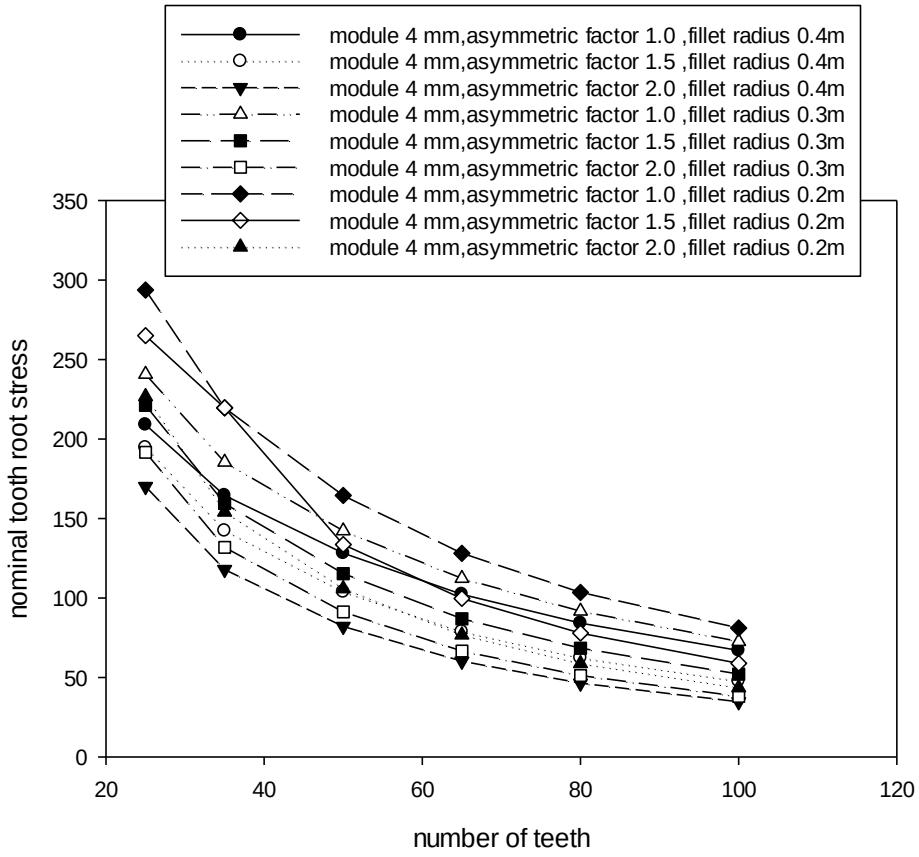

FIGURE 5.16 Effect of number of teeth on bending stress with different fillet radius and asymmetric factor for module = 4

As a number of teeth increase a nominal bending stress decreases but simultaneously at a higher module, asymmetric factor as well as fillets radius this effect also increases as shown in figure 5.16.

Analysis shows effects of higher pressure angle on drive side effect on tooth geometry. The parametric analysis helps to understand the effect of drive side pressure angle on tooth geometry of asymmetric spur gear.

This way parametric analysis of gear gives idea about effect on gear tooth parameter by changing pressure angle on drive side. It is very useful to take decision about input design parameters for desire output in terms of bending stress to improve load carrying capacity. Figure 5.15 and 5.16 shows cumulation of various parameters in terms of bending stress.

CHAPTER – 6

OPTIMIZATION OF DRIVE SIDE PRESSURE ANGLE

6.1 Introduction

For symmetric spur gear, both side involute profiles are same. Equation for involute profile is presented in section 3.2 and 3.3. It depends on pressure angle (α) and radius r. It locates the point at any radius r on the involute profile of gear tooth for given pressure angle.

In design of gear, most important thing is bending stress must be low at critical section. So it is necessary to minimize bending stress of tooth at critical section. To minimize bending stress one way is optimize geometrical shape of standard symmetric gear [1-2]. In order to achieve this goal, pressure angle on drive side profile (as compare to coast side) can be increases. It is found that, in asymmetric involute spur gear, at the critical section the bending stress decreases as the pressure angle on drive side is higher than coast side [45-57]. Higher value of drive side pressure angle gives better reduction in bending stress [55]. But contact ratio and tip thickness are limiting factor for higher drive side pressure angle.

6.2 Constraint to optimize drive side pressure angle

As the pressure angle on drive side (as compare to coast side) increases, the bending stress decreases at root of tooth [45-57]. But contact ratio (ε) and tip thickness (S_t) are constraint for same.

6.2.1 Contact ratio

Contact ratio is a measure of the average number of teeth in contact during the period in which a tooth comes and goes out of contact with the mating gear [2]. Contact Ratio is the ratio of the arc of action to the circular pitch.

Figure 6.1[95] show that position of tooth load variation .A'B' show that this duration only a single pair of gear teeth is in contact which is subject to the maximum load. If contact ratio is very low this duration becomes high which is not desirable.

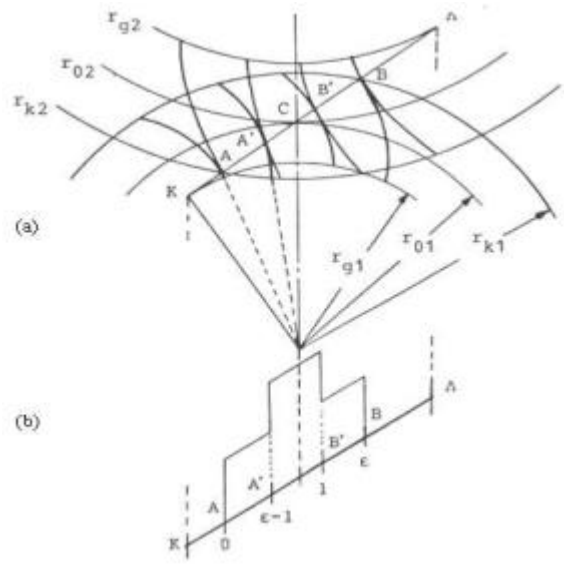

FIGURE 6.1: Positions of tooth load variation

Gear standard procedures recommend that, the contact ratio should be higher or equal to 1.1 [1-2]. Below this contact ratio tooth loading period increases and it is undesirable condition for cyclic loading.

The formula for calculating contact ratio [1, 2] is:

$$\varepsilon = \frac{\sqrt{r_{tp}^2 - r_{bp}^2} + \sqrt{r_{tg}^2 - r_{bg}^2} - C \cdot \sin\alpha}{p \cdot \cos\alpha} \tag{6.1}$$

6.2.2 Tip thickness

Tip thickness is main constraints for higher value of drive side pressure angle. Small thickness makes tooth very sharp and pointed.

The formula for calculating tip thickness of tooth (considered from ch-3) is:

a) Tip Thickness for symmetric spur gear tooth

$$S_t = 2 \cdot r_t \cdot \theta_t \tag{6.2}$$

$$\theta_t = \frac{\pi}{2.z} + \tan\alpha - \alpha - \left(\tan\left(\cos^{-1}\left(\frac{r_p}{r_t}.\cos\alpha \right) \right) - \left(\cos^{-1}\left(\frac{r_p}{r_t}.\cos\alpha \right) \right) \right)$$

b) Tip Thickness of asymmetric spur gear tooth

$$S_t = r_t.\theta_{td} + r_t.\theta_{td} \tag{6.3}$$

$$\theta_{td} = \frac{\pi}{2.z} + \tan\alpha_d - \alpha_d - \left(\tan\left(\cos^{-1}\left(\frac{r_p}{r_t}.\cos\alpha_d \right) \right) - \left(\cos^{-1}\left(\frac{r_p}{r_t}.\cos\alpha_d \right) \right) \right)$$

$$\theta_{tc} = \frac{\pi}{2.z} + \tan\alpha_c - \alpha_c - \left(\tan\left(\cos^{-1}\left(\frac{r_p}{r_t}.\cos\alpha_c \right) \right) - \left(\cos^{-1}\left(\frac{r_p}{r_t}.\cos\alpha_c \right) \right) \right)$$

Gear standard procedures recommend that, the tip thickness should be ≥ *0.4m* for hardened gears. In exceptional cases, tip thickness decreases to *0.25m* [1-2]. Below this tip thickness it becomes more pointed.

6.2.3 Condition

Niels L. Pedersen has suggested that higher reduction in the bending stress can be obtained when the drive side pressure angle is greater than the coast side pressure angle [55].

6.3 Flow chart to optimized drive side pressure angle

Figure 6.2 gives a flow chart to optimized drive side pressure angle.

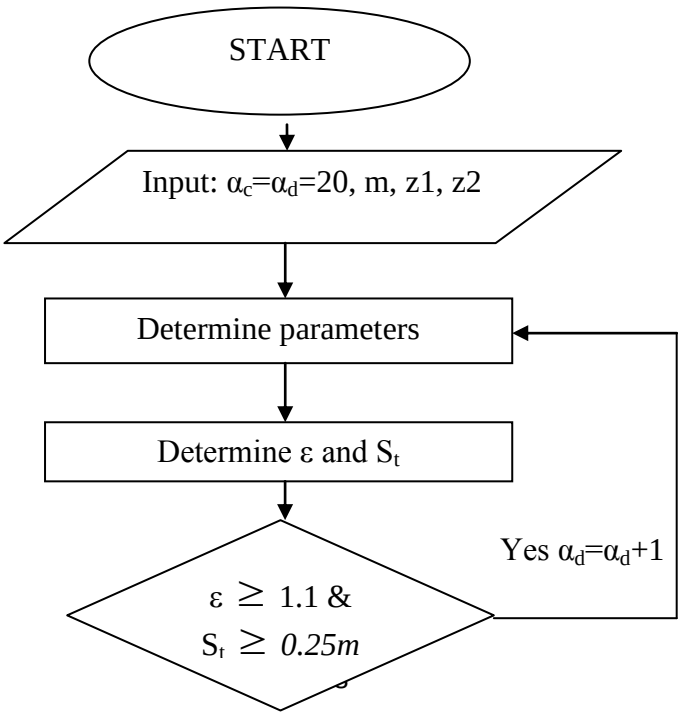

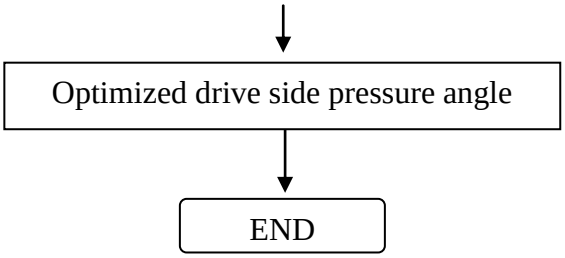

FIGURE 6.2: Flow chart to optimized drive side pressure angle

6.4 Algorithm to optimized drive side pressure angle

1. Input : m , Z_p, Z_g, $\alpha_d = \alpha_c = 20^0$
2. Calculate S_t, ε
3. If $S_t \geq 0.25m$ *and* $\varepsilon \geq 1.1$ then go to step 5 otherwise go to step 4
4. $\alpha_d = \alpha_d + 1$ then goto step 2
5. Print α_d
6. *END*

6.5 Optimization of drive side pressure angle

With help of above developed equations and as per gear parameters presented in table 5.1, a code has been developed. Code is available in APPENDIX I. Based on that data various graphs have been created. Figure 6.3 shows a pressure angle on drive side verses contact ratio.

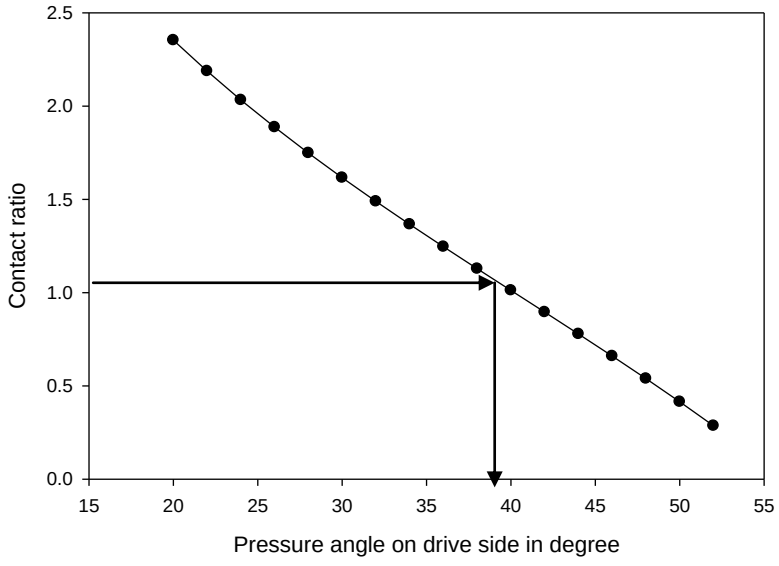

FIGURE 6.3: Pressure angle on drive side verses contact ratio

In this illustration at 1.1, contact ratio pressure angle is 38^0 as per fig. 6.3, which is safe condition.

Figure 6.4 shows a pressure angle on drive side verses tip thickness of asymmetric spur gear.

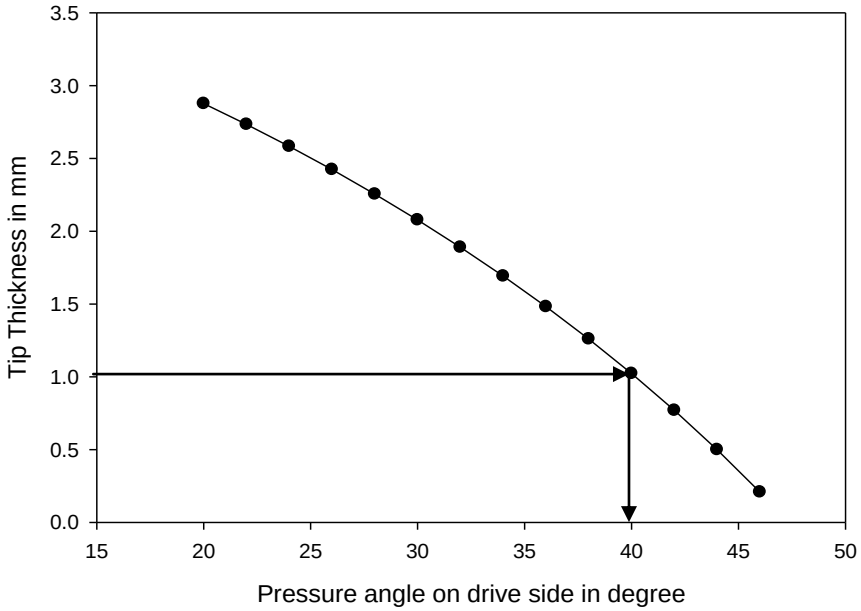

FIGURE 6.4: Pressure angle on drive side verses tip thickness

In this illustration at 1unit (*0.25m*) tip thickness pressure angle is 40^0 as shown figure 6.4, which is safe condition.

But decision on maximum magnitude of drive side pressure angle is constraint by the safe contact ratio and top land tip thickness (figure 6.3, 6.4). At 38^0 pressure angle on drive side profile it satisfies conditions and constraints. So, based on above conditions and constraint optimise drive side pressure angle is 38^0.

CHAPTER – 7

OPTIMIZATION OF FILLET WITH G2 CONTINUITY AT CRITICAL SECTION

The gear tooth-root is exposed to a combination of both shearing and bending. Due to repeated excessive stresses a bending fatigue often occurs at the root of tooth. The first crack initiates at the regions with the highest stress concentrations and propagates until failure occurs. The fatigue of gear tooth due to bending is always a challenge to designers.

At the critical section of tooth, stress concentration occurs due to curvature discontinuity [68]. At the connection point of involute profile of tooth and circular fillet at root, stress concentration occurs due to curvature discontinuity. Such discontinuities cause a sudden rise in stress values, so it is necessary to making these regions prone to mechanical failure [68]. Hence, stress concentration plays a important role to reduce or avoid mechanical failure. Reduction in stress concentration will improve the gear tooth strength. This research focuses on the minimization of stress concentration by optimizing root profile at critical section of asymmetric gear. It will reduce stress concentration. Geometric continuity of order 2 at connection point of involute profile and root profile plays a very important role in reducing stress concentration [93]. A Bezier curve [94] is used with geometric continuity of order 2 at the critical section of an asymmetric spur gear tooth to reduce curvature discontinuity. It will reduce bending fatigue which is challenge of designers.

7.1 G2 continuity

In order to reduce concentration of stress, an important condition of criterion is geometric continuity of order 2(G2 continuity) [93]. G2 continuity gives connection between two curves with equal tangent and equal curvature [93]. G2 continuity is very important to decrease stress concentration at the root of tooth. G2 continuity at the

connection points of tooth profile and root profile of gear plays very important role in reducing stress concentration [93]. Here in this work a Bezier curve is used.

7.2 Bezier curve

Bezier curve mimics the shape of its control polygon. Main characteristic of Bezier curve is, it is always tangent to end points and also passes through its end points [94]. If we select point B1 and B2 in tangent direction of curve DE and GH as shown in figure 7.3, it will create G1 continuity condition. It represents position of end point and equal tangent and continuity between two geometric curves. It is very easy to select point B1 and B2 in tangent direction of curve DE and GH during drawing in CAD software. This is a main reason to select Bezier curve to optimize root of tooth.

Bezier Curve

A Bezier Curve [94] is obtained by a defining polygon.

$$P(t)=\sum_{i=0}^{n} B_i J_{n,i}(t) \tag{7.1}$$

Where,

$$J_{n,i}(t)=\frac{n!}{i!(n-1)!}t^i(1-t)^{n-i} \quad , \; 0\le t\le 1$$

or

$$P(t)=(1-t)^3\cdot B_0+3\cdot(1-t)^2\cdot t\cdot B_1+3\cdot(1-t)\cdot t^2\cdot B_2+t^3\cdot B_3, \qquad 0\le t\le 1$$

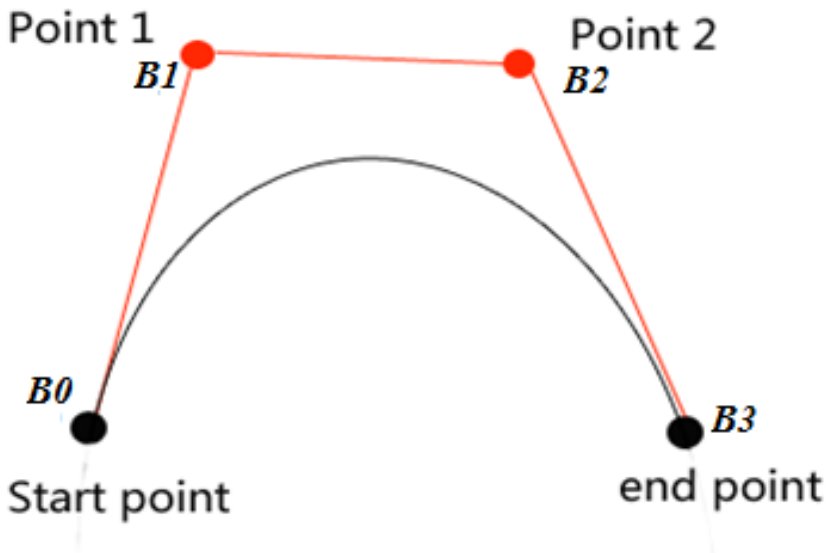

FIGURE 7.1: Bezier curve

7.3 Establishment of optimize fillet with G2 continuity at critical section

Connection point of involute profile of tooth and at root a circular fillet creates discontinuity causes stress concentration occurs [68]. In order to minimize stress concentration, G2 continuity at the blending of gear tooth plays very important role [93].

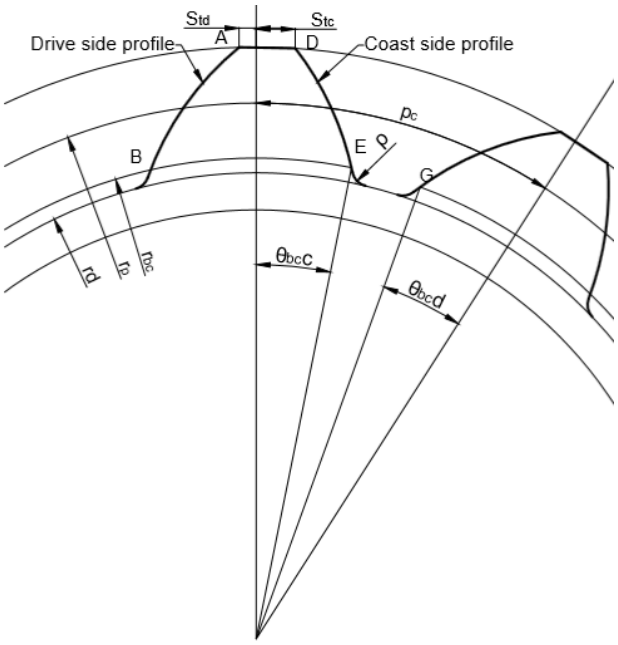

FIGURE 7.2: Circular fillet at gear tooth root

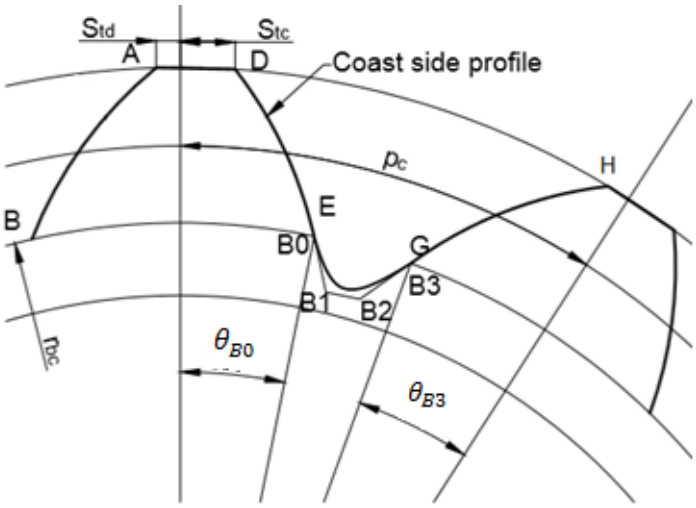

FIGURE 7.3: Developed fillet at tooth root with G2 continuity

To reduce stress concentration a curve with G2 continuity using Bezier curve at the connection point of involute tooth profile and root profile has been developed as shown in figure 7.3.

If the radius of curvature is same at common end point, curves are known as curvature continuous [93]. Tangent and curvature continuous is possible only when both

first and second derivations of the equations are equal at common end point [93]. First and second derivations of Bezier curve at end points are [94].

$$P'(0) = n(B_1 - B_0) \tag{7.2}$$

$$P'(n) = n(B_n - B_{n-1}) \tag{7.3}$$

$$P''(0) = n(n-1)(B_0 - 2B_1 - B_2) \tag{7.4}$$

$$P''(n) = n(n-1)(B_n - 2B_{n-1} - B_{n-2}) \tag{7.5}$$

For Cubic Bezier curve n = 3

$$P'(0) = 3(B_1 - B_0) \tag{7.6}$$

$$P'(3) = 3(B_3 - B_2) \tag{7.7}$$

$$P''(0) = 6(B_0 - 2B_1 - B_2) \tag{7.8}$$

$$P''(3) = 6(B_3 - 2B_2 - B_1) \tag{7.9}$$

First and second order derivative of the curve DE and GH at end points gives value of P`(0), P``(0), P`(3) and P``(3) respectively. B0 and B3 are end points of curve DE and GH respectively. B0 and B3 are known points. Solve the equation 7.6 to 7.9 to obtain required points B1 and B2 of Bezier curve.

Code has been developed and available in APENDIX I to calculate that coordinate of known points B0 and B3. Equations to obtain coordinate of known points B0 and B3 are given below.

Location of point B0:

$$x_{B0} = r_{bc} \cdot \cos(\theta_{B0}) \tag{7.10}$$

$$y_{B0} = r_{bc} \cdot \sin(\theta_{B0}) \tag{7.11}$$

$$\theta_{B0} = \frac{\pi}{2 \cdot z} + \tan\alpha_c - \alpha_c - \left(\tan\left(\cos^{-1}\left(\frac{r_p}{r_{bc}} . \cos\alpha_c \right) \right) - \left(\cos^{-1}\left(\frac{r_p}{r_{bc}} . \cos\alpha_c \right) \right) \right)$$

Location of point B3:

$$x_{B3} = r_{bc} \cdot \cos\left(\frac{2\pi}{z} - \theta_{B3} \right) \tag{7.12}$$

$$y_{B3} = r_{bc} \cdot \sin\left(\frac{2\pi}{z} - \theta_{B3} \right) \tag{7.13}$$

$$\theta_{B3} = \frac{\pi}{2 \cdot z} + \tan\alpha_d - \alpha_d - \left(\tan\left(\cos^{-1}\left(\frac{r_p}{r_{bc}} . \cos\alpha_d \right) \right) - \left(\cos^{-1}\left(\frac{r_p}{r_{bc}} . \cos\alpha_d \right) \right) \right)$$

A Bezier curve with G2 continuity at critical section of tooth has been successfully established to reduce stress concentration which occurs due to curvature discontinuity.

CHAPTER – 8

GEOMETRIC MODEL OF INVOLUTE SPUR GEAR

A computer program has been presented to develop an exact CAD model for analysis. This chapter divided in two parts. In First part algorithm has been developed to create a CAD model of symmetric spur gear with standard fillet, asymmetric spur gear with standard fillet and asymmetric spur gear with the modified root. Second part presents a developed CAD models in AutoCAD software using algorithm.

Current researchers are works on the optimization of tooth root fillet which improve load carrying capacity and life. Gear design required FEA analysis to predict gear failure, estimates gears life in service which is necessary for good gear design.CAD model is required for FEA. Involute profile and root profile of gear is very important in gear modeling. It is very difficult to develop exact involute profile and root profile. Various papers are available to develop involute profile and root profile, but they are based on programming which required knowledge of programming and manual method is very time consuming. In this paper, author explores hybrid approach to develop exact involute profile and root profile. A code has been developed which gives a points on involute profile and root profile. Using these points, it is very easy to create involute profile and root profile in AutoCAD software or any modeling software.

8.1 Algorithm to develop CAD Model

Involute profile and root profile of gear is very important in gear modeling. So, computer program has been created, to develop exact involute profile and root profile. It is very difficult to understand a computer program without its knowledge. So, an algorithm is presented.

Algorithm to create location of point on involute profile and root profile has been developed and presented in next section. Using these points a required curve has been developed in AutoCAD modeling software.

8.1.1 Algorithm for symmetric spur gear with standard fillet

For symmetric spur gear, both side involute profiles are same. Equation for involute profile is presented in section 3.2 and 3.3, has been considered. Equation 8.1is used to develop an involute tooth profile of a gear. It depends on pressure angle (α) and radius r. It locates the point at any radius r on the involute profile of gear tooth as shown in figure 8.1. Circular root profile is widely used in design [68]. In this symmetric spur gear, a circular root profile is considered at root of the tooth.

$$\theta_r = \frac{\pi}{2 \cdot z} + \tan\alpha - \alpha - \left(\tan\left(\cos^{-1}\left(\frac{r_p}{r}.\cos\alpha \right) \right) - \left(\cos^{-1}\left(\frac{r_p}{r}.\cos\alpha \right) \right) \right) \qquad (8.1)$$

Figure 1 shows the symmetric spur gear tooth profile. Arc AB is a circular arc with center o1. Arc BC is involute arc developed by equation 1. Arc CD is a circular arc with center o. Arc DE is involute arc developed by equation 1. Arc EF is a circular arc with center o2. Arc FG is a circular arc with center o. To develop profile in software each point location is required. So, the locations of the points are given in table 8.1.

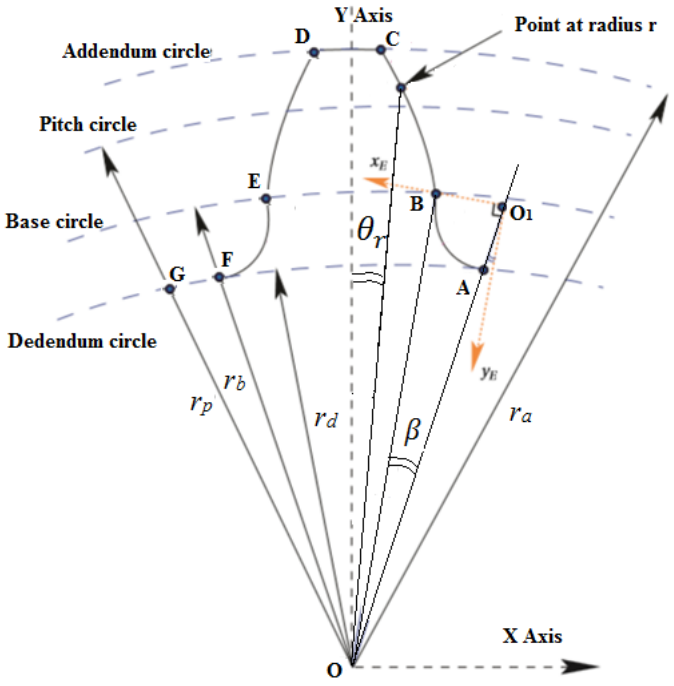

FIGURE 8.1: Symmetric spur gear geometry

TABLE 8.1: Cartesian coordinates of a point on symmetric spur gear tooth profile

Point	Cartesian Coordinates Equation
A	$x_A = r_d \cdot \cos(\theta_B + \beta)$ $y_A = r_d \cdot \sin(\theta_B + \beta)$ $\beta = \tan^{-1}\left(\frac{r}{r_b}\right)$ and $r = \frac{r_b^2 - r_d^2}{2r_b}$ $\theta_A = \frac{\pi}{2 \cdot z} + \tan\alpha - \alpha - \left(\tan\left(\cos^{-1}\left(\frac{r_p}{r_b}.\cos\alpha\right)\right) - \left(\cos^{-1}\left(\frac{r_p}{r_b}.\cos\alpha\right)\right)\right)$
B	$x_B = r_b \cdot \cos(\theta_B)$ $y_B = r_b \cdot \sin(\theta_B)$ $\theta_B = \frac{\pi}{2 \cdot z} + \tan\alpha - \alpha - \left(\tan\left(\cos^{-1}\left(\frac{r_p}{r_b}.\cos\alpha\right)\right) - \left(\cos^{-1}\left(\frac{r_p}{r_b}.\cos\alpha\right)\right)\right)$
C	$x_C = r_a \cdot \cos(\theta_C)$ $y_C = r_a \cdot \sin(\theta_C)$ $\theta_C = \frac{\pi}{2 \cdot z} + \tan\alpha - \alpha - \left(\tan\left(\cos^{-1}\left(\frac{r_p}{r_a}.\cos\alpha\right)\right) - \left(\cos^{-1}\left(\frac{r_p}{r_a}.\cos\alpha\right)\right)\right)$
D	$x_D = -r_a \cdot \cos(\theta_D)$ $y_D = r_a \cdot \sin(\theta_D)$ $\theta_D = \frac{\pi}{2 \cdot z} + \tan\alpha - \alpha - \left(\tan\left(\cos^{-1}\left(\frac{r_p}{r_a}.\cos\alpha\right)\right) - \left(\cos^{-1}\left(\frac{r_p}{r_a}.\cos\alpha\right)\right)\right)$
E	$x_E = -r_b \cdot \cos(\theta_E)$ $y_E = r_b \cdot \sin(\theta_E)$ $\theta_E = \frac{\pi}{2 \cdot z} + \tan\alpha - \alpha - \left(\tan\left(\cos^{-1}\left(\frac{r_p}{r_b}.\cos\alpha\right)\right) - \left(\cos^{-1}\left(\frac{r_p}{r_b}.\cos\alpha\right)\right)\right)$
F	$x_F = -r_d \cdot \cos(\theta_F + \beta)$ $y_F = r_d \cdot \sin(\theta_F + \beta)$ $\beta = \tan^{-1}\left(\frac{r}{r_b}\right)$ and $r = \frac{r_b^2 - r_d^2}{2r_b}$

	$\theta_F = \frac{\pi}{2 \cdot z} + \tan\alpha - \alpha - \left(\tan\left(\cos^{-1}\left(\frac{r_p}{r_b}.\cos\alpha \right) \right) - \left(\cos^{-1}\left(\frac{r_p}{r_b}.\cos\alpha \right) \right) \right)$
G	$x_G = -r_d \cdot \cos\left(\frac{2 \cdot \pi}{z} - (\theta_G + \beta) \right)$ $y_G = r_d \cdot \sin\left(\frac{2 \cdot \pi}{z} - (\theta_G + \beta) \right)$ $\beta = \tan^{-1}\left(\frac{r}{r_b} \right)$ and $r = \frac{r_b^2 - r_d^2}{2r_b}$ $\theta_G = \frac{\pi}{2 \cdot z} + \tan\alpha - \alpha - \left(\tan\left(\cos^{-1}\left(\frac{r_p}{r_b}.\cos\alpha \right) \right) - \left(\cos^{-1}\left(\frac{r_p}{r_b}.\cos\alpha \right) \right) \right)$

Algorithm to develop gear profile

Segment vies an algorithms has been presented for symmetric involute spur gear.

Algorithm for involute curve BC

for (I = r_b, I <= r_a, I++)

{

$$\theta_I = \frac{\pi}{2 \cdot z} + \tan\alpha - \alpha - \left(\tan\left(\cos^{-1}\left(\frac{r_p}{I}.\cos\alpha \right) \right) - \left(\cos^{-1}\left(\frac{r_p}{I_b}.\cos\alpha \right) \right) \right)$$

$$X = I \cdot \cos(\theta_I)$$

$$Y = I \cdot \sin(\theta_I)$$

Plot X Y
}

Algorithm for involute curve DE

for (J = r_a, J <= r_b, J--)

{

$$\theta_J = \frac{\pi}{2 \cdot z} + \tan\alpha - \alpha - \left(\tan\left(\cos^{-1}\left(\frac{r_p}{J}.\cos\alpha \right) \right) - \left(\cos^{-1}\left(\frac{r_p}{J}.\cos\alpha \right) \right) \right)$$

$$X = -J \cdot \cos(\theta_J)$$

$$Y = J \cdot \sin(\theta_J)$$

Plot X Y
}

8.1.2 Algorithm for asymmetric spur gear with standard fillet

Gears with higher load-carrying capacity and increased fatigue life are current demand from industry. There are lots of ways to achieve that, namely using novel materials, heat-treatment or novel gear geometries [88]. For involute spur gear, there is mainly two way to optimize tooth geometry.

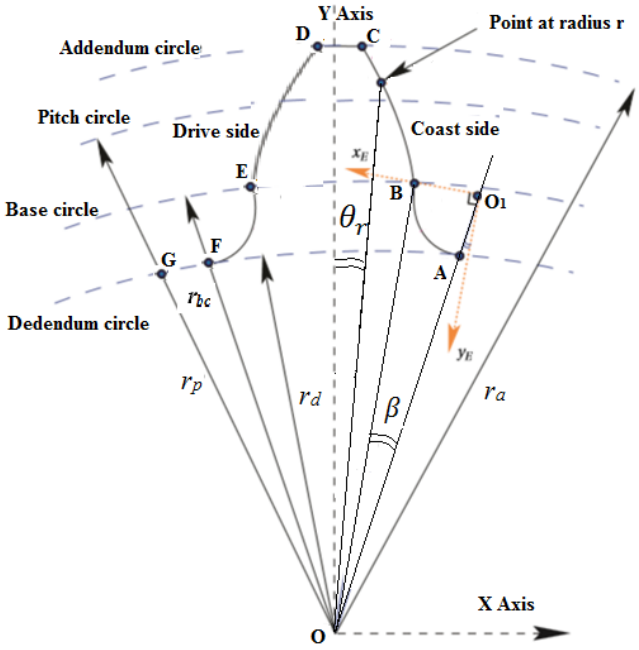

FIGURE 8.2: Asymmetric spur gear geometry

The first way is to optimize tooth root profile [68, 69, 76, 78] and the second way is to optimize the drive side involute tooth profile [44-57]. Drive side means loaded side. The involute profile depends on pressure angle. So, we need to optimize it. When we change pressure angle on the drive side, both sides involute profile becomes different and spur gear becomes asymmetric.

Past and current research shows that higher pressure angle on the drive side as compare coast side within the limit will reduce stress at the root of the tooth [44-57] which improve load carrying capacity and longer life. Contact ratio and tip thickness are a limiting factor for higher drive side pressure angle. Gear standard procedures recommend that the contact ratio should be higher or equal to 1.1 [1] and tip thickness should be ≥ 0.25m [1].

Figure 8.2 shows the asymmetric spur gear tooth profile. Arc AB is a circular arc with center o1. Arc BC is involute arc developed by equation 8.1. Arc CD is a circular arc with center o. Arc DE is involute arc developed by equation 8.1 but with different pressure

angle as compare to involute arc BC. Due to higher pressure angle on involute profile DE, it becomes longer then involute arc BC. In this paper, both side involute profiles considered from tip of the tooth to base circle of coast side. Arc EF is a circular arc with center o2. Arc FG is a circular arc with center o. To develop profile each point location is required. So, the locations of the points are given in table 8.2.

TABLE 8.2: Cartesian coordinates of a point on asymmetric spur gear tooth profile

Point	Equations for Cartesian coordinates of a point
A	$x_A = r_d \cdot \cos(\theta_B + \beta)$ $y_A = r_d \cdot \sin(\theta_B + \beta)$ $\beta = \tan^{-1}\left(\frac{r}{r_{bc}}\right)$ and $r = \frac{r_{bc}^2 - r_d^2}{2r_{bc}}$ $\theta_A = \frac{\pi}{2 \cdot z} + \tan\alpha_c - \alpha_c - \left(\tan\left(\cos^{-1}\left(\frac{r_p}{r_{bc}}.\cos\alpha_c\right)\right) - \left(\cos^{-1}\left(\frac{r_p}{r_{bc}}.\cos\alpha_c\right)\right)\right)$
B	$x_B = r_{bc} \cdot \cos(\theta_B)$ $y_B = r_{bc} \cdot \sin(\theta_B)$ $\theta_B = \frac{\pi}{2 \cdot z} + \tan\alpha_c - \alpha_c - \left(\tan\left(\cos^{-1}\left(\frac{r_p}{r_{bc}}.\cos\alpha_c\right)\right) - \left(\cos^{-1}\left(\frac{r_p}{r_{bc}}.\cos\alpha_c\right)\right)\right)$
C	$x_C = r_a \cdot \cos(\theta_C)$ $y_C = r_a \cdot \sin(\theta_C)$ $\theta_C = \frac{\pi}{2 \cdot z} + \tan\alpha_c - \alpha_c - \left(\tan\left(\cos^{-1}\left(\frac{r_p}{r_a}.\cos\alpha_c\right)\right) - \left(\cos^{-1}\left(\frac{r_p}{r_a}.\cos\alpha_c\right)\right)\right)$
D	$x_D = -r_a \cdot \cos(\theta_D)$ $y_D = r_a \cdot \sin(\theta_D)$ $\theta_D = \frac{\pi}{2 \cdot z} + \tan\alpha_d - \alpha_d - \left(\tan\left(\cos^{-1}\left(\frac{r_p}{r_a}.\cos\alpha_d\right)\right) - \left(\cos^{-1}\left(\frac{r_p}{r_a}.\cos\alpha_d\right)\right)\right)$
E	$x_E = -r_{bc} \cdot \cos(\theta_E)$ $y_E = r_{bc} \cdot \sin(\theta_E)$ $\theta_E = \frac{\pi}{2 \cdot z} + \tan\alpha_d - \alpha_d - \left(\tan\left(\cos^{-1}\left(\frac{r_p}{r_{bc}}.\cos\alpha_d\right)\right) - \left(\cos^{-1}\left(\frac{r_p}{r_{bc}}.\cos\alpha_d\right)\right)\right)$

F	$x_F = -r_d \cdot \cos(\theta_F + \beta)$ $y_F = r_d \cdot \sin(\theta_F + \beta)$ $\beta = \tan^{-1}\left(\frac{r}{r_{bc}}\right)$ and $r = \frac{r_{bc}^2 - r_d^2}{2r_{bc}}$ $\theta_F = \frac{\pi}{2 \cdot z} + \tan\alpha_d - \alpha_d - \left(\tan\left(\cos^{-1}\left(\frac{r_p}{r_{bc}}.\cos\alpha_d\right)\right) - \left(\cos^{-1}\left(\frac{r_p}{r_{bc}}.\cos\alpha_d\right)\right)\right)$
G	$x_G = -r_d \cdot \cos\left(\frac{2 \cdot \pi}{z} - (\theta_G + \beta)\right)$ $y_G = r_d \cdot \sin\left(\frac{2 \cdot \pi}{z} - (\theta_G + \beta)\right)$ $\beta = \tan^{-1}\left(\frac{r}{r_{bc}}\right)$ and $r = \frac{r_{bc}^2 - r_d^2}{2r_{bc}}$ $\theta_G = \frac{\pi}{2 \cdot z} + \tan\alpha_d - \alpha_d - \left(\tan\left(\cos^{-1}\left(\frac{r_p}{r_{bc}}.\cos\alpha_d\right)\right) - \left(\cos^{-1}\left(\frac{r_p}{r_{bc}}.\cos\alpha_d\right)\right)\right)$

Algorithm to develop gear profile

Segment vies algorithms has been presented for asymmetric involute spur gear.

Algorithm for involute curve BC

for (I = r_b, I <= r_a, I++)

{

$$\theta_I = \frac{\pi}{2 \cdot z} + \tan\alpha_c - \alpha_c - \left(\tan\left(\cos^{-1}\left(\frac{r_p}{I}.\cos\alpha_c\right)\right) - \left(\cos^{-1}\left(\frac{r_p}{I}.\cos\alpha_c\right)\right)\right)$$

$X = I \cdot \cos(\theta_I)$

$Y = I \cdot \sin(\theta_I)$

Plot X Y

}

Algorithm for involute curve DE

for (J = r_a, J <= r_b, J--)

{

$$\theta_J = \frac{\pi}{2 \cdot z} + \tan\alpha_d - \alpha_d - \left(\tan\left(\cos^{-1}\left(\frac{r_p}{J}.\cos\alpha_d \right) \right) - \left(\cos^{-1}\left(\frac{r_p}{J}.\cos\alpha_d \right) \right) \right)$$

$$X = -J \cdot \cos(\theta_J)$$

$$Y = J \cdot \sin(\theta_J)$$

Plot X Y
}

8.1.3 Algorithm for asymmetric spur gear with modified root profile

Modified root profile is presented in chapter 8.3. Asymmetric spur with modified root profile is shown in figure.

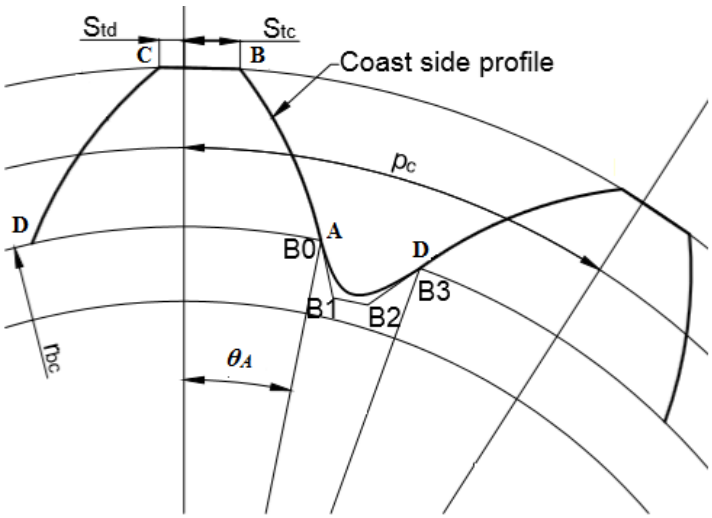

FIGURE 8.3: Asymmetric gear with optimized fillet at tooth root with G2 continuity

TABLE 8.3: Cartesian coordinates of a point on asymmetric spur gear tooth profile with modified fillet

Point	Equations of Cartesian Coordinates of points
A	$x_A = r_{bc} \cdot \cos(\theta_A)$ $y_A = r_{bc} \cdot \sin(\theta_A)$ $\theta_A = \frac{\pi}{2 \cdot z} + \tan\alpha_c - \alpha_c - \left(\tan\left(\cos^{-1}\left(\frac{r_p}{r_{bc}}.\cos\alpha_c \right) \right) - \left(\cos^{-1}\left(\frac{r_p}{r_{bc}}.\cos\alpha_c \right) \right) \right)$
B	$x_B = r_a \cdot \cos(\theta_B)$ $y_B = r_a \cdot \sin(\theta_B)$ $\theta_B = \frac{\pi}{2 \cdot z} + \tan\alpha_c - \alpha_c - \left(\tan\left(\cos^{-1}\left(\frac{r_p}{r_a}.\cos\alpha_c \right) \right) - \left(\cos^{-1}\left(\frac{r_p}{r_a}.\cos\alpha_c \right) \right) \right)$

C	$x_C = -r_a \cdot \cos(\theta_C)$ $y_C = r_a \cdot \sin(\theta_C)$ $\theta_C = \frac{\pi}{2 \cdot z} + \tan\alpha_d - \alpha_d - \left(\tan\left(\cos^{-1}\left(\frac{r_p}{r_a}.\cos\alpha_d \right) \right) - \left(\cos^{-1}\left(\frac{r_p}{r_a}.\cos\alpha_d \right) \right) \right)$
D	$x_D = -r_{bc} \cdot \cos(\theta_D)$ $y_D = r_{bc} \cdot \sin(\theta_D)$ $\theta_D = \frac{\pi}{2 \cdot z} + \tan\alpha_d - \alpha_d - \left(\tan\left(\cos^{-1}\left(\frac{r_p}{r_{bc}}.\cos\alpha_d \right) \right) - \left(\cos^{-1}\left(\frac{r_p}{r_{bc}}.\cos\alpha_d \right) \right) \right)$

Algorithm for involute curve AB

for (I = r_{bc}, I <= r_a, I++)

{

$$\theta_I = \frac{\pi}{2 \cdot z} + \tan\alpha_c - \alpha_c - \left(\tan\left(\cos^{-1}\left(\frac{r_p}{I}.\cos\alpha_c \right) \right) - \left(\cos^{-1}\left(\frac{r_p}{I}.\cos\alpha_c \right) \right) \right)$$

$$X = I \cdot \cos(\theta_I)$$

$$Y = I \cdot \sin(\theta_I)$$

Plot X Y

}

Algorithm for involute curve CD

for (J = r_a, J <= r_{bc}, J--)

{

$$\theta_J = \frac{\pi}{2 \cdot z} + \tan\alpha_d - \alpha_d - \left(\tan\left(\cos^{-1}\left(\frac{r_p}{J}.\cos\alpha_d \right) \right) - \left(\cos^{-1}\left(\frac{r_p}{J}.\cos\alpha_d \right) \right) \right)$$

$$X = -J \cdot \cos(\theta_J)$$

$$Y = J \cdot \sin(\theta_J)$$

Plot X Y

}

Algorithm to develop root profile

Calculate

Location of point B0:

$$x_{B0} = r_{bc} \cdot \cos(\theta_{B0})$$

$$y_{B0} = r_{bc} \cdot \sin(\theta_{B0})$$

$$\theta_{B0} = \frac{\pi}{2 \cdot z} + \tan\alpha_c - \alpha_c - \left(\tan\left(\cos^{-1}\left(\frac{r_p}{r_{bc}} . \cos\alpha_c \right) \right) - \left(\cos^{-1}\left(\frac{r_p}{r_{bc}} . \cos\alpha_c \right) \right) \right)$$

Location of point B3:

$$x_{B3} = r_{bc} \cdot \cos\left(\frac{2\pi}{z} - \theta_{B3} \right)$$

$$y_{B3} = r_{bc} \cdot \sin\left(\frac{2\pi}{z} - \theta_{B3} \right)$$

$$\theta_{B3} = \frac{\pi}{2 \cdot z} + \tan\alpha_d - \alpha_d - \left(\tan\left(\cos^{-1}\left(\frac{r_p}{r_{bc}} . \cos\alpha_d \right) \right) - \left(\cos^{-1}\left(\frac{r_p}{r_{bc}} . \cos\alpha_d \right) \right) \right)$$

Location of point B1 and B2 can be achieved by method presented in chapter 7.

```
for (t = 0.0; t < 1.0; t += 0.05)

{
xt=((1-t)*(1-t)*(1-t)*x0)+(3*t*(1-t)*(1-t)*x1)+(3*t*t*(1-t)*x2)+(t*t*t*x3)

yt=((1-t)*(1-t)*(1-t)*y0)+(3*t*(1-t)*(1-t)*y1)+(3*t*t*(1-t)*y2)+(t*t*t*y3)

Plot (xt, yt);

}
```

8.2 CAD Model

Previous section presents an algorithm to create location of point on involute profile and root profile. Using these points a required curve has been developed in AutoCAD modeling software. Chapter 6 present a technique to optimize drive side pressure angle and chapter 7 present a technique to optimized root profile. Both things are considered in programming and developed universal program which is capable to capable to calculate optimize drive side pressure angle and optimized root profile by inputting basic parameters. For asymmetric spur gear with the modified root, parameters are pressure angle on coast side, module and number of teeth. For asymmetric spur gear with standard fillet, parameters are pressure angle on coast side, module, number of teeth and root fillet radius. For symmetric spur gear with standard fillet, parameters are pressure angle, module, number of teeth and root fillet radius.

To validate developed concept input parameters are required. For demonstration purpose any input parameters can be used with consideration of parameter selection presented in section 5. In this work all developed equations and programs are in generalization foam. So, any input can be used, But for illustration the parameters and material presented in table 8.1[96] & 8.2 [88, 96] are considered.

Table 8.4 Design parameters [96]

Design Parameters	**Value**	**Unit**
Pressure angle, Coast side	20^0	Degree
Number of teeth on pinion	25	-
Number of teeth on gear	25	-
Module	4	mm
Power	18	KW
Rotation	1600	RPM

Table 8.5 Material-Steel (Used for ANSYS analysis)[88,96]

Parameters	**Value**	**Unit**
Young Modules	$2x10^{11}$	N/m^2
Poisson ratio	0.266	-
Density	7860	Kg/m^3
Yield strength	$2.5x10^8$	N/m^2

Table 8.6 represent input and calculated parameters of symmetric involute spur gear ($\alpha_d=20^0$, $\alpha_c=20^0$) with normal fillet (ρ_F =1.2 mm) at root of tooth.

TABLE 8.6: Design parameters for Symmetric involute spur gear $\alpha_d=20^0$, $\alpha_c=20^0$) with normal fillet (ρ_F =1.2 mm) at root of tooth

	Parameter	**Symbol**	**Value**	**Unit**
Input Parameter	Pressure angle	α	20	Degree
	Module	m	4	-
	Number of teeth on pinion	Z_p	25	-
	Number of teeth on gear	Z_q	25	-
	Power	P	18	KW
	Rotation	RPM	1600	RPM
Selected input parameters	Radius of curvature of fillet curve	ρ_F	1.2 (*0.3m)*	mm
Calculated basic parameters	Pitch circle diameter	d_p	100	mm
	Pitch circle radius	r_p	50	mm
	Base circle radius	r_b	46.9876	mm
	Tip circle diameter	d_t	108	mm
	Tip circle radius	r_t	54	mm
Calculated Bending stress	Radius at HPSTC	r_{HPSTC}	50.5339	mm
	Contact ratio	ε	1.6128	-
	Tooth thickness at pitch circle	S_p	6.274	mm

equation parameters	Tip thickness at tip circle	S_t	2.876	mm
	Thickness of tooth at critical section	S_{Fn}	7.292	mm
	Bending moment arm height	h_{Fe}	2.6234	mm
	Load angle	α_{Fen}	0.3180	rad
	Torque	T_P	107.4295866	Nm
	Tangential load	F_t	2148.5	N

Table 8.7 represent input and calculated parameters of asymmetric involute spur gear ($\alpha_d=38^0$, $\alpha_c=20^0$) with normal fillet (ρ_F =1.2 mm) at root of tooth.

TABLE 8.7: Design parameters for asymmetric involute spur gear ($\alpha_d=38^0$, $\alpha_c=20^0$) with normal fillet (ρ_F =1.2 mm) at root of tooth

	Parameter	**Symbol**	**Value**	**Unit**
Input Parameter	Pressure angle on coast side	α_c	20	Degree
	Module	m	4	-
	Number of teeth on pinion	Z_p	25	-
	Number of teeth on gear	Z_g	25	-
	Power	P	18	KW
	Rotation	RPM	1600	RPM
Selected input parameters	Radius of curvature of fillet curve	ρ_F	1.2 (*0.3m)*	mm
Calculated basic parameters	Pitch circle diameter	d_p	100	mm
	Pitch circle radius	r_p	50	mm
	Base circle radius at coast side	r_{bc}	46.98766	mm
	Base circle radius at drive side	r_{bd}	39.41089	mm
	Tip circle diameter	d_t	108	mm
	Tip circle radius	r_t	54	mm
Calculated constrain to optimize drive side pressure angle	Contact ratio	ε	1.2416	-
	Tip thickness at tip circle	S_t	1.259	mm
Optimized drive side pressure angle	Pressure angle on drive side	α_d	38	Degree
Calculated Bending stress equation parameters	Radius at HPSTC	r_{HPSTC}	52.295	mm
	Tooth thickness at pitch circle	S_p	6.274	mm
	Thickness of tooth at critical section	S_{Fn}	8.6769	mm
	Tip thickness at tip circle	S_t	2.876	mm
	Bending moment arm height	h_{Fe}	4.4480	mm
	Load angle	α_{Fen}	0.691546	rad
	Torque	T_P	107.4295866	Nm
	Tangential load	F_t	2148.5	N

8.2.1 Symmetric involute spur gear $\alpha_d=20^0$, $\alpha_c=20^0$) with normal fillet (ρ_F =1.2 mm) at root of tooth

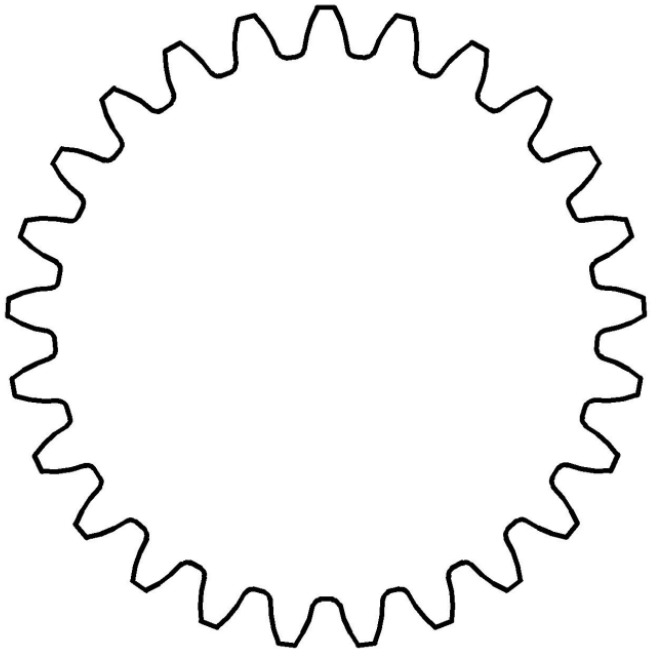

FIGURE 8.4: Profile of symmetric involute spur gear ($\alpha_d=20^0$, $\alpha_c=20^0$) with normal fillet (ρ_F =1.2 mm)

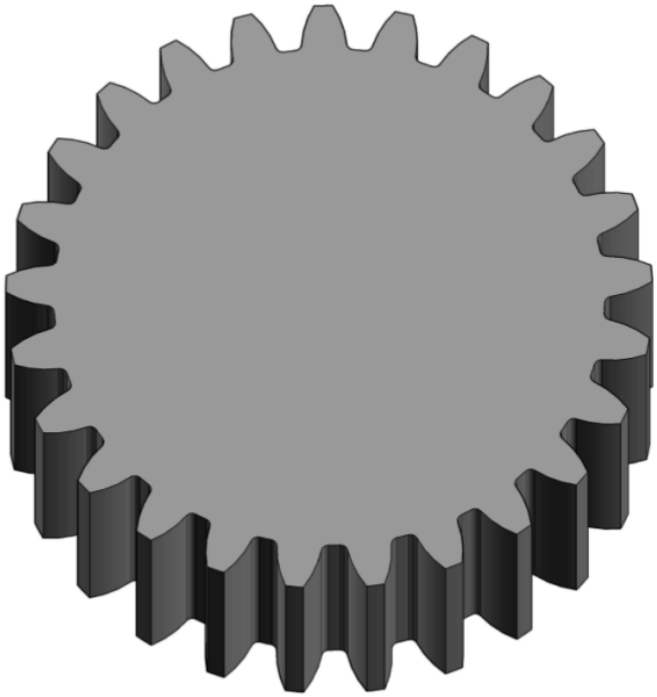

FIGURE 8.5: CAD model of Symmetric involute spur gear ($\alpha_d=20^0$, $\alpha_c=20^0$) with normal fillet (ρ_F =1.2 mm)

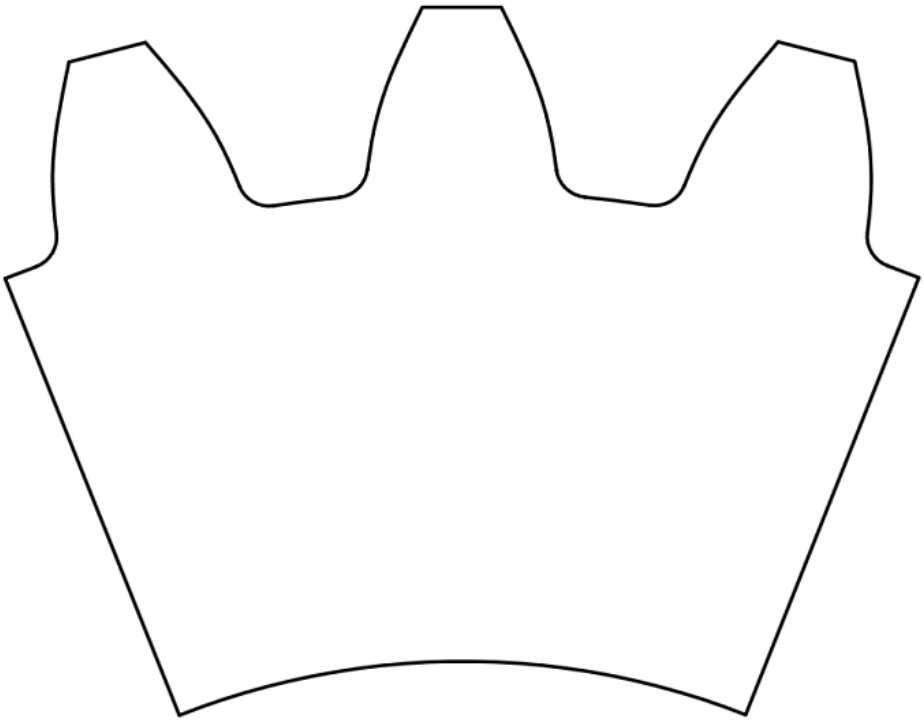

FIGURE 8.6: Segment of symmetric involute spur gear ($\alpha_d=20^0$, $\alpha_c=20^0$) with normal fillet (ρ_F =1.2 mm)

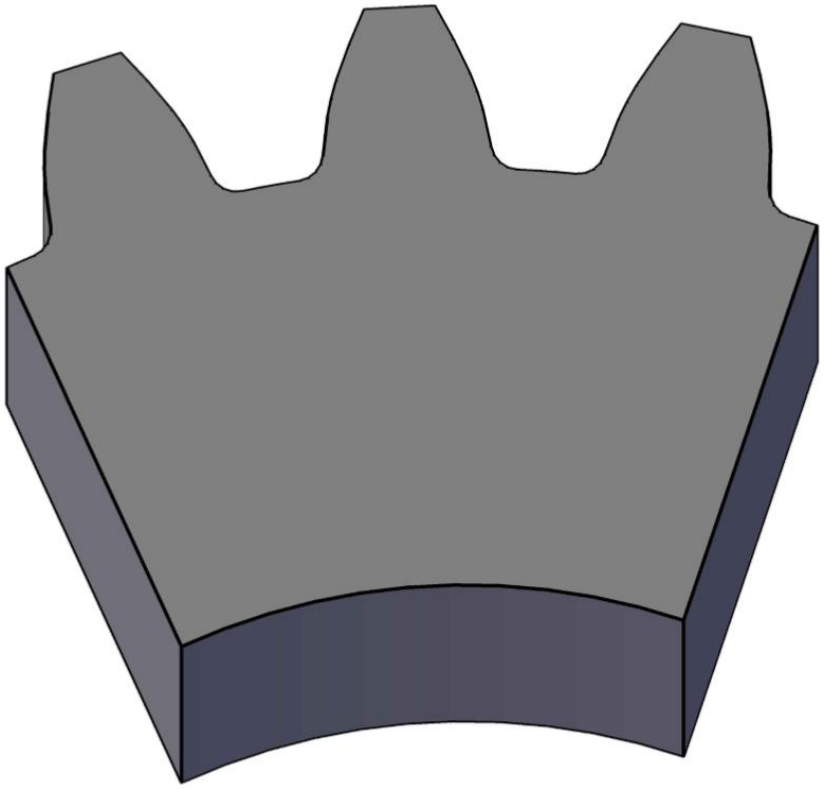

FIGURE 8.7: CAD model of segment of symmetric involute spur gear ($\alpha_d=20^0$, $\alpha_c=20^0$) with normal fillet (ρ_F =1.2 mm)

8.2.2 Asymmetric involute spur gear ($\alpha_d=38^0$, $\alpha_c=20^0$) with normal fillet (ρ_F =1.2 mm) at root of tooth

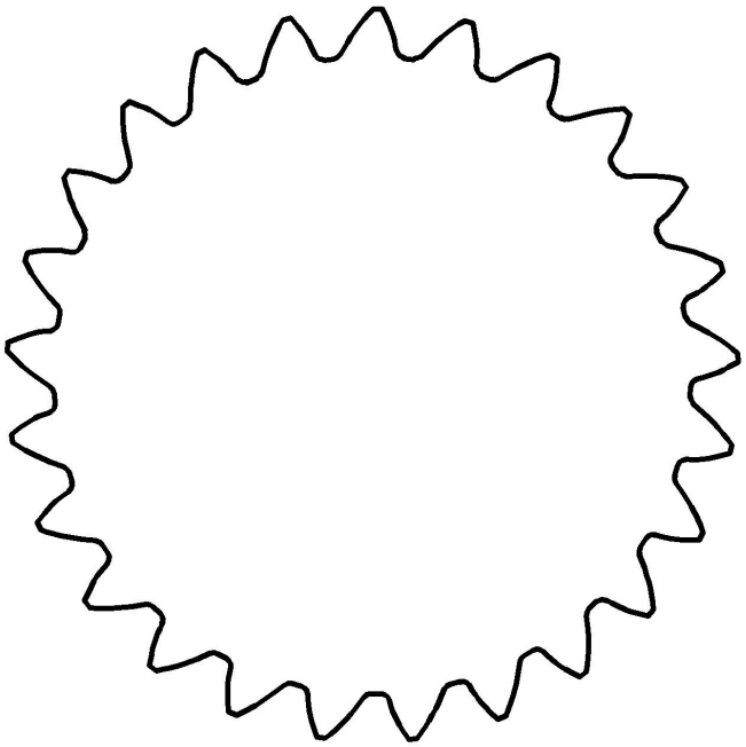

FIGURE 8.8: Profile of asymmetric involute spur gear ($\alpha d=38^0$, $\alpha c=20^0$) with normal fillet (ρ_F =1.2 mm) at root of tooth

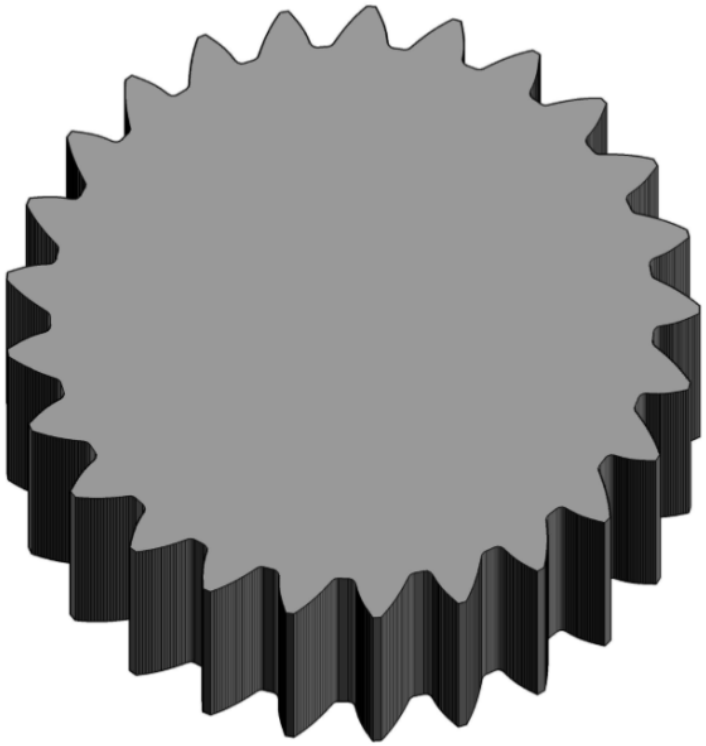

FIGURE 8.9: CAD model of asymmetric involute spur gear ($\alpha_d=38^0$, $\alpha_c=20^0$) with normal fillet (ρ_F =1.2 mm)

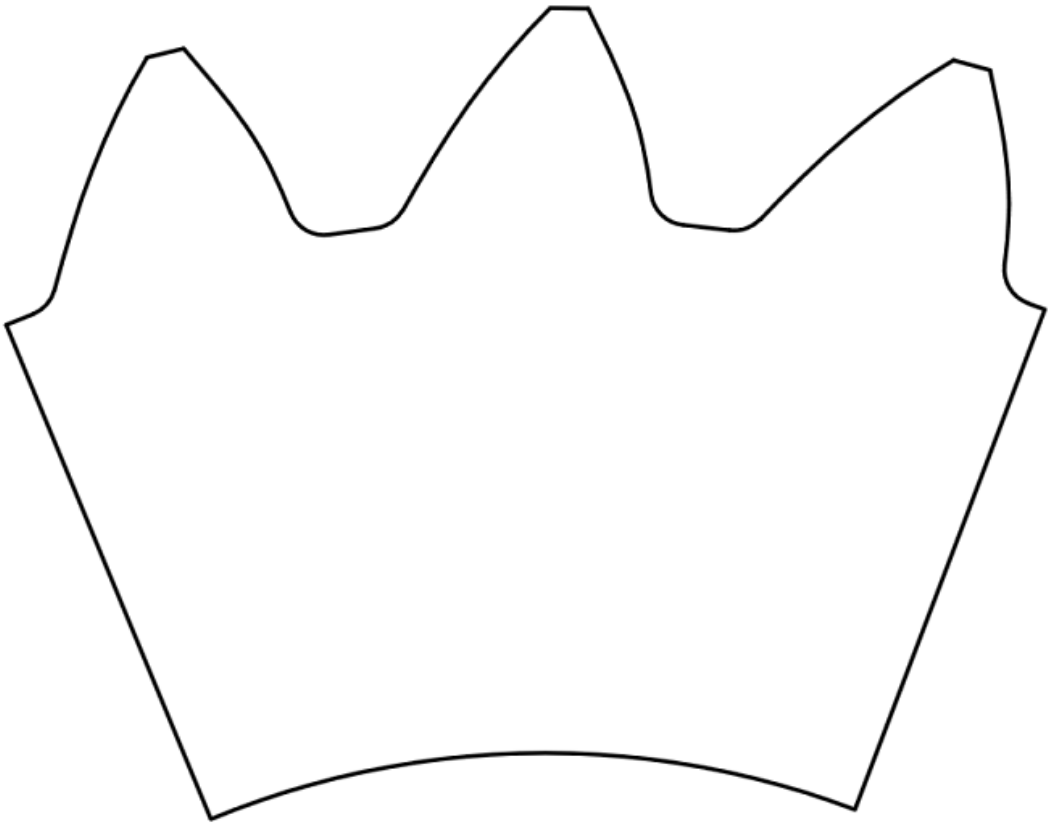

FIGURE 8.10: Segment of asymmetric involute spur gear ($\alpha d=38^0$, $\alpha c=20^0$) with normal fillet (ρ_F =1.2 mm) at root of tooth

FIGURE 8.11: CAD model of segment of asymmetric involute spur gear ($\alpha d=38^0$, $\alpha c=20^0$) with normal fillet (ρ_F =1.2 mm) at root of tooth

8.2.3 Asymmetric involute spur gear ($\alpha_d=38^0$, $\alpha_c=20^0$) with G2 continuity at root of tooth

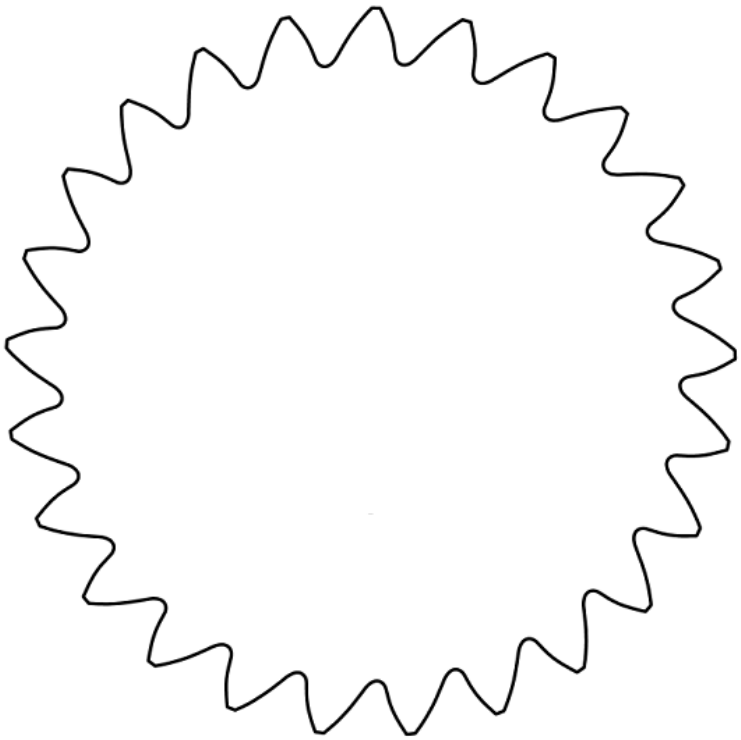

FIGURE 8.12: Profile of asymmetric involute spur gear ($\alpha_d=38^0$, $\alpha_c=20^0$) with G2 continuity at root of tooth

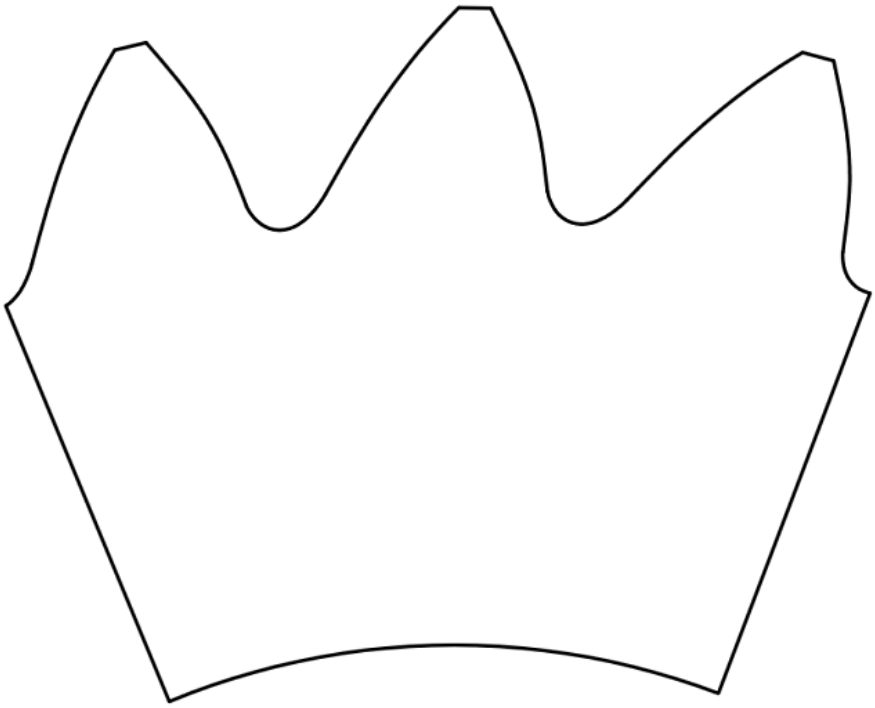

FIGURE 8.13: Segment of asymmetric involute spur gear ($\alpha_d=38^0$, $\alpha_c=20^0$) with G2 continuity at root of tooth

Developed algorithm is very useful to create location of point on involute profile and root profile. Using these points a required curve has been developed in AutoCAD modeling software. Involute profile and root profile of gear is very important in gear modeling and very difficult to develop exact geometry in CAD software. So, this algorithm useful to creates point on involute profile and root profile. Using these points a required curve has been developed in AutoCAD modeling software.

CHAPTER – 9

FINITE ELEMENT ANALYSIS

9.1 Introduction to Finite Element Analysis

Finite Element Analysis (FEA) is also known as Finite Element Method (FEM).It is a numerical method [85] to solve complex elastic and structural problems. This method is developed by Alexander Hrennikoff and Richard Courant [86].

Gear design is very complex procedure [1]. Good gear design will give high durability and consistency in power transmission [1]. AGMA [7] and ISO [8] published many numerical standards used to design gear. Gear design as per ISO and AGMA standard required FEA analysis to predict gear failure, estimates gears life in service [87] which is necessary for good gear design [88]. Then result will verified by experimental test on bending strength.

9.2 Procedure for finite element analysis

Finite element analysis is divided in three parts. First part is pre processing part which create virtual environment of object by given inputs, inform of geometry of object, element type, material of object, load location, boundary condition and discretization of object etc,. Second part is solution in which a desire effect has been given. Last part is post processing in which various or desire data is generated.

Since, gear tooth is considered as a cantilever beam which subjected load on drive side profile in line contact.

9.2.1 Preprocessing

In preprocessing stage following input data are required.

Geometric of gear: It is very difficult to generate CAD model in ANSYS directly. So, a required model has been generated in AutoCAD. Then that geometry is converted into IGES file. It can be transferred from AutoCAD to ANSYS.

Element type: Tetrahedral Solid element [85, 96, 97]

Material properties: Structural steel material is used and its property is presented in table 8.5 is used

Boundary conditions: in this analysis a gear is fixed from two sides and at rim.

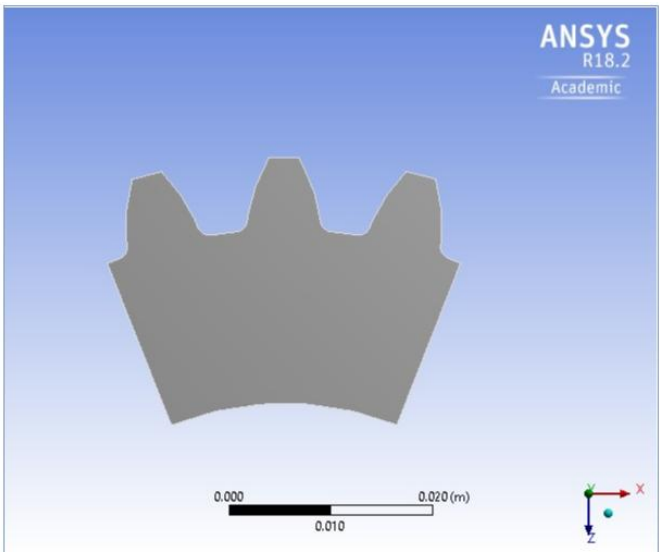

FIGURE 9.1: Imported model Geometric model for FEA

Discretization: It is a process of converting whole 3D model into very small elements. Tetrahedral solid elements [85, 96, 97] are used in this analysis. Meshed model as shown in figure 9.2

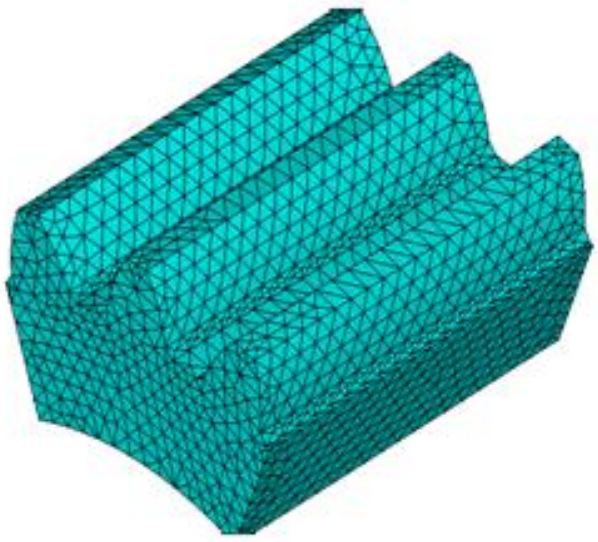

FIGURE 9.2: Meshed model of gear

Define the loadings: The gear tooth is loaded at HPSTC on drive side. Applied load is 2148.5 N.

9.2.2 Solution

Solution stage performed a task in software as per out requirements.

9.2.3 Post processing

The post processing stage involves with generation of required data by the software. Since in post processing a Von missed stress a shown in figure 9.3, 9.4 and 9.5 files are generated.

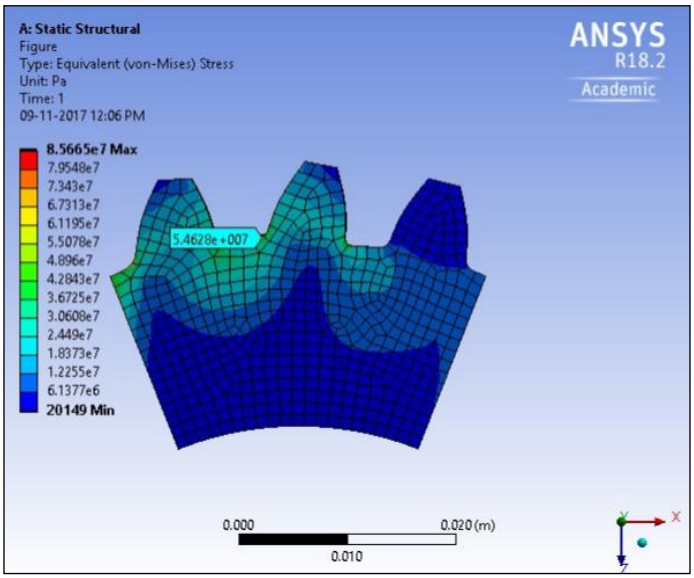

FIGURE 9.3: ANSYS Result for symmetric involute spur gear $\alpha_d=20^0$, $\alpha_c=20^0$) with normal fillet (ρ_F =1.2 mm) at root of tooth

Similar analyses were carried out for asymmetric spur gear with standard fillet and asymmetric spur gear with the modified root.

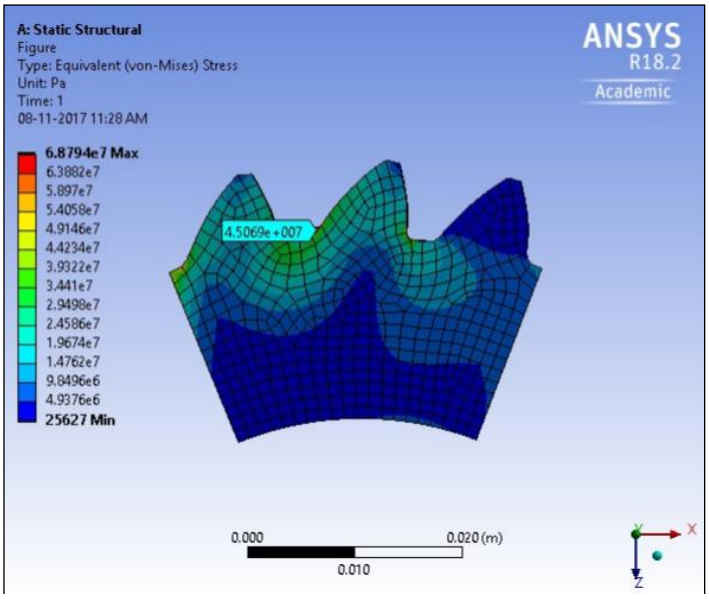

FIGURE 9.4: ANSYS Result for asymmetric involute spur gear ($\alpha_d=38^0$, $\alpha_c=20^0$) with normal fillet (ρ_F =1.2 mm) at root of tooth

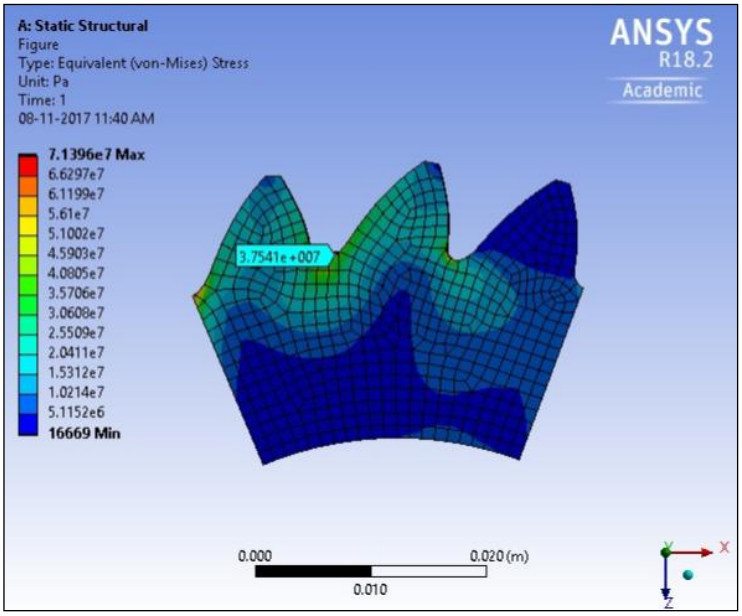

FIGURE 9.5: ANSYS Result for asymmetric involute spur gear ($\alpha_d=38^0$, $\alpha_c=20^0$) with G2 continuity at root of tooth

From this FEA analysis, obtained result of von-Mises stress for symmetric involute spur gear $\alpha_d=20^0$, $\alpha_c=20^0$) with normal fillet (ρ_F =1.2 mm) at root of tooth is 54.62 MPa. Obtained result of von-Mises stress for asymmetric involute spur gear ($\alpha_d=38^0$, $\alpha_c=20^0$) with normal fillet (ρ_F =1.2 mm) at root of tooth is 45.06 MPa. Obtained result of von-Mises stress for asymmetric involute spur gear ($\alpha_d=38^0$, $\alpha_c=20^0$) with G2 continuity at root of tooth is 37.54 MPa.

CHAPTER – 10

G- CODE FOR INVOLUTE SPUR GEAR

10.1 Introduction

Gear is a very important part of all machines. Gear design is very complicated process [1]. After a careful design of the gear, the next task is gear manufacturing. It is divided into two main categories namely forming and machining [1]. Forming include direct casting, drawing, molding, extrusion, powdered, heat softened materials. Machining involves roughing and finishing operations. Metal gears are produced by machining from the cast, hot rolled or forged blanks. Roughing processes include milling the tooth shape with formed cutters, generating the shape with a rack cutter, a shaping cutter or a hob cutter. It consists of forming, generation, shaping and hobbing processes [1]. Secondary finishing operation consists of Shaving, Grinding, Burnishing, Lapping and Honing [1].

Current researchers are works on the optimization of tooth root fillet which improve load carrying capacity and life [26-27, 29, 65, 67-68, 78-79, 84]. Roughing processes generates trochoidal at the root of the tooth [72, 74]. So, roughing processes are unable to obtain desire root profile as per design [72]. This thing will reduce the performance of gear in terms of load caring capacity and longer life [72]. So, an alternative manufacturing technique is required. Some researches have developed a form tool for desire root profile [89]. It makes a very costly manufacturing technique. Another approach is CNC wire cut machine to manufacture a gear as per the design parameter [90].

CNC (computer numerical control) works on a set of instruction in which the process is controlled by numbers, letters, and symbols. In CNC, the numbers, symbols form an instruction based program designed for a gear [90]. These instructions are called G-code. CNC works as per instruction given by G codes in the form of program to perform a task. Writing a program using G-code is very much complicated task and it requires high knowledge of the machine. Written codes may have faults which without performing the

operations is very difficult to find. Trial and error method is needed to identify the problems and make a successful product [90]. So, CAM software is required CAD model of gear to generate G-code [91]. CAD model requires modeling software.

CNC wire cut machine capable of manufacturing gear as per desire parameter [89] but require G code generation software and modeling software to create a CAD model [91,92].Optimize profile developed by a researcher is on equation-based and it is very difficult to create in CAD model [92]. So, Use of CNC wire cut depend on complicated CAD model [92] and G code generation software which is also complicated [91]. An alternative is required in this situation.

In this paper, authors generate G code without using a G code generation software and CAD model. The author used SciLab open source software to generate G code.

Very few works have been done in the area of profile cutting or G code generation. In 2002, Joseph B. Ferreira developed spreadsheets to cut profile of gear using laser cutters [98]. In 2008, O.Reyes et. al, developed an algorithm to describe spur gear profile[99]. In 2016, N K Mandal et. al, developed interactive spur gear generation using parametric programming with CNC end milling [100].

10.2 Symmetric involute spur gear tooth

Lots of researchers have been developed a gear tooth profile. In this work gear tooth profile given in section 3.2 and 3.3, has been considered. Equation 1[2] is used to develop an involute tooth profile of a gear. It depends on pressure angle (α) and radius r. It locates the point at any radius r on the involute profile of gear tooth as shown in figure 1. Circular root profile is widely used in design [68]. In this work, a circular root profile is considered at root of the tooth.

$$\theta_r = \frac{\pi}{2 \cdot z} + \tan\alpha - \alpha - \left(\tan\left(\cos^{-1}\left(\frac{r_p}{r}.\cos\alpha \right) \right) - \left(\cos^{-1}\left(\frac{r_p}{r}.\cos\alpha \right) \right) \right) \tag{9.1}$$

10.2.1Symmetric spur gear geometry

Figure 1 shows the symmetric spur gear tooth profile. Arc AB is a circular arc with center o1. Arc BC is involute arc developed by equation 1. Arc CD is a circular arc with center o. Arc DE is involute arc developed by equation 1. Arc EF is a circular arc with center o2. Arc FG is a circular arc with center o. To develop G code each point location is required. So, the locations of the points are given in table 1.

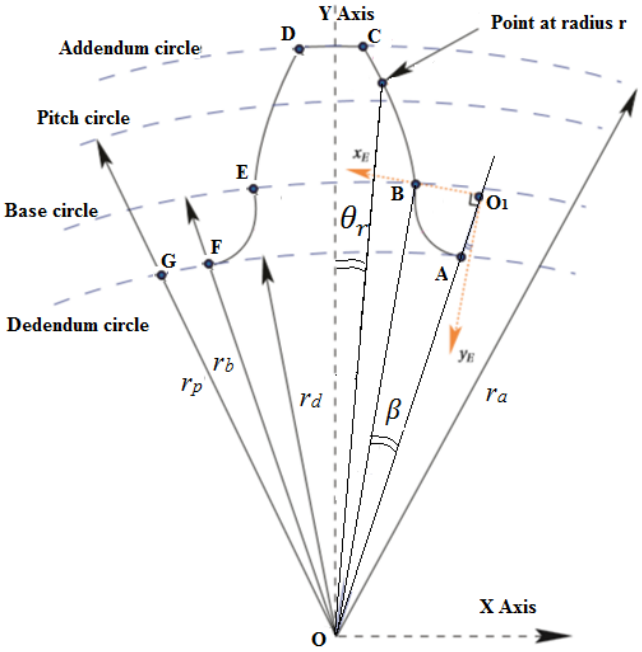

FIGURE 10.1: Symmetric spur gear geometry

TABLE 10.1: Cartesian coordinates of a point on symmetric spur gear tooth profile

Point	Cartesian Coordinates Equation
A	$x_A = r_d \cdot \cos(\theta_B + \beta)$ $y_A = r_d \cdot \sin(\theta_B + \beta)$ $\beta = \tan^{-1}\left(\frac{r}{r_b}\right)$ and $r = \frac{r_b^2 - r_d^2}{2r_b}$ $\theta_A = \frac{\pi}{2 \cdot z} + \tan\alpha - \alpha - \left(\tan\left(\cos^{-1}\left(\frac{r_p}{r_b}.\cos\alpha\right)\right) - \left(\cos^{-1}\left(\frac{r_p}{r_b}.\cos\alpha\right)\right)\right)$
B	$x_B = r_b \cdot \cos(\theta_B)$ $y_B = r_b \cdot \sin(\theta_B)$ $\theta_B = \frac{\pi}{2 \cdot z} + \tan\alpha - \alpha - \left(\tan\left(\cos^{-1}\left(\frac{r_p}{r_b}.\cos\alpha\right)\right) - \left(\cos^{-1}\left(\frac{r_p}{r_b}.\cos\alpha\right)\right)\right)$
C	$x_C = r_a \cdot \cos(\theta_C)$ $y_C = r_a \cdot \sin(\theta_C)$ $\theta_C = \frac{\pi}{2 \cdot z} + \tan\alpha - \alpha - \left(\tan\left(\cos^{-1}\left(\frac{r_p}{r_a}.\cos\alpha\right)\right) - \left(\cos^{-1}\left(\frac{r_p}{r_a}.\cos\alpha\right)\right)\right)$

D	$x_D = -r_a \cdot \cos(\theta_D)$ $y_D = r_a \cdot \sin(\theta_D)$ $\theta_D = \frac{\pi}{2 \cdot z} + \tan\alpha - \alpha - \left(\tan\left(\cos^{-1}\left(\frac{r_p}{r_a}.\cos\alpha \right) \right) - \left(\cos^{-1}\left(\frac{r_p}{r_a}.\cos\alpha \right) \right) \right)$
E	$x_E = -r_b \cdot \cos(\theta_E)$ $y_E = r_b \cdot \sin(\theta_E)$ $\theta_E = \frac{\pi}{2 \cdot z} + \tan\alpha - \alpha - \left(\tan\left(\cos^{-1}\left(\frac{r_p}{r_b}.\cos\alpha \right) \right) - \left(\cos^{-1}\left(\frac{r_p}{r_b}.\cos\alpha \right) \right) \right)$
F	$x_F = -r_d \cdot \cos(\theta_F + \beta)$ $y_F = r_d \cdot \sin(\theta_F + \beta)$ $\beta = \tan^{-1}\left(\frac{r}{r_b} \right)$ and $r = \frac{r_b^2 - r_d^2}{2r_b}$ $\theta_F = \frac{\pi}{2 \cdot z} + \tan\alpha - \alpha - \left(\tan\left(\cos^{-1}\left(\frac{r_p}{r_b}.\cos\alpha \right) \right) - \left(\cos^{-1}\left(\frac{r_p}{r_b}.\cos\alpha \right) \right) \right)$
G	$x_G = -r_d \cdot \cos\left(\frac{2 \cdot \pi}{z} - (\theta_G + \beta) \right)$ $y_G = r_d \cdot \sin\left(\frac{2 \cdot \pi}{z} - (\theta_G + \beta) \right)$ $\beta = \tan^{-1}\left(\frac{r}{r_b} \right)$ and $r = \frac{r_b^2 - r_d^2}{2r_b}$ $\theta_G = \frac{\pi}{2 \cdot z} + \tan\alpha - \alpha - \left(\tan\left(\cos^{-1}\left(\frac{r_p}{r_b}.\cos\alpha \right) \right) - \left(\cos^{-1}\left(\frac{r_p}{r_b}.\cos\alpha \right) \right) \right)$

10.2.2Algorithm to develop G code for symmetric involute spur gear

Algorithm for circular curve AB

In CNC machine for circular cutting G02 and G03 codes are available. G02 and G03 codes are used for clockwise and anticlockwise cutting operation respectively. Both codes require a current or starting position (point A), end or targeted position (point B) and radius of a circular arc. Syntax to write code is G02/G03 X Y Z R. G92 command is used to assign program zero. Point A is our program zero.

Calculate

$$r = \frac{r_b^2 - r_d^2}{2r_b} \text{ and } \beta = \tan^{-1}\left(\frac{r}{r_b}\right)$$

$$\theta_A = \frac{\pi}{2 \cdot z} + \tan\alpha - \alpha - \left(\tan\left(\cos^{-1}\left(\frac{r_p}{r_b}.\cos\alpha\right)\right) - \left(\cos^{-1}\left(\frac{r_p}{r_b}.\cos\alpha\right)\right)\right)$$

$$\theta_B = \frac{\pi}{2 \cdot z} + \tan\alpha - \alpha - \left(\tan\left(\cos^{-1}\left(\frac{r_p}{r_b}.\cos\alpha\right)\right) - \left(\cos^{-1}\left(\frac{r_p}{r_b}.\cos\alpha\right)\right)\right)$$

Start position: $x_A = r_d \cdot \cos(\theta_B + \beta)$ and $y_A = r_d \cdot \sin(\theta_B + \beta)$

End position: $x_B = r_b \cdot \cos(\theta_B)$ and $y_B = r_b \cdot \sin(\theta_B)$

Print G92 x_a y_a

Print G02 x_b y_b r

Algorithm for involute curve BC

In CNC machine for the involute cutting readymade code is not available. Using "for loop" code has been developed. Code G01 available for point to point cutting operation.

for (I = rb, I <= ra, I++)

{

$$\theta_I = \frac{\pi}{2 \cdot z} + \tan\alpha - \alpha - \left(\tan\left(\cos^{-1}\left(\frac{r_p}{I}.\cos\alpha\right)\right) - \left(\cos^{-1}\left(\frac{r_p}{I}.\cos\alpha\right)\right)\right)$$

$X = I \cdot \cos(\theta_I)$

$Y = I \cdot \sin(\theta_I)$

Print G01 X Y

}

Algorithm for circular curve CD

Circular curve CD starts from c point and end at d point with addendum circle radius. In G code program current location is known to the machine so, the endpoint only requires. Cutting operation takes place in an anticlockwise direction so G03 code is used.

Calculate

$$\theta_D = \frac{\pi}{2 \cdot z} + \tan\alpha - \alpha - \left(\tan\left(\cos^{-1}\left(\frac{r_p}{r_a}.\cos\alpha\right)\right) - \left(\cos^{-1}\left(\frac{r_p}{r_a}.\cos\alpha\right)\right)\right)$$

$x_D = -r_a \cdot \cos(\theta_D)$

$y_D = r_a \cdot \sin(\theta_D)$

Print G03 x_D y_D r_a

Algorithm for involute curve DE

In CNC machine for the involute cutting readymade code is not available. Here cutting operation takes place from point D to point E.

for (J = r_a, J <= r_b, J--)

{

$$\theta_J = \frac{\pi}{2 \cdot z} + \tan\alpha - \alpha - \left(\tan\left(\cos^{-1}\left(\frac{r_p}{J}.\cos\alpha \right) \right) - \left(\cos^{-1}\left(\frac{r_p}{J}.\cos\alpha \right) \right) \right)$$

$$X = -J \cdot \cos(\theta_J)$$

$$Y = J \cdot \sin(\theta_J)$$

Print G01 X Y

}

Algorithm for circular curve EF

Circular curve EF is started from E point and end at F point. In G code program current location is known to the machine so, the endpoint only requires. Cutting operation takes place in a clockwise direction so G02 code is used.

Calculate

$$x_F = -r_d \cdot \cos(\theta_F + \beta)$$

$$y_F = r_d \cdot \sin(\theta_F + \beta)$$

$$\beta = \tan^{-1}\left(\frac{r}{r_b} \right) \text{ and } r = \frac{r_b^2 - r_d^2}{2r_b}$$

$$\theta_F = \frac{\pi}{2 \cdot z} + \tan\alpha - \alpha - \left(\tan\left(\cos^{-1}\left(\frac{r_p}{r_b}.\cos\alpha \right) \right) - \left(\cos^{-1}\left(\frac{r_p}{r_b}.\cos\alpha \right) \right) \right)$$

Print G02 x_F y_F r

Algorithm for circular curve FG

Cutting operation takes place in an anticlockwise direction so G03 code is used.

Calculate

$$x_G = -r_d \cdot \cos\left(\frac{2\cdot\pi}{z} - (\theta_G + \beta)\right)$$

$$y_G = r_d \cdot \sin\left(\frac{2\cdot\pi}{z} - (\theta_G + \beta)\right)$$

$$\beta = \tan^{-1}\left(\frac{r}{r_b}\right) \text{ and } r = \frac{r_b^2 - r_d^2}{2r_b}$$

$$\theta_G = \frac{\pi}{2\cdot z} + \tan\alpha - \alpha - \left(\tan\left(\cos^{-1}\left(\frac{r_p}{r_b}.\cos\alpha\right)\right) - \left(\cos^{-1}\left(\frac{r_p}{r_b}.\cos\alpha\right)\right)\right)$$

Print G03 x_G y_G r

Above algorithm created for one tooth of gear as per input data. Using "for loop" for a given number of tooth repeat above cycle for complete gear profile.

10.3 Asymmetric involute spur gear tooth

10.3.1Asymmetric spur gear geometry

Figure 10.2 shows the asymmetric spur gear tooth profile.

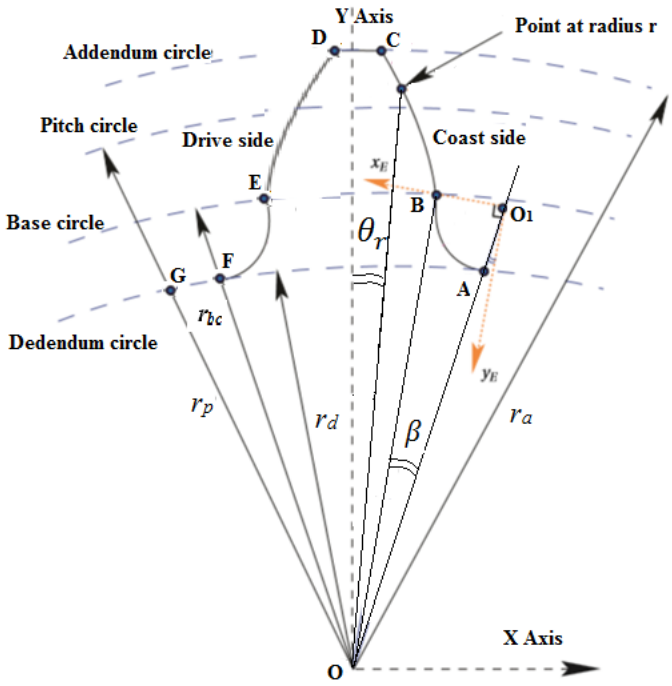

FIGURE 10.2: Asymmetric spur gear geometry

Arc AB is a circular arc with center o1. Arc BC is involute arc developed by equation 1. Arc CD is a circular arc with center o. Arc DE is involute arc developed by equation 1 but with different pressure angle as compare to involute arc BC. Due to higher pressure angle on involute profile DE, it becomes longer then involute arc BC. In this paper, both side involute profiles considered from tip of the tooth to base circle of coast side. Arc EF is a circular arc with center o2. Arc FG is a circular arc with center o. To develop G code each point location is required. So, the locations of the points are given in table 2.

TABLE 10.2: Cartesian coordinates of a point on asymmetric spur gear tooth profile

Point	Equation
A	$x_A = r_d \cdot \cos(\theta_B + \beta)$ $y_A = r_d \cdot \sin(\theta_B + \beta)$ $\beta = \tan^{-1}\left(\frac{r}{r_{bc}}\right)$ and $r = \frac{r_{bc}^2 - r_d^2}{2r_{bc}}$ $\theta_A = \frac{\pi}{2 \cdot z} + \tan\alpha_c - \alpha_c - \left(\tan\left(\cos^{-1}\left(\frac{r_p}{r_{bc}}.\cos\alpha_c\right)\right) - \left(\cos^{-1}\left(\frac{r_p}{r_{bc}}.\cos\alpha_c\right)\right)\right)$
B	$x_B = r_{bc} \cdot \cos(\theta_B)$ $y_B = r_{bc} \cdot \sin(\theta_B)$ $\theta_B = \frac{\pi}{2 \cdot z} + \tan\alpha_c - \alpha_c - \left(\tan\left(\cos^{-1}\left(\frac{r_p}{r_{bc}}.\cos\alpha_c\right)\right) - \left(\cos^{-1}\left(\frac{r_p}{r_{bc}}.\cos\alpha_c\right)\right)\right)$
C	$x_C = r_a \cdot \cos(\theta_C)$ $y_C = r_a \cdot \sin(\theta_C)$ $\theta_C = \frac{\pi}{2 \cdot z} + \tan\alpha_c - \alpha_c - \left(\tan\left(\cos^{-1}\left(\frac{r_p}{r_a}.\cos\alpha_c\right)\right) - \left(\cos^{-1}\left(\frac{r_p}{r_a}.\cos\alpha_c\right)\right)\right)$
D	$x_D = -r_a \cdot \cos(\theta_D)$ $y_D = r_a \cdot \sin(\theta_D)$ $\theta_D = \frac{\pi}{2 \cdot z} + \tan\alpha_d - \alpha_d - \left(\tan\left(\cos^{-1}\left(\frac{r_p}{r_a}.\cos\alpha_d\right)\right) - \left(\cos^{-1}\left(\frac{r_p}{r_a}.\cos\alpha_d\right)\right)\right)$
E	$x_E = -r_{bc} \cdot \cos(\theta_E)$ $y_E = r_{bc} \cdot \sin(\theta_E)$

	$\theta_E = \frac{\pi}{2 \cdot z} + \tan\alpha_d - \alpha_d - \left(\tan\left(\cos^{-1}\left(\frac{r_p}{r_{bc}} . \cos\alpha_d \right) \right) - \left(\cos^{-1}\left(\frac{r_p}{r_{bc}} . \cos\alpha_d \right) \right) \right)$
F	$x_F = -r_d \cdot \cos(\theta_F + \beta)$ $y_F = r_d \cdot \sin(\theta_F + \beta)$ $\beta = \tan^{-1}\left(\frac{r}{r_{bc}} \right)$ and $r = \frac{r_{bc}^2 - r_d^2}{2 r_{bc}}$ $\theta_F = \frac{\pi}{2 \cdot z} + \tan\alpha_d - \alpha_d - \left(\tan\left(\cos^{-1}\left(\frac{r_p}{r_{bc}} . \cos\alpha_d \right) \right) - \left(\cos^{-1}\left(\frac{r_p}{r_{bc}} . \cos\alpha_d \right) \right) \right)$
G	$x_G = -r_d \cdot \cos\left(\frac{2 \cdot \pi}{z} - (\theta_G + \beta) \right)$ $y_G = r_d \cdot \sin\left(\frac{2 \cdot \pi}{z} - (\theta_G + \beta) \right)$ $\beta = \tan^{-1}\left(\frac{r}{r_{bc}} \right)$ and $r = \frac{r_{bc}^2 - r_d^2}{2 r_{bc}}$ $\theta_G = \frac{\pi}{2 \cdot z} + \tan\alpha_d - \alpha_d - \left(\tan\left(\cos^{-1}\left(\frac{r_p}{r_{bc}} . \cos\alpha_d \right) \right) - \left(\cos^{-1}\left(\frac{r_p}{r_{bc}} . \cos\alpha_d \right) \right) \right)$

10.3.2Algorithm to develop G code for asymmetric spur gear

Algorithm for circular curve AB

In CNC machine for circular cutting G02 and G03 codes are available. G02 and G03 codes are used for clockwise and anticlockwise cutting operation respectively. Both codes require a current or starting position (point A), end or targeted position (point B) and radius of a circular arc. Syntax to write code is G02/G03 X Y Z R. G92 command is used to assign program zero. Point A is our program zero.

Calculate

$$\beta = \tan^{-1}\left(\frac{r}{r_{bc}} \right) \text{ and } r = \frac{r_{bc}^2 - r_d^2}{2 r_{bc}}$$

$$\theta_A = \frac{\pi}{2 \cdot z} + \tan\alpha_c - \alpha_c - \left(\tan\left(\cos^{-1}\left(\frac{r_p}{r_{bc}} . \cos\alpha_c \right) \right) - \left(\cos^{-1}\left(\frac{r_p}{r_{bc}} . \cos\alpha_c \right) \right) \right)$$

$$\theta_B = \frac{\pi}{2 \cdot z} + \tan\alpha_c - \alpha_c - \left(\tan\left(\cos^{-1}\left(\frac{r_p}{r_{bc}} . \cos\alpha_c \right) \right) - \left(\cos^{-1}\left(\frac{r_p}{r_{bc}} . \cos\alpha_c \right) \right) \right)$$

Start position: $x_A = r_d \cdot \cos(\theta_B + \beta)$ and $y_A = r_d \cdot \sin(\theta_B + \beta)$

End position: $x_B = r_{bc} \cdot \cos(\theta_B)$ and $y_B = r_{bc} \cdot \sin(\theta_B)$

Print G92 x_a y_a

Print G02 x_b y_b r

Algorithm for involute curve BC

In CNC machine for the involute cutting readymade code is not available. Using "for loop" code has been developed. Code G01 available for point to point cutting operation.

for (I = r_{bc}, I <= r_a, I++)

{

$$\theta_I = \frac{\pi}{2 \cdot z} + \tan\alpha_c - \alpha_c - \left(\tan\left(\cos^{-1}\left(\frac{r_p}{I}.\cos\alpha_c \right) \right) - \left(\cos^{-1}\left(\frac{r_p}{I}.\cos\alpha_c \right) \right) \right)$$

$$X = I \cdot \cos(\theta_I)$$

$$Y = I \cdot \sin(\theta_I)$$

Print G01 X Y

}

Algorithm for circular curve CD

Circular curve CD starts from c point and end at d point with addendum circle radius. In G code program current location is known to the machine so, the endpoint only requires. Cutting operation takes place in an anticlockwise direction so G03 code is used.

Calculate

$$\theta_D = \frac{\pi}{2 \cdot z} + \tan\alpha_d - \alpha_d - \left(\tan\left(\cos^{-1}\left(\frac{r_p}{r_a}.\cos\alpha_d \right) \right) - \left(\cos^{-1}\left(\frac{r_p}{r_a}.\cos\alpha_d \right) \right) \right)$$

$$x_D = -r_a \cdot \cos(\theta_D)$$

$$y_D = r_a \cdot \sin(\theta_D)$$

Print G03 x_D y_D r_a

Algorithm for involute curve DE

In CNC machine for the involute cutting readymade code is not available. Here cutting operation takes place from point D to point E.

for (J = r_a, J <= r_{bc}, J--)

{

$$\theta_J = \frac{\pi}{2 \cdot z} + \tan\alpha_d - \alpha_d - \left(\tan\left(\cos^{-1}\left(\frac{r_p}{J}.\cos\alpha_d \right) \right) - \left(\cos^{-1}\left(\frac{r_p}{J}.\cos\alpha_d \right) \right) \right)$$

$$X = -J \cdot \cos(\theta_J)$$

$$Y = J \cdot \sin(\theta_J)$$

Print G01 X Y
}

Algorithm for circular curve EF

Circular curve EF is started from E point and end at F point. In G code program current location is known to the machine so, the endpoint only requires. Cutting operation takes place in a clockwise direction so G02 code is used.

Calculate

$$x_F = -r_d \cdot \cos(\theta_F + \beta)$$

$$y_F = r_d \cdot \sin(\theta_F + \beta)$$

$$\beta = \tan^{-1}\left(\frac{r}{r_{bc}} \right) \text{ and } r = \frac{r_{bc}^2 - r_d^2}{2 r_{bc}}$$

$$\theta_F = \frac{\pi}{2 \cdot z} + \tan\alpha_d - \alpha_d - \left(\tan\left(\cos^{-1}\left(\frac{r_p}{r_{bc}}.\cos\alpha_d \right) \right) - \left(\cos^{-1}\left(\frac{r_p}{r_{bc}}.\cos\alpha_d \right) \right) \right)$$

Print G02 x_F y_F r

Algorithm for circular curve FG

Cutting operation takes place in an anticlockwise direction so G03 code is used.

Calculate

$$x_G = -r_d \cdot \cos\left(\frac{2 \cdot \pi}{z} - (\theta_G + \beta) \right)$$

$$y_G = r_d \cdot \sin\left(\frac{2 \cdot \pi}{z} - (\theta_G + \beta) \right)$$

$$\beta = \tan^{-1}\left(\frac{r}{r_{bc}} \right) \text{ and } r = \frac{r_{bc}^2 - r_d^2}{2 r_{bc}}$$

$$\theta_G = \frac{\pi}{2 \cdot z} + \tan\alpha_d - \alpha_d - \left(\tan\left(\cos^{-1}\left(\frac{r_p}{r_{bc}} . \cos\alpha_d \right) \right) - \left(\cos^{-1}\left(\frac{r_p}{r_{bc}} . \cos\alpha_d \right) \right) \right)$$

Print G03 x_G y_G r

Above algorithm created for one tooth of gear as per input data. Using "for loop" for a given number of tooth repeat above cycle for complete gear profile.

Similarly, an algorithm can be created for asymmetric spur gear and internal symmetric, asymmetric spur gear.

10.4 Asymmetric involute spur gear with modified root profile

10.4.1 Asymmetric spur gear with modified root profile geometry

Modified root profile is presented in chapter 8.3. Asymmetric spur with modified root profile is shown in figure.

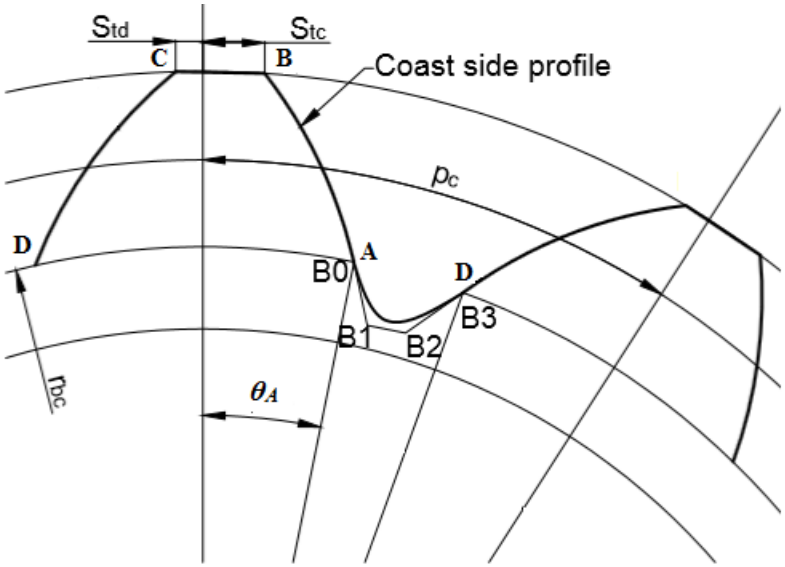

FIGURE 10.3: Asymmetric gear with optimized fillet at tooth root with G2 continuity

TABLE 10.3: Cartesian coordinates of a point on asymmetric spur gear tooth profile with modified fillet

Point	Equations of Cartesian Coordinates of points
A	$x_A = r_{bc} \cdot \cos(\theta_A)$ $y_A = r_{bc} \cdot \sin(\theta_A)$ $\theta_A = \frac{\pi}{2 \cdot z} + \tan\alpha_c - \alpha_c - \left(\tan\left(\cos^{-1}\left(\frac{r_p}{r_{bc}} . \cos\alpha_c \right) \right) - \left(\cos^{-1}\left(\frac{r_p}{r_{bc}} . \cos\alpha_c \right) \right) \right)$
B	$x_B = r_a \cdot \cos(\theta_B)$

	$y_B = r_a \cdot \sin(\theta_B)$ $\theta_B = \frac{\pi}{2 \cdot z} + \tan\alpha_c - \alpha_c - \left(\tan\left(\cos^{-1}\left(\frac{r_p}{r_a}.\cos\alpha_c \right) \right) - \left(\cos^{-1}\left(\frac{r_p}{r_a}.\cos\alpha_c \right) \right) \right)$
C	$x_C = -r_a \cdot \cos(\theta_C)$ $y_C = r_a \cdot \sin(\theta_C)$ $\theta_C = \frac{\pi}{2 \cdot z} + \tan\alpha_d - \alpha_d - \left(\tan\left(\cos^{-1}\left(\frac{r_p}{r_a}.\cos\alpha_d \right) \right) - \left(\cos^{-1}\left(\frac{r_p}{r_a}.\cos\alpha_d \right) \right) \right)$
D	$x_D = -r_{bc} \cdot \cos(\theta_D)$ $y_D = r_{bc} \cdot \sin(\theta_D)$ $\theta_D = \frac{\pi}{2 \cdot z} + \tan\alpha_d - \alpha_d - \left(\tan\left(\cos^{-1}\left(\frac{r_p}{r_{bc}}.\cos\alpha_d \right) \right) - \left(\cos^{-1}\left(\frac{r_p}{r_{bc}}.\cos\alpha_d \right) \right) \right)$

10.4.2Algorithm to develop G code for asymmetric spur gear with modified root profile

Algorithm for circular curve AB

In CNC machine for circular cutting G02 and G03 codes are available. G02 and G03 codes are used for clockwise and anticlockwise cutting operation respectively. Both codes require a current or starting position (point A), end or targeted position (point B) and radius of a circular arc. Syntax to write code is G02/G03 X Y Z R. G92 command is used to assign program zero. Point A is our program zero.

Calculate

$$\theta_A = \frac{\pi}{2 \cdot z} + \tan\alpha_c - \alpha_c - \left(\tan\left(\cos^{-1}\left(\frac{r_p}{r_{bc}}.\cos\alpha_c \right) \right) - \left(\cos^{-1}\left(\frac{r_p}{r_{bc}}.\cos\alpha_c \right) \right) \right)$$

$$\theta_B = \frac{\pi}{2 \cdot z} + \tan\alpha_c - \alpha_c - \left(\tan\left(\cos^{-1}\left(\frac{r_p}{r_a}.\cos\alpha_c \right) \right) - \left(\cos^{-1}\left(\frac{r_p}{r_a}.\cos\alpha_c \right) \right) \right)$$

Start position: $x_A = r_{bc} \cdot \cos(\theta_A)$ and $y_A = r_{bc} \cdot \sin(\theta_A)$

End position: $x_B = r_a \cdot \cos(\theta_B)$ and $y_B = r_a \cdot \sin(\theta_B)$

Print G92 x_a y_a

for (I = r_{bc}, I <= r_a, I++)

{

$$\theta_I = \frac{\pi}{2 \cdot z} + \tan\alpha_c - \alpha_c - \left(\tan\left(\cos^{-1}\left(\frac{r_p}{I}.\cos\alpha_c \right) \right) - \left(\cos^{-1}\left(\frac{r_p}{I}.\cos\alpha_c \right) \right) \right)$$

$$X = I \cdot \cos(\theta_I)$$

$$Y = I \cdot \sin(\theta_I)$$

Print G01 X Y

}

Algorithm for circular curve BC

Circular curve BC starts from B point and end at C point with addendum circle radius. In G code program current location is known to the machine so, the endpoint only requires. Cutting operation takes place in an anticlockwise direction so G03 code is used.

Calculate

$$x_C = -r_a \cdot \cos(\theta_C)$$

$$y_C = r_a \cdot \sin(\theta_C)$$

$$\theta_C = \frac{\pi}{2 \cdot z} + \tan\alpha_d - \alpha_d - \left(\tan\left(\cos^{-1}\left(\frac{r_p}{r_a}.\cos\alpha_d \right) \right) - \left(\cos^{-1}\left(\frac{r_p}{r_a}.\cos\alpha_d \right) \right) \right)$$

Print G03 x_C y_C r_a

Algorithm for involute curve CD

In CNC machine for the involute cutting readymade code is not available. Here cutting operation takes place from point C to point D.

for (J = r_a, J <= r_{bc}, J--)

{

$$\theta_J = \frac{\pi}{2 \cdot z} + \tan\alpha_d - \alpha_d - \left(\tan\left(\cos^{-1}\left(\frac{r_p}{J}.\cos\alpha_d \right) \right) - \left(\cos^{-1}\left(\frac{r_p}{J}.\cos\alpha_d \right) \right) \right)$$

$$X = -J \cdot \cos(\theta_J)$$

$$Y = J \cdot \sin(\theta_J)$$

Print G01 X Y

}

Algorithm to develop G code for root profile

Calculate

Location of point B0:

$$x_{B0} = r_{bc} \cdot \cos(\theta_{B0})$$

$$y_{B0} = r_{bc} \cdot \sin(\theta_{B0})$$

$$\theta_{B0} = \frac{\pi}{2 \cdot z} + \tan\alpha_c - \alpha_c - \left(\tan\left(\cos^{-1}\left(\frac{r_p}{r_{bc}} . \cos\alpha_c \right) \right) - \left(\cos^{-1}\left(\frac{r_p}{r_{bc}} . \cos\alpha_c \right) \right) \right)$$

Location of point B3:

$$x_{B3} = r_{bc} \cdot \cos\left(\frac{2\pi}{z} - \theta_{B3} \right)$$

$$y_{B3} = r_{bc} \cdot \sin\left(\frac{2\pi}{z} - \theta_{B3} \right)$$

$$\theta_{B3} = \frac{\pi}{2 \cdot z} + \tan\alpha_d - \alpha_d - \left(\tan\left(\cos^{-1}\left(\frac{r_p}{r_{bc}} . \cos\alpha_d \right) \right) - \left(\cos^{-1}\left(\frac{r_p}{r_{bc}} . \cos\alpha_d \right) \right) \right)$$

Location of point B1 and B2 can be achieved by method presented in chapter 7.

```
for (t = 0.0; t < 1.0; t += 0.05)
{
xt=((1-t)*(1-t)*(1-t)*x0)+(3*t*(1-t)*(1-t)*x1)+(3*t*t*(1-t)*x2)+(t*t*t*x3)
yt=((1-t)*(1-t)*(1-t)*y0)+(3*t*(1-t)*(1-t)*y1)+(3*t*t*(1-t)*y2)+(t*t*t*y3)
print G01 xt yt
}
```

Developed algorithm is very useful to create G code for CNC.

CHAPTER – 11

RESULTS, DISCUSSION AND APPLICATION

11.1 Parametric analysis

In the Parametric analysis for the various parameters have been generated using developed equations. So, it is globally applicable. For given input parameter it is easy to create data set and predict optimize drive side pressure angle and % reduction in bending stress without using FEA.

Application - to obtain optimize pressure angle of drive side

Parametric analysis help to identify value of constraint parameters for optimization of drive side pressure angle. For parameter presented in table 5.1, at contact ratio (ε) $\leq$ 1.1, pressure angle is 38^0 as per table 2, which is a safe condition and at 1unit (*0.25m*) tip thickness pressure angle is 40^0 as per table 8, which is a safe condition. At 38^0 pressure angle on the drive side profile, it satisfies both conditions/constraints. So, based on above constraint optimize drive side pressure angle is 38^0.

Application - to obtain % reduction of bending stress at the root of tooth

From table 5.16, it is found that for symmetric spur gear tooth ($\alpha_d = \alpha_c = 20^0$ and ρ_F = *0.3m* = 1.2 mm) and asymmetric spur gear tooth ($\alpha_d = 38^0$, $\alpha_c = 20^0$ and ρ_F = *0.3m* =1.2 mm) bending stress obtain from parametric analysis is 240.46 and 198.58 respectively. For comparison result is presented in table 11.1.

Based on parametric analysis it is found that banding stress is reducing by 17.41 % compared with normal profile symmetric gear.

From FEA conducted in chapter 10, it is found that for symmetric spur gear tooth ($\alpha_d = \alpha_c = 20^0$ and ρ_F = *0.3m* = 1.2 mm) and asymmetric spur gear tooth ($\alpha_d = 38^0$, $\alpha_c = 20^0$ and ρ_F = 0.3m =1.2 mm) Von Mises stress is 54.62 MPa and 45.06 MPa respectively. For comparison result is presented in table 11.1

Based on FEA analysis it observed that Von Mises stress is reducing by 17.50 %

compared to normal profile symmetric gear.

From table 11.1, it is observed that % reduction in bending stress obtained from FEA and parametric analysis is approximately the same so it justifies parametric analysis.

TABLE 11.1: Comparison of ANSYS and parametric analysis result

Sr. No.	Condition	ANSYS result of bending stress	Parametric analysis result obtain form equations
1	Bending stress of symmetric gear ($\alpha_d = \alpha_c = 20^0$ and $\rho_F = 1.2$ mm)	54.62	240.46 [table 5.16]
2	Bending stress if asymmetric gear ($\alpha_d = 38^0$, $\alpha_c = 20^0$ and $\rho_F = 1.2$ mm)	45.06	198.58 [table 5.16]
3	% reduction in bending stress	17.50%	17.41%

It shows that parametric analysis can be replacing FEA to predict or calculate % reduction in bending stress at the root of the tooth.

In addition to above from table 5.16, it is observed that for *($\rho_F = 0.2m$)* at $\alpha_d = 38^0$, $\alpha_c = 20^0$, nominal bending stress is 235.319. Which is higher than *($\rho_F = 0.3m$)* at $\alpha_d = 38^0$, $\alpha_c = 20^0$.simillaly for *($\rho_F = 0.4m$)* at $\alpha_d = 38^0$, $\alpha_c = 20^0$, nominal bending stress is 176.056. Which is less than for *($\rho_F = 0.3m$)* at $\alpha_d = 38^0$, $\alpha_c = 20^0$.

But for *($\rho_F = 0.2m$)* at $\alpha_d = 38^0$, $\alpha_c = 20^0$, 19.89% reduction in bending stress can be achieved which is higher in all three cases. These types of prediction only possible using parametric analysis.

For given input parameter it is easy to create data set and predict optimize drive side pressure angle and % reduction in bending stress without using FEA.

11.2 Objective function

Objective function has been developed using standard bending stress equation and developed equations of "bending stress equation parameters" to minimize bending stress at critical section of tooth.

Objective function gives nominal bending stress for given input parameters. Main application of objective function is to calculate multiplication factor.

Application - Multiplication factor

In research, many researcher works on same design of gear with different parameters to obtain optimize design parameters. Researcher develops various CAD model for FEM. For example in asymmetric gear to optimize pressure angle, different pressure angle drive side CAD model is required. Then all CAD model are analyzed in FEM simulator to predict bending stress at root of tooth. In such situation, researchers need to develop each CAD model and also need to create virtual environment in FEM simulator. It required lots of time and work. To avoid such situation, in this research author developed method to calculate multiplication factor (MF) for given material and gear design parameters (module, number of tooth on gear and pinion). Multiplication factor is eliminates multiple FEM analysis to calculate bending stress at root of symmetric and asymmetric gear.

To demonstrate concept of multiplication factor current case has been considered. Author calculate multiplication factor by comparing result of bending stress obtain from developed equations and FEA for symmetric spur gear. Using multiplication factor, author calculate bending stress for asymmetric gear and then it is compared to FEA result of asymmetric gear.

Multiplication factor has been calculated by comparing the bending stress obtains from FEA and developed equations result of symmetric gear.

TABLE 11.2: Comparison of result of bending stress obtained from FEA and equations

Gear	Bending stress obtain from objective function	Bending stress obtain from FEA	Multiplication factor
Bending stress of symmetric gear ($\alpha_d = \alpha_c = 20^0$ and $\rho_F = 1.2$ mm)	240.762	54.62 Mpa	0.22686

From table 11.2, Multiplication factor is 0.22686. Now calculate Bending stress for asymmetric gear.

TABLE 11.3: Calculation of bending stress for asymmetric gear using multiplication factor

Gear	Bending stress obtain from objective function	Multiplication factor	Bending stress obtain from MF	FEA result
Bending stress of asymmetric gear ($\alpha_d = 38^0$, $\alpha_c = 20^0$ and $\rho_F = 1.2$ mm)	198.58	0.22686	45.52	45.06

It is found that result calculated from multiplication factor and FEA for asymmetric gear is nearly same. So, concept of multiplication factor is verified. Multiplication factor is eliminates multiple FEM analysis to calculate bending stress at root of symmetric and asymmetric gear.

In this research author developed method to calculate multiplication factor (MF) for given material and gear design parameters (module, number of tooth on gear and pinion) for different pressure angle condition. But it is need to verify this phenomena for other different condition like load, material, thickness of gear and many more.

12.3 Optimization of root profile

An algorithm to create exact CAD model has been developed. Code presented in ANEXTURE I is used to obtain required coordinate points on involute profile are presented in table 11.4.

TABLE 11.4: Created coordinate points on involute profile spur using code

	Symmetric involute spur gear	Asymmetric involute spur gear
Input	Enter module in mm =4 Enter number of teeth on gear =25 Enter pressure angle on coast side in degree =20 Enter pressure angle on drive side in degree =20	Enter module in mm =4 Enter number of teeth on gear =25 Enter pressure angle on coast side in degree =20 Enter pressure angle on drive side in degree =38
Output	POINT 46.842856,3.647239 POINT 47.850439,3.586123 POINT 48.866108,3.405524 POINT 49.885747,3.142547 POINT 50.907163,2.809506 POINT 51.928593,2.413104 POINT 52.948455,1.957619 POINT 53.965261,1.446037 POINT 53.980857,-1.437749 POINT 52.964109,-1.950174 POINT 51.944283,-2.406542 POINT 50.922866,-2.803880 POINT 49.901436,-3.137936 POINT 48.881755,-3.402062 POINT 47.866004,-3.584080 POINT 46.858199,-3.648171	POINT 46.842856,3.647239 POINT 47.850439,3.586123 POINT 48.866108,3.405524 POINT 49.885747,3.142547 POINT 50.907163,2.809506 POINT 51.928593,2.413104 POINT 52.948455,1.957619 POINT 53.965261,1.446037 POINT 53.999696,0.181260 POINT 52.994945,-0.731984 POINT 51.975683,-1.590099 POINT 50.943858,-2.392344 POINT 49.901436,-3.137936 POINT 48.850400,-3.826015 POINT 47.792757,-4.455604 POINT 46.730544,-5.025558

Using created points a curve has been developed in AutoCAD software. It is shown in figure 11.1 and 11.2. Using these points a required curve has been developed in

AutoCAD modeling software. Involute profile and root profile of gear is very important in gear modeling and very difficult to develop exact geometry in CAD software. So, this algorithm useful to creates point on involute profile and root profile. Using these points a required curve has been developed in AutoCAD modeling software.

Using above method a involute profile for symmetric and asymmetric spur gear is generated as shown in figure 8.4 to 8.13 in AutoCAD.

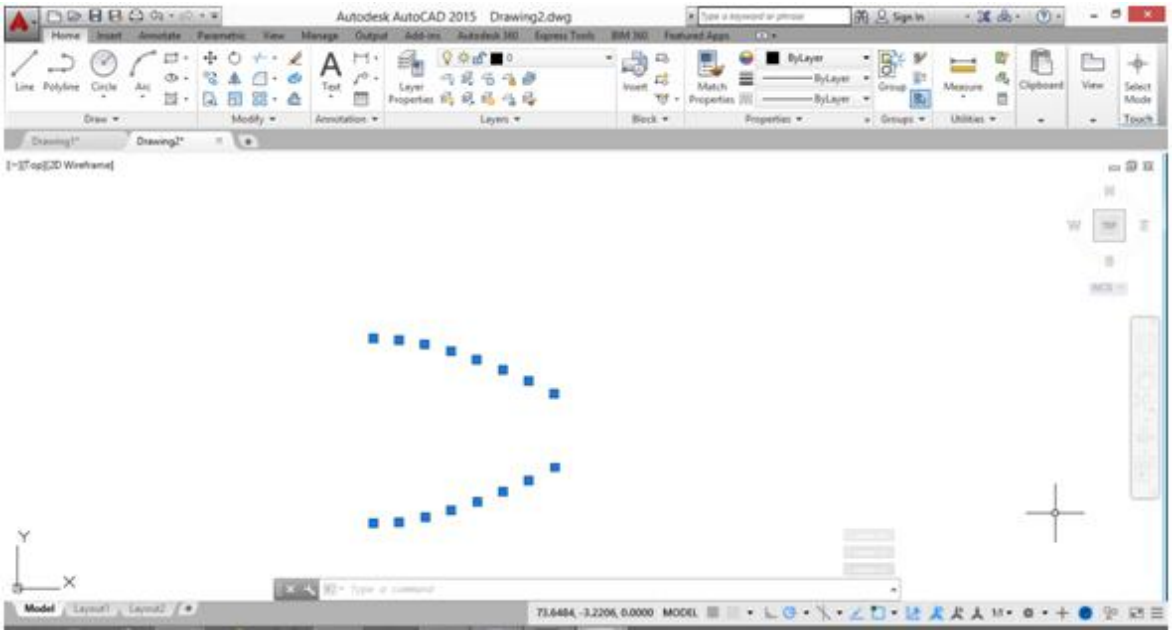

FIGURE 11.1: Developed involute profile for symmetric gear using obtained points from code

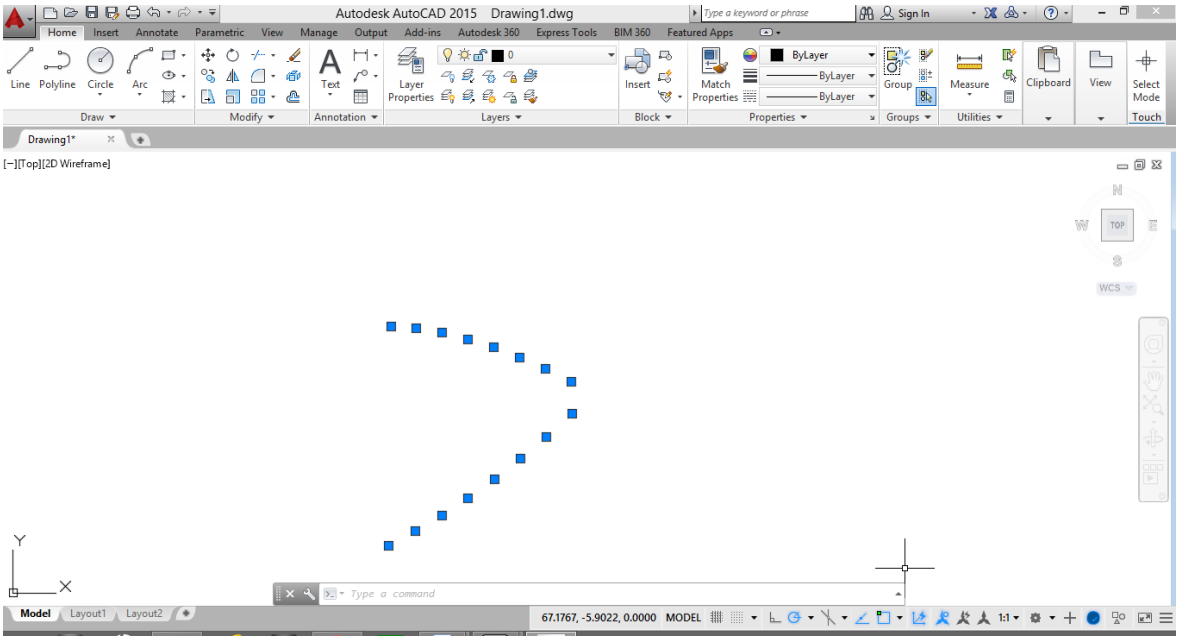

FIGURE 11.2: Developed involute profile for asymmetric gear using obtained points from code

FEA analysis has been carried out for developed CAD models. FEA simulation show that von-Mises stress at root of symmetric gear ($\alpha_d = 20^0$ and $\alpha_c = 20^0$) with normal fillet is 54.62 MPa. von-Mises stress at root of tooth of asymmetric gear ($\alpha_d = 38^0$ and $\alpha_c = 20^0$) with normal fillet and G2 continuity at root are 45.06 MPa and 37.54 MPa respectively. von-Mises stress is reducing by 31.27% compared to normal fillet symmetric gear. Result has been presented in table 11.5.

TABLE 11.5: Result table

Bending stress	**Value**	**Unit**
Bending stress of symmetric gear ($\alpha_d = \alpha_c = 20^0$ and $\rho_F = 1.2$ mm)	54.62	MPa
Bending stress of asymmetric gear ($\alpha_d = 38^0$, $\alpha_c = 20^0$ and $\rho_F = 1.2$ mm)	45.06	MPa
Bending stress of asymmetric gear ($\alpha_d = 38^0$, $\alpha_c = 20^0$) with G2 continuity	37.54	MPa
% reduction in bending stress of asymmetric gear compare to symmetric gear with normal fillet	17.50	%
% reduction in bending stress of asymmetric gear with G2 continuity at root compare to symmetric gear with normal fillet	31.27	%

Result of past work for different criteria has been presented in table 11.6 for better comparison of result of bending stress. It is presented in form of % reduction in bending stress for given optimization.

TABLE 11.6: Comparison of result of past work

Sr. No.	Reference number	Maximum Bending Stress Reduction in %
1	46 (Asymmetric gear optimization)	15%
2	52 (Asymmetric gear with root fillet optimization)	28%
3	61 (Direct Gear Design)	30%
4	62 (Direct Gear Design of asymmetric gear)	30%
5	55 (Asymmetric gear optimization)	18%
6	53 (Asymmetric gear with fillet optimization)	20%
7	84 (Symmetric gear with root fillet optimization)	21%

12.4 G- code

The G code is very essential for manufacturing using CNC machine. To achieve the desired parameter for better performance it is necessary to use CNC for manufacturing a gear. Currently, the industry uses CAD model and G code generation software to develop G code. This research presented an innovative approach to develop a G code for symmetric

and asymmetric involute spur gear without using CAD model and G code generation software.

An algorithm has been presented to obtain G code for CNC without using CAD model and G code generation software. Code to develop G code is presented in ANEXTURE I and input – output of program is presented in table 11.7, 11.8 and 11.9.

TABLE 11.7: Created G code for symmetric involute gear as per input

	Symmetric involute spur gear
Input	Enter module in mm =4 Enter number of teeth on gear =25 Enter pressure angle on coast side in degree =20 Enter pressure angle on drive side in degree =20
Output	G90,M03,G71,G94,F500,S1000 G41,T1 G00 X46.842856,Y3.647239,Z2.000000 G01 X46.842856,Y3.647239,Z-10.000000 G01 X47.850439,Y3.586123 Z-10.000000 G01 X48.866108,Y3.405524 Z-10.000000 G01 X49.885747,Y3.142547 Z-10.000000 G01 X50.907163,Y2.809506 Z-10.000000 G01 X51.928593,Y2.413104 Z-10.000000 G01 X52.948455,Y1.957619 Z-10.000000 G01 X53.965261,Y1.446037 Z-10.000000 G02 X53.980857,Y1.437749,Z-10.000000,R54 G01 X53.980857,Y-1.437749,Z-10.000000 G01 X52.964109,Y-1.950174,Z-10.000000 G01 X51.944283,Y-2.406542,Z-10.000000 G01 X50.922866,Y-2.803880,Z-10.000000 G01 X49.901436,Y-3.137936,Z-10.000000 G01 X48.881755,Y-3.402062,Z-10.000000 G01 X47.866004,Y-3.584080,Z-10.000000 G01 X46.858199,Y-3.648171,Z-10.000000

Using above developed G code, In CNC simulation developed profiles are presented in below figure 11.3, 11.4 and 11.5.

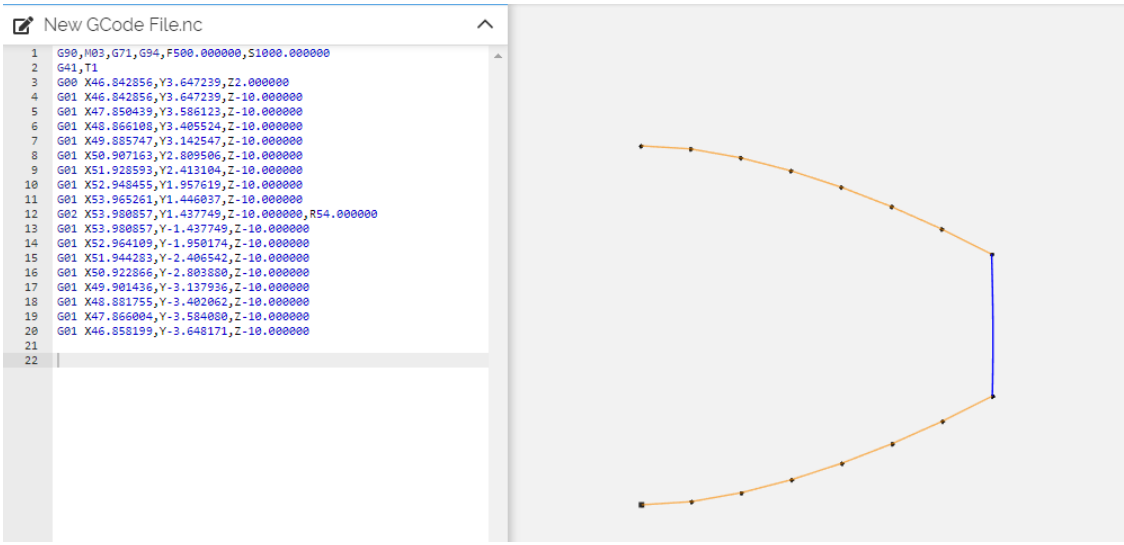

FIGURE 11.3: G code simulation for symmetric gear

TABLE 11.8: Created G code for asymmetric involute gear as per input

	Asymmetric involute spur gear
Input	Enter module in mm =4 Enter number of teeth on gear =25 Enter pressure angle on coast side in degree =20 Enter pressure angle on drive side in degree =38
Output	G90,M03,G71,G94,F500.000000,S1000.000000 G41,T1 G00 X46.842856,Y3.647239,Z2.000000 G01 X46.842856,Y3.647239,Z-10.000000 G01 X47.850439,Y3.586123,Z-10.000000 G01 X48.866108,Y3.405524,Z-10.000000 G01 X49.885747,Y3.142547,Z-10.000000 G01 X50.907163,Y2.809506,Z-10.000000 G01 X51.928593,Y2.413104,Z-10.000000 G01 X52.948455,Y1.957619,Z-10.000000 G01 X53.965261,Y1.446037,Z-10.000000 G02 X53.999696,Y0.181260,Z-10.000000,R54.000000 G01 X53.999696,Y0.181260,Z-10.000000 G01 X52.994945,Y-0.731984,Z-10.000000 G01 X51.975683,Y-1.590099,Z-10.000000 G01 X50.943858,Y-2.392344,Z-10.000000 G01 X49.901436,Y-3.137936,Z-10.000000 G01 X48.850400,Y-3.826015,Z-10.000000 G01 X47.792757,Y-4.455604,Z-10.000000 G01 X46.730544,Y-5.025558,Z-10.000000

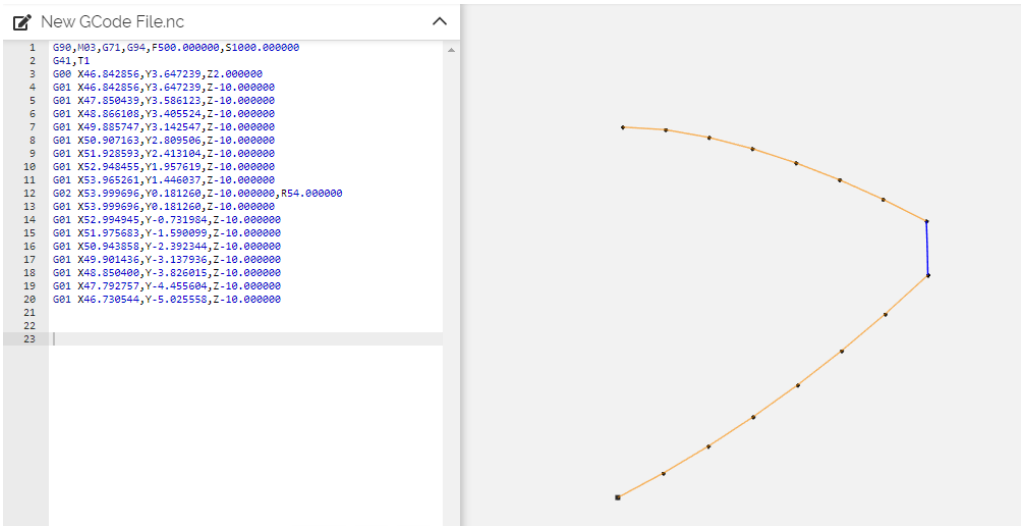

FIGURE 11.4: G code simulation for asymmetric gear

TABLE 11.9: Created G code for asymmetric involute gear with modified root profile as per input

	Asymmetric involute spur gear with G2 Continuity at root
Input	Enter module in mm =4 Enter number of teeth on gear =25 Enter pressure angle on coast side in degree =20 Enter pressure angle on drive side in degree =38
Output	G90,M03,G71,G94,F500.000000,S1000.000000 G41,T1 G00 X46.499307,Y6.735725,Z2.000000 G01 X46.499307,Y6.735725,Z-10.000000 G01 X46.042458,Y6.301251,Z-10.000000 G01 X45.706548,Y5.875949,Z-10.000000 G01 X45.487159,Y5.466849,Z-10.000000 G01 X45.379873,Y5.080980,Z-10.000000 G01 X45.380270,Y4.725371,Z-10.000000 G01 X45.483933,Y4.407050,Z-10.000000 G01 X45.686441,Y4.133048,Z-10.000000 G01 X45.983377,Y3.910392,Z-10.000000 G01 X46.370321,Y3.746113,Z-10.000000 G01 X46.842856,Y3.647239,Z-10.000000 G01 X47.850439,Y3.586123,Z-10.000000 G01 X48.866108,Y3.405524,Z-10.000000 G01 X49.885747,Y3.142547,Z-10.000000 G01 X50.907163,Y2.809506,Z-10.000000 G01 X51.928593,Y2.413104,Z-10.000000 G01 X52.948455,Y1.957619,Z-10.000000 G01 X53.965261,Y1.446037,Z-10.000000

	G02 X53.999696,Y0.181260,Z-10.000000,R54.000000 G01 X53.999696,Y0.181260,Z-10.000000 G01 X52.994945,Y-0.731984,Z-10.000000 G01 X51.975683,Y-1.590099,Z-10.000000 G01 X50.943858,Y-2.392344,Z-10.000000 G01 X49.901436,Y-3.137936,Z-10.000000 G01 X48.850400,Y-3.826015,Z-10.000000 G01 X47.792757,Y-4.455604,Z-10.000000 G01 X46.730544,Y-5.025558,Z-10.000000

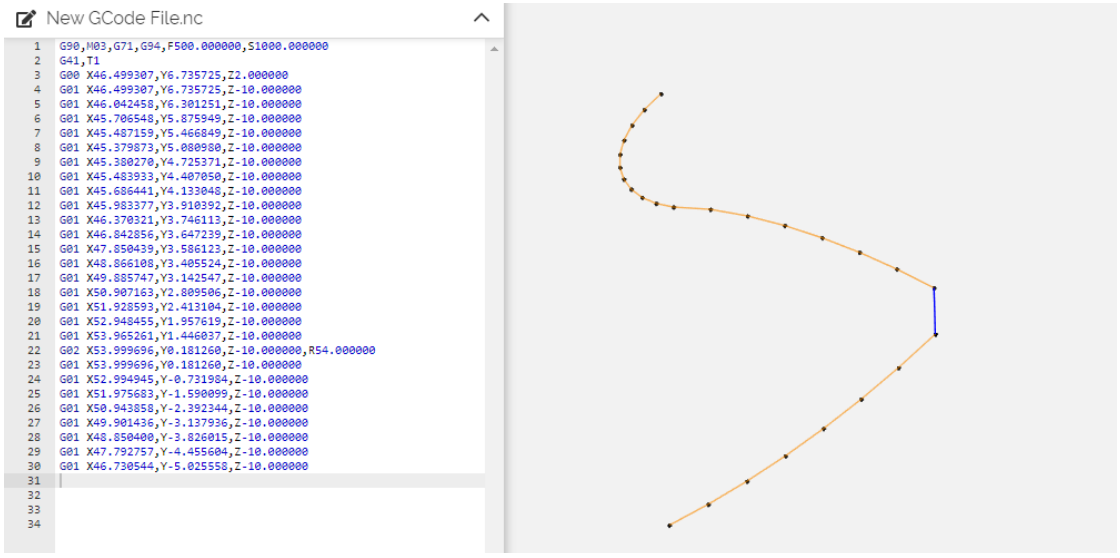

FIGURE 11.5: G code simulation for asymmetric gear with modified root profile

CONCLUSIONS

Based on presented work following conclusions has been made.

Mathematical model

- Mathematical model has been successfully developed of symmetric and asymmetric involute spur gear.
- Equations to calculate "bending stress equation parameters" of symmetric and asymmetric of involute spur gear has been derived.

Objective function

- Based on standard bending stress equation and developed equations of "bending stress equation parameters" an objective function has been developed to minimize bending stress at critical section of tooth.
- Concept of multiplication factor has been successfully verified.

Parametric analysis

Based on the parametric analysis, the following conclusions can be drawn:

- Basic aspects of the geometry of asymmetric involute spur gears have been represented.
- Parametric analysis of gear tooth has been successfully completed.
- Higher module means stronger tooth, it gives lower bending stress at the critical section of the tooth. Since the value of the higher pressure angle on the drive side is constraint by the safe contact ratio and top land tip thickness. As per parametric analysis change of tooth module does not affect contact ratio at any number of teeth, means one constraint (safe contact ratio) does not allow a higher value of pressure angle which is desirable to minimize bending stress.
- For the same diameter (before and after increasing number of teeth) higher Number of teeth increase contact ratio but one constraint (top land tip thickness) does not allow a higher value of pressure angle which is desirable to minimize bending stress. For the same diameter (before and after increasing number of teeth) low Number of teeth increase top land tip thickness but one constraint (contact ratio) is not allow a higher value of pressure angle which is desirable to minimize bending stress.

- The data can be used for the design of asymmetric involute spur gear tooth.
- The data can be used to help in understanding the effect of drive side pressure angle on tooth geometry of asymmetric involute spur gear.
- The data can be potentially used to predict the tooth geometry of asymmetric involute spur gear.
- The data can be used to develop a tooth profile of asymmetric involute spur gear.
- Parametric analysis replaces FEA to predicts or calculate % reduction in bending stress at the root of the tooth. It is successfully verified.

Algorithm to generate CAD model

- Algorithm to create location of point on involute profile and root profile has been developed.
- Using these points a CAD model has been generated in AutoCAD.
- FEA analysis has been carried out for developed CAD models.

Optimization of pressure angle and root profile

At the critical section of tooth, concentration occurs due to curvature discontinuity. Such discontinuities cause a drastic jump in stress values, thereby making these regions prone to mechanical failure. Hence, the optimization of the gear tooth-root profile plays a significant role in reducing the stress concentration and improving the gear tooth strength. This research focuses on the minimization of stress concentration by optimizing root profile at critical section of asymmetric gear. For asymmetric gear bending stress at critical section is always lower then symmetric gear. Combined effect of asymmetric gear and optimized root profile gives better reduction in bending stress at critical section. It will reduce stress concentration. Geometric continuity of order 2 at connection point of involute profile and root profile plays a very important role in reducing stress concentration. A Bezier curve is used with geometric continuity of order 2 at the critical section of an asymmetric spur gear tooth to reduce curvature discontinuity. It will reduce bending fatigue which is challenge of designers.

- von-Mises stress of asymmetric with normal fillet is compared with normal filleted symmetric gear and found that, it is reducing by 17.50 %.
- von-Mises stress of optimized root profile with asymmetric is compared with normal filleted symmetric gear and found that, it is reducing by 31.27%.

- It is observed that modified tooth and root profile was reduced stress concentration.

G- Code

- Algorithm has been successfully developed to generate G code for symmetric and asymmetric involute spur gear.
- G Code has been successfully generated for symmetric and asymmetric involute spur gear without using CAD model and G code software.
- Developed technique save lots of time to generate G code
- G code for complicated root profile can be generated easily.

Overall conclusion

Equation for geometric dimension of tooth in generalization foam has been developed. Based on that an objective function to minimize bending stress has been developed. With help of this, input parameters can be decided as per output in terms of bending stress. After finalization of parameter, using algorithm to create location of point on involute profile and root profile has been developed. With helps of these points a CAD models developed. CAD models are analyzed in FEA. von-Mises stress of optimized root profile with asymmetric is compared with normal filleted symmetric gear and found that, it is reducing by 31.27%. So, it is observed that modified tooth and root profile was reduced stress concentration. Since main aim of this research has been successfully achieved. It is very difficult to developed modified profile using conventional manufacturing technique. So, Algorithm for G Code has been successfully generated for symmetric and asymmetric involute spur gear.

FUTURE SCOPE

In this research, method to calculate multiplication factor (MF) for given material and gear design parameters (module, number of tooth on gear and pinion) for different pressure angle condition has been developed. But need to verify this phenomenon for other different condition like load, material, thickness of gear and many more. It will reduce multiple FEA analysis.

In this research, FEA analysis to calculate bending stress at root of symmetric and asymmetric gear has been conducted successfully. But experimental analysis will give more exact result as per actual condition.

Software to generate G code for internal spur, helical gear and other gear can be developed.

Integrated module of design, modeling and manufacturing of symmetric and asymmetric for internal and external involute spur gear can be developed.

REFERENCES

1. Dudley Darle W, 2009, Handbook of practical gear design, Ist Edition, CRC Press London
2. Maitra Gitin M, 1994, Handbook of gear design, TMH Publication, New Delhi, IInd Edition
3. Prof. K.Gopinath & Prof. M.M.Mayuram, Module 1 to 10, Machine Design II, Indian Institute of Technology Madras.
4. P. J. L. Fernandes, 1996, Tooth bending fatigue failures in gears, Engineering Failure Analysis, vol. 3, pp. 219-225
5. Q. J. Yang, 1996, Fatigue test and reliability design of gears, International Journal of Fatigue, vol. 18, pp. 171-177
6. Timoshenko, S.P., and Baud, R.V., 1926, Strength of Gear Teeth, Mechanical Engineering, 48, pp. 1105.
7. AGMA 908-B89 Standard, Geometry factors for spur, helical and herringbone gear teeth.
8. ISO 6336 Standard, Calculation of Load Capacity of Spur and Helical Gears.
9. Timoshenko, S., and Baud, R.V., 1926, Strength of Gear is Greatly Affected by Fillet Radius, Automat. Ind., 55, pp. 138-142.
10. Kelley, B.W., and Pederson, R., 1958, The Beam Strength of Modern Gear-Tooth Design, SAE Transactions, 66, pp. 137-157.
11. Aida, T., and Terauchi, Y., 1962, On the Bending Stress of a Spur Gear, Bulletin of JSME, 5, pp. 161-183.
12. Wilcox, L., and Coleman, W., 1972, Application of Finite Elements to the Analysis of Gear Tooth Stresses, ASME, 72-PTG-30, pp. 1-12.
13. Francavilla, A., Ramakrishnan, C. V., and Zienkiewicz, O. C., 1975, Optimization of shape to minimize stress concentration, J. Strain Analysis, 10(2), pp. 62–70.
14. Drago, R.J., 1976, Limitations of Current Tooth Root Stress Analysis, AGMA Paper, 220.20, pp. 1-19.
15. Winter, H., and Wirth, X., 1977, The Effect of Notches at the Tooth Root Fillet on the Endurance Strength of Gears, ASME, 77-DET-54, pp. 1-7.
16. Oda, J., 1977, On a technique to obtain an optimum strength shape by the finite element method, Bulletin of the JSME, 20(140), pp. 160–167.
17. Drago, R.J., and Lutthans, R.V., 1981, An Experimental Investigation of the Combined Effects of Rim Thickness and Pitch Diameter on Spur Gear Tooth Root and Fillet Stresses, AGMA, P229.22, pp. 1-24.
18. Angeles, J., 1983, Synthesis of plane curves with prescribed local geometric properties using periodic splines, J. Computer-Aided Design, 15(3), pp. 147– 155.
19. Andrews, J.D., and Hearn, E.J., 1987, An Automatic Design Optimization Procedure to Minimize Fillet Bending Stresses in Involute Spur Gears, International Journal for Numerical Methods in Engineering, 24, pp. 975–991.
20. Duraisamy, S., 1988, Optimal Root Geometry and Fatigue Testing of Spur Gears, M S Thesis, The Ohio State University, Columbus, Ohio.

21. Der Hovanesian, J., Erickson, M.A., Hathaway, R.B., and Savoyard, J.P. JR, 1989, Gear Root Stress Optimization Using Photoelastic Optimization Techniques, Society of Automotive Engineers, SAE Technical Papers, 97, pp. 748-755.
22. Mabie, H.H., C.A. Rogers and C.F. Reinholtz, 1990, Design of Nonstandard Spur Gears Cut by a Hob, Mechanism and Machine Theory, 25: 635-644.
23. Rogers, C.A., Mabie, H.H., and Reinholtz, C.F., 1990, Design of Spur Gears Generated with Pinion Cutters, Mechanism and Machine Theory, 25, 6, pp. 623-634.
24. Clapper, M., 1993, Gear Root Stress Prediction and Comparisons to Experimental and FEM Results, M S Thesis, the Ohio State University, Columbus, Ohio.
25. Tsai, M. and Y. Tsai, 1998, Design of High Contact Ratio Spur Gears Using Quadratic Parametric Tooth Profiles, Mechanism and Machine Theory, 33: 551-564.
26. Pulley FT, Kipling MW, Matson GA, Thurman DL, Avery BW, 2000, Method for producing and controlling a fillet on a gear. US Patent 6,164,880
27. Spitas, V., Costopoulos, T., and Spitas, C., 2005, Increasing the strength of standard involute geat teeth with novel circular root fillet design, American Journal of Applied Sciences, 2(6), pp. 1058–1064.
28. Tiwari, S. K., and Joshi, U. K., 2012, Stress analysis of mating involute spur gear tooth, International Journal of Engineering Research & Technology, 1(9), pp. 1–11.
29. Zou, T., Shaker, M., Angeles, J., and Morozov, A., 2014, Optimization of tooth root profile of spur gears for maximum load-carrying capacity, Proc. ASME Design Egineering Technical Conferences, Buffalo, NY, Aug. 17-20, CD-ROM DETC2014-34568.
30. Kawalec, A., Wiktor, J., and Ceglarek, D., 2005, Comparative analysis of tooth-root strength using ISO and AGMA standards in spur and helical gears with fem-based verification, ASME J. Mechanical Design, 128(5), pp. 1141–1158.
31. Pedrero, J. I., Vallejo, I. I., and Pleguezuelos, M., 2006, Calculation of tooth bending strength and surface durability of high transverse contact ratio spur and helical gear drives, ASME J. Mechanical Design, 129(1), pp. 69–74.
32. Buenneke, R. W., Slane, M. B., Dunham, C. R., Semenek, M. P., Shea, M. M., Tripp, J. E., 1982, Gear Single Tooth Bending Fatigue Test, SAE Technical Paper Series
33. Wheitner, J. A., 1992, Investigation of the Effects of Manufacturing Variations and Materials on Fatigue Crack Detection Methods in Gear Teeth, MS Thesis, The Ohio State University, Columbus, Ohio.
34. Fernandes P, 1996, Tooth bending fatigue analysis in gears, Eng Fail Anal 3(3):219–225
35. Lewicki D, Ballarini R, 1997, Effects of rim thickness on gear crack propagation path, ASME J Mech Des 119:88–95
36. Blarasin A, Guagliano M, Vergani L, 1997, Fatigue crack growth prediction in specimens similar to spur gear teeth, Fatigue Fract Eng Mater Struct 20:1171–1182
37. Daniewicz, S.R. and D.H. Moore, 1998, Increasing the bending Fatigue Resistance of Spur Gear Teeth Using a Presetting Process, Intl. J. Fatigue, 20: 537-542.
38. Ciavarella, M. and G. Demelio, 1999, Numerical Methods for the Optimization of Specific Sliding, Stress Concentration and Fatigue Life of Gears, Intl. J. Fatigue, 21: 465-474.
39. Glodez S, Sraml M, Kramberger J, 2002, A computational model for determination of service life of gears, Int J Fatigue 24:1013–1020
40. Jelaska D, Podrug S, 2007, Gear tooth root fatigue behaviour, Adv Eng 2:187–198

41. Pehan, S., Kramberger, J., Flasker, J., and Zafosnik, B., 2008, Investigation of crack propagation scatter in gear tooth's root, J. Engineering Fracture Mechanics, 75, pp. 1266–1283.
42. Ananda K, Ravichandra R, Mustaffa M, 2012, Spur gear crack propagation path analysis using finite element method. In: Proceedings of the international multi conference of engineers and computer scientists, Hong Kong, March 14–16
43. Willis, 1838, Engineer and Machinist's Assistant, 2nd Edition, pp. 142.
44. DiFrancesco, G., and Marini, S., 1997, Structural Analysis of Teeth with Asymmetric Profiles, Gear Technology, July/August Issue, pp. 16-22
45. Kapelevich, 2000, Geometry and design of involute spur gears with asymmetric teeth, Mech. Mach. Theory, vol. 35, no. 1, pp. 117-130
46. Faydor L. Litvin , Qiming Lian , Alexander L. Kapelevich, 2000, Asymmetric modified spur gear drives: reduction of noise, localization of contact, simulation of meshing and stress analysis, Computer methods applied mechanics and engineering, 188, 363 to 390.
47. Deng, G., and Nakanishi, T., 2001, Bending Tooth Root Stress Decrease Using an Asymmetric Tooth Profile, Proceedings of the International Conference on Mechanical Transmissions, pp. 404-407, Chongqing, China.
48. Deng, G., Nakanishi, T., and Inoue, K., 2003, Bending Load Capacity Enhancement Using an Asymmetric Tooth Profile, JSME International Journal Series C, 46, pp. 1171-1177.
49. F. Karpat, K. Cavdar, F.C. Babalık, 2005, Computer aided analysis of involute spur gears with asymmetric teeth, Proceedings of International Conference on Gears, Garching, Germany, VDI BERICHTE, pp. 145-163, 2005.
50. Karpat, F., Ekwaro-Osire, S., Cavdar, K., and Babalik, F., 2008, Dynamic Analysis of Involute Spur Gears with Asymmetric Teeth, International Journal of Mechanical Sciences, 50, 1598-1610.
51. V. Senthil Kumar, D.V. Muni, G. Muthuveerappan, 2008, Optimization of asymmetric spur gear drives to improve the bending load capacity, Mechanism and machine theory 43 (2008) 829–858.
52. Th. Costopoulos, V. Spitas, 2009, Reduction of gear fillet stresses by using one-sided involute asymmetric teeth, Mechanism and machine theory, 44, 1524–1534.
53. Kapelevich, A., and Shekhtman, Y., 2009, Tooth Fillet Profile Optimization for Gears with Symmetric and Asymmetric Teeth, Gear Technology, September/October Issue, pp. 73-79.
54. Brown, F.W., Davidson, S.R., Hanes, D.B., Kapelevich, A., and Weires, D.J., 2010, Analysis and Testing of Gears with Asymmetric Involute Tooth Form and Optimized Fillet Form for Potential Application in Helicopter Main Drives, AGMA Technical Paper, pp. 1-15, Paper No. 10FTM14.
55. Niels L. Pedersen, 2011, Improving bending stress in spur gears using asymmetric gears and Shape optimization, Mechanism and machine theory, 45, 1707–1720.
56. Alipiev, O., 2011, Geometric design of involute spur gear drives with symmetric and asymmetric teeth using the Realized Potential Method, Mechanism and Machine Theory, 46(1), 10–32.
57. Prabhu Sekar, R., & Muthuveerappan, G., 2015, Estimation of tooth form factor for normal contact ratio asymmetric spur gear tooth, Mechanism and Machine Theory, 90, 187–218.
58. Kapelevich, A. L., and Shekhtman, Y. V., 2002, Direct gear design for spur and helical involute gears, Gear Technology, September/October, pp. 29–35.

59. Kapelevich, A. L., and Shekhtman, Y. V., 2003, Direct gear design: Bending stress minimization, Gear Technology, September/October, pp. 44–47.
60. Kapelevich, A., 2007, Direct Gear Design for High-Performance Gear Transmissions, Gear Solutions, December Issue, pp. 22-31.
61. Alexander L. Kapelevich and Yuriy V. Shekhtman, 2003, Direct gear design: bending stress minimization, Gear technology, september/october 2003.
62. Alex Kapelevich, AKGears, 2009, direct design of asymmetric gears: approach and application, Proceedings of MPT2009-Sendai JSME International conference on motion and power transmissions,
63. Muni, D.V., Kumar, V.S., and Muthuveerappan, G., 2007, Optimization of Asymmetric Spur Gear Drives for Maximum Bending Strength Using Direct Gear Design Method, Mechanics Based Design of Structures and Machines, 35, pp. 127-145.
64. Marimuthu, P., & Muthuveerappan, G., 2014, Optimum Profile Shift Estimation on Direct Design Asymmetric Normal and High Contact Ratio Spur Gears Based on Load Sharing, Procedia Engineering, 86, 709–717.
65. Sekar, R. P., & Muthuveerappan, G., 2014, Load sharing based maximum fillet stress analysis of asymmetric helical gears designed through direct design — A parametric study, Mechanism and Machine Theory, 80, 84–102.
66. Marimuthu, P., & Muthuveerappan, G., 2016, Design of asymmetric normal contact ratio spur gear drive through direct design to enhance the load carrying capacity, Mechanism and Machine Theory, 95, 22–34.
67. Spitas, V.A. and T. Costopoulos, 2001, New Concepts in Numerical Modeling and Calculation of the Maximum Root Stress in Spur Gears versus Standard Methods: A Comparative Study, Proc. 1st National Conf. Recent Advances in Mechanical Eng., ASME-Greek Section, Patras.
68. Spitas, V., Costopoulos, T., and Spitas, C., 2005, Increasing the strength of standard involute gear teeth with novel circular root fillet design, American Journal of Applied Sciences, 2(6), pp. 1058–1064.
69. Spitas, V. A., Costopoulos, T. N., and Spitas, C. A., 2006, Optimum gear tooth geometry for minimum fillet stresses using bem and experimental verification with photoelasticity, ASME J. Mechanical Design, 128, pp. 1159–1164.
70. Spitas, V., and Spitas, C., 2007, Optimizing Involute Gear Design for Maximum Bending Strength and Equivalent Pitting Resistance, Proceedings of the Institution of Mechanical Engineers, Part C, Journal of Mechanical Engineering Science, 221, pp. 479-488.
71. Spitas C, Spitas V, 2007, Four-parametric study of the bending strength of circular fillet versus trochoidal fillet in gear tooth design using BEM, Mech Based Des Struct Mach, 35(2),163–178.
72. C. Spitas and V. Spitas, 2007, A FEM study of the bending strength of circular fillet gear teeth compared to trochoidal fillets produced with enlarged cutter tip radius, Mech. Based Des. Struc., vol. 35, no. 1, pp. 59-73.
73. Pedersen, N.L., 2009, Reducing Bending Stress in External Spur Gears by Redesign of the Standard Cutting Tool, Structural and Multidisciplinary Optimization, 38, pp. 215-227.
74. Cuneyt Fetvaci, 2010, Generation simulation of involute spur gears machined by pinion-type shaper cutters, Journal of Mechanical Engineering, 56(10), 644-652.

75. Sanders A A, 2010, An experimental investigation of the influence of elliptical root shapes and asymmetric teeth on root stresses and bending fatigue lives, Master's thesis, The Ohio State University, Columbus.
76. Zhao X, 2014, Increasing bending strength in spur gears using shape optimisation of cutting tool profile, Aust J Mech Eng, 12(2), 208–216.
77. Kawalec, A., Wiktor, J., and Ceglarek, D., 2005, Comparative analysis of tooth-root strength using ISO and AGMA standard in spur and helical gear with FEM-based verification, Journal of Mechanical Design, ASME, 128(5), pp. 1141–1158.
78. Xiao, H., Zaton, W., and Zu, J.W., 2005, Fillet Shape Optimization for Gear Teeth, Proceedings of the ASME International Design Engineering Technical Conferences and Computers and Information in Engineering Conference, pp. 815-820, Long Beach, California.
79. Yeh, T., Yang, D., and Tong, S., 2001, Design of New Tooth Profiles for High-Load Capacity Gears, Mechanism and Machine Theory, 36, pp. 1105-1120.
80. Senthilvelan, S., and Gnanamoorthy, R., 2006, Effect of Gear Tooth Fillet Radius on the Performance of Injection Molded Nylon 6/6 Gears, Materials and Design, 27, pp. 632-639.
81. Flodin, A., and Andersson, M., 2012, Tooth root optimization of powder metal gears: reducing stress from bending and transient loads, Proc. of Powder Metal World Congress and Exhibition, Yokohama, Japan.
82. Sankar, S., Raj, M., and Nataraj, M., 2010, Profile modification for increasing the tooth strength in spur gear using CAD, Engineering, 2(9), pp. 740–749.
83. Wang Z, Zhang N, Dong D, Chen X, 2012, Analysis of the influence of fillet curves on gear bending strength based on space contact, Appl Mech Mater, 155–156(2), 1203–1207.
84. Zou, T., Shaker, M., Angeles, J., and Morozov, A., 2014, Optimization of tooth root profile of spur gears for maximum load-carrying capacity, Proc. ASME Design Egineering Technical Conferences, Buffalo, NY
85. S.S Bhavikatti , Finite Element Analysis.
86. J.S Rao, History of Rotating Dynamics.
87. J. Kramberger, M. Šraml, I. Potrč, and J. Flašker, 2004, Numerical calculation of bending fatigue life of thin-rim spur gears, Engineering Fracture Mechanics, vol. 71, pp. 647-656.
88. Joseph R. Davis, Davis & Associates, 2005, Gear Materials, Properties, and Manufacture, Ist Edition, ASM International, USA.
89. Nitin Chaphalkar, Gregory Hyatt, and Nicklas Bylund, 2014, Analysis of Gear Root Forms: A Review of Designs, Standards and Manufacturing Methods for Root Forms in Cylindrical Gears, Gear solution.
90. M.P. Groover, E.W. Zimmers, 1984, Conventional Numerical Control, in: CAD/CAM: Computer-Aided Design and Manufacturing, Prentice-Hall, Inc., New Jersey, USA.
91. Nazma Sultana, 2016, SolidCAM iMachining (2D): A Simulation Study of a Spur Gear Machining and G-code Generation for CNC Machine, Int. J. Mech. Eng. Autom., Volume 3, Number 1, pp. 1-9.
92. Oladejo KA, Ogunsade AA, 2014, Drafting of involute spurgears in AutoCAD-VBA customized, Adv Sci Tech Res, 1(2):18-26.
93. Lizheng Lu, 2006, Optimal multi-degree reduction of Bezier curve with G2 continuity, Computer aided geometric design, 23, 673-683.
94. D.Rogers, J. Adams, 1990, Mathematical element for computer graphics.

95. Konstandinos G. Raptis, Theodore N. Costopoulos, Georgios A. Papadopoulos and Andonios D. Tsolakis,2010, Rating of spur gear strength using photo elasticity and the Finite Element Method, American Journal of Applied Sciences, 3(1), pp. 222-231.
96. P A Vaghela, 2011, Master degree thesis "Effect of Rim Thickness on Asymmetric Spur Gear Tooth Bending Stress", Gujarat technological university, Gujarat, India.
97. Bommisetty, V.S.N. Karthik, 2012, Finite Element Analysis of Spur Gear Set, ETD Archive. 630.
98. Joseph B. Ferreira, 2002, Bachelor of Science in Mechanical Engineering Thesis, Using Spreadsheets to Parameterize Spur Gear Design for Laser Cutters, Massachusetts institute of technology.
99. O.Reyes, A.Rebolledo, G.Sanchez, 2008, Algorithm to Describe the Ideal Spur Gear Profile, Proceedings of the World Congress on Engineering,Vol II WCE, London, U.K.
100. N K Mandal, N K Singh and UC Kumar, 2016, Interactive Spur Gear Generation Using Parametric Programming with CNC End Milling , International Journal of Mechatronics, Electrical and Computer Technology, Vol. 6(22), Oct. pp. 3172-3187.

PUBLICATIONS

J M Prajapati & P A Vaghela, “Factor affecting the bending stress at critical section of asymmetric spur gear” at international journal of mechanical engineering and technology, volume 4, issue 4, (2013), pp. 266-273.
https://www.scimagojr.com/journalsearch.php?q=21100808402&tip=sid&clean=0
SJR 2018:0.209

J M Prajapati & P A Vaghela, “Objective function to optimize bending stress at critical section of asymmetric spur gear ” at ISOR international journal of mechanical and civil engineering, vol. 10 , issue 1 , (2013) , pp 58-65.
https://doi.org/10.9790/1684-1015865

J M Prajapati & P A Vaghela “Constraints affect the optimization of bending stress at critical section of asymmetric spur gear tooth” at international journal of mechanical engineering and robotics research, vol. 3 , issue 1, (2014), pp 138-144.
https://www.scimagojr.com/journalsearch.php?q=21100788860&tip=sid&clean=0
SJR 2018:0.154

P.A. Vaghela, J.M. Prajapati, “Hybridization of Taguchi and Genetic Algorithm to minimize iteration for optimization of solution” MethodsX, 6(2019), 230–238
https://doi.org/10.1016/j.mex.2019.01.002
Scopus (Elsevier) and web of science indexed

Priyakant Vaghela and Jagdish Prajapati, ”Optimization of tooth root profile using bezier curve with G2 continuity to reduce bending stress of asymmetric spur gear tooth”, MATEC Web Conf.,237 (2018)03010.
https://doi.org/10.1051/matecconf/201823703010
Scopus (Elsevier), EI and web of science indexed

P A Vaghela & J M Prajapati “Parametric analysis of asymmetric involute spur gear tooth” at International journal of powertrains, Inderscience publication (In press)
https://www.inderscience.com/info/ingeneral/forthcoming.php?jcode=IJPT
Scopus (Elsevier) indexed

P.A. Vaghela, J.M. Prajapati, “Integrated Symmetric and Asymmetric Involute Spur Gear Modelling and Manufacturing” Materials Today: Proceedings (In press).
http://www.icmmm-vit.com
https://www.journals.elsevier.com/materials-today-proceedings
Scopus (Elsevier) and Conference Proceedings Citation Index indexed

Submitted papers

J.M. Prajapati & P.A. Vaghela, “G Code for Symmetric and Asymmetric involute spur gear without using CAD model and G code generation software”, International journal of powertrains.
https://www.inderscience.com/jhome.php?jcode=ijpt
Scopus (Elsevier) indexed

J.M. Prajapati & P.A. Vaghela, “Modelling of symmetric and asymmetric involute spur gear”, International Journal of Computer Aided Engineering and Technology.
https://www.inderscience.com/jhome.php?jcode=ijcaet
Scopus (Elsevier) indexed

APENDIX-I (CODE)

1. Code to calculate contact ratio

```
function [contact]=CR(m, ng, np, ac, ad)
rpg= (m*ng)/2
rtg=rpg+m
radiansd = ad*(%pi/180)
rbg=rpg*(cos(radiansd))
p1=((rtg^2-rbg^2)^0.5)
rpp= (m*np)/2
rtp=rpp+m
radiansc = ac*(%pi/180)
rbp=rpp*(cos(radiansd))
p2=((rtp^2-rbp^2)^0.5)
p3=( (rpg+rpp)*sin(radiansd))
p4=(3.14*m*cos(radiansd))
contact=( (p1+p2-p3)/ (p4))
endfunction
```

2. Code to Calculate HPSTC radius

```
function [HPSTC]=HP(m, ng, np, a)
rpg=(m*ng)/2
rtg=rpg+m
radians = a*(%pi/180)
rbg=rpg*(cos(radians))
p1=((rtg^2-rbg^2)^0.5)
rpp=(m*np)/2
rtp=rpp+ m
rbp=rpp*(cos(radians))
p2=((rtp^2-rbp^2)^0.5)
p3=((rpg*(cos(radians)))+(rpp*(cos(radians)))
p4=(3.14*m*cos(radians))
CR=((p1+p2-p3)/(p4))
tg=3.14*m*cos(radians)
HPSTC=((rtg^2)+((CR-1)*tg)*(((CR-1)*tg)-(2*p1))^0.5)
endfunction
```

3. Code to calculate tip thickness

```
function [St]=St(m, z, ad, ac)
rp=(m*z)/2
rt=rp+ m
radiansd = ad*(%pi/180)
rb=rp*(cos(radiansd))
```

```
p1=(3.14/(2*z))
p2= tan(radiansd)
p3=acos((rp/rt)* cos(radiansd))
td=p1+(p2- radiansd)-((tan(p3))-p3)
radiansc = ac*(%pi/180)
rb=rp*(cos(radiansc))
p4= tan(radiansc)
p5= acos((rp/rt)* cos(radiansc))
tc=p1+(p4- radiansc)-((tan(p5))-p5)
St=td+tc
endfunction
```

4. Code to calculate critical section thickness

```
function [CST]=cst(m, z, ad, ac)
rp=(m*z)/2
rt=rp+ m
radiansd = ad*(%pi/180)
rbd=rp*(cos(radiansd))
radiansc = ac*(%pi/180)
rbc=rp*(cos(radiansc))
p1=(3.14/(2*z))
p2= tan(radiansd)
p3=acos((rp/rbc)* cos(radiansd))
tfnd=p1+(p2- radiansd)-((tan(p3))-p3)
p4= tan(radiansc)
p5= acos((rp/rbc)* cos(radiansc))
tfnc=p1+(p4- radiansc)-((tan(p5))-p5)
cst=(rbc*sin(tfnd))+(rbc*sin(tfnc)
endfunction
```

5. Code to calculate load angle

```
function [AFEN]=afen(m, z, ad, r)
rp=(m*z)/2
radiansd = ad*(%pi/180)
p1=(3.14/(2*z))
p2= tan(radiansd)
p3=acos((rp/r)* cos(radiansd))
afen=tan(p3)-p1-tan(p2)+ radiansd
endfunction
```

6. Code to calculate bending moment arm height

```
function [BMAH]=bmah(m, zg, np, ad, ac)
rpg=(m*ng)/2
rtg=rpg+m
radiansd = ad*(%pi/180)
rbg=rpg*(cos(radiansd))
p1=((rtg^2-rbg^2)^0.5)
rpp=(m*np)/2
```

```
rtp=rpp+ m
rbp=rpp*(cos(radiansd))
p2=((rtp^2-rbp^2)^0.5)
p3=((rpg*(cos(radiansd)))+(rpp*(cos(radiansd)))
p4=(3.14*m*cos(radiansd))
CR=((p1+p2-p3)/(p4))
tg=3.14*m*cos(radiansd)
HPSTC=((rtg^2)+((CR-1)*tg)*(((CR-1)*tg)-(2*p1))^0.5)
p5=(3.14/(2*z))
p6= tan(radiansd)
p7=acos((rp/r)* cos(radiansd))
afen=tan(p7)-p5-tan(p6)+ radiansd
rtp=rpg+m
radiansd = ad*(%pi/180)
rbd=rp*(cos(radiansd))
radiansc = ac*(%pi/180)
rbc=rp*(cos(radiansc))
p0=(3.14/(2*z))
p8=acos((rp/rbc)* cos(radiansd))
tfnd=p0+(p6- radiansd)-((tan(p8))-p8)
p9= acos((rp/ rhpstc)* cos(radiansd))
thpstc=p0+( p6- radiansd)-((tan(p9))-p9)
bmah=(rhpstc*cos(thpstc))-((rbc*cos(tfnd))+( rhpstc*sin(thpstc)*tan(afen)))
endfunction
```

7. Code to calculate optimize drive side pressure angle

```
function [OPA]=opa(m, z, ac)
cr= CR(4,25,47,20)   // calling of function
st= St(4,25,20,20)   // calling of function
if (cr > 1.1) & ( st < 0.3*m)
opa=ac+1
then
disp(opa),
end
opa=opa
endfunction
```

8. Code to calculate nominal bending stress at the root of tooth

```
function [BS]=bs(m, zp, zg, ac, P, S)
T=P/S
d=m*zp
rf=0.3*m
ft=(2000*T)/d
b=10*m
ad= OPA(m,zp,ac)   // calling of function
afen=AFEN(m,zp,ac,(d/2))    // calling of function
bmah=BMAH(m,zp,ad,ac)      // calling of function
cst=CST(m,zp,ad,ac)     // calling of function
```

```
Yf=(6*(bmah/m)*(cos(afen)))/(((cst/m)^2)*cos(ad))
Yb=1
L=cst/bmah
Qs=cst/(2*rf)
Ys=(((1.21)+(2.3/L))^-1)
bs=(ft*Yf*Yb*Ys)/(b*m)
endfunction
```

9. Code to calculate coordinate of B0 and B3 point

```
function [CB0B3]=cb0b3(m, z, ad, ac)
rp=(m*z)/2
rt=rp+ m
radiansd = ad*(%pi/180)
rbd=rp*(cos(radiansd))
radiansc = ac*(%pi/180)
rbc=rp*(cos(radiansc))
p1=(3.14/(2*z))
p2= tan(radiansd)
p3=acos((rp/rbc)* cos(radiansd))
p4= tan(radiansc)
p5= acos((rp/rbc)* cos(radiansc))
b0=p1+(p4- radiansc)-((tan(p5))-p5)
xb0=rbc* cos(b0)
yb0=rbc* sin(b0)
b3=p1+(p2- radiansd)-((tan(p3))-p3)
xb3=rbc* cos((3.14*2)/(z))-b3)
yb3=rbc* sin((3.14*2)/(z))-b3)
endfunction
```

10. Code to calculate coordinate of involute path points

```
m=input("Enter module in mm =")
z=input("Enter number of teeth on gear =")
ac=input("Enter pressure angle on coast side in degree =")
ad=input("Enter pressure angle on drive side in degree =")
rp=(m*z)/2
rt=rp+ m
radians = ac*(%pi/180)
rb=rp*(cos(radians))
for i=rb : rt
p1=(3.14/(2*z))
p2= tan(radians)
p3=acos((rp/i)* cos(radians))
p4= tan(radians)
p5= acos((rp/i)* cos(radians))
b0=p1+(p4- radians)-((tan(p5))-p5)
xi=i* cos(b0)
yi=i* sin(b0)
```

```
mprintf('POINT %f,%f \n',xi,yi)
end
radiansd = ad*(%pi/180)
p1=(3.14/(2*z))
p2= tan(radiansd)
p3=acos((rp/rt)* cos(radiansd))
p4= tan(radiansd)
p5= acos((rp/rt)* cos(radiansd))
b0=p1+(p4- radiansd)-((tan(p5))-p5)
xi=-rt* cos(b0)
yi=rt* sin(b0)
rp=(m*z)/2
rt=rp+ m
radiansd = ad*(%pi/180)
rb=rp*(cos(radians))
for j= rt:-1:rb
p6=(3.14/(2*z))
p7= tan(radiansd)
p8=acos((rp/j)* cos(radiansd))
p9= tan(radiansd)
p10= acos((rp/j)* cos(radiansd))
b1=p6+(p9- radiansd)-((tan(p10))-p10)
xi1=j* cos(b1)
yi1=-j* sin(b1)
mprintf('POINT %f,%f \n',xi1,yi1)
end
```

11. Code to create point on modified root profile

```
function [BCURVE]=bcurve(x0, y0, x1, y1, x2, y2, x3, y3)
for  t = 0: t <= 1: 0.1
xt = ((1-t) * (1-t) * (1-t) * x0) + (3 * t * (1-t) * (1-t) * x1) + (3 * t * t * (1-t) * x2) + (t * t *
t * x3)
yt = ((1-t) * (1-t) * (1-t) * y0) + (3 * t * (1-t) * (1-t) * y1) + (3 * t * t * (1-t) * y2) + (t * t *
t * y3)
disp(xt,yt)
end
endfunction
```

12. Code to create G code for symmetric involute spur gear (root circle and involute profile)

```
function [GCODE]=gcode(m, z, pa)
rp=(m*z)/2
rt=rp+ m
```

```
radians = pa*(%pi/180)
rb=rp*(cos(radians))
rd=rp-m
r=(((rb*rb)-(rd*rd))/2*rb)
b=atan(r/rb)
p1=(3.14/(2*z))
p2= tan(radians)
p3=acos((rp/rb)* cos(radians))
p4= tan(radians)
p5= acos((rp/rb)* cos(radians))
b0=p1+(p4- radians)-((tan(p5))-p5)
x2=rb* cos(b0)
y2=rb* sin(b0)
x1=rd* cos(b0+b)
y1=rd* sin(b0+b)
disp(G92,x1,y1)
disp(G02,x2,y2,r)
for i=rb : rt
p1=(3.14/(2*z))
p2= tan(radians)
p3=acos((rp/i)* cos(radians))
p4= tan(radians)
p5= acos((rp/i)* cos(radians))
b0=p1+(p4- radians)-((tan(p5))-p5)
xi=i* cos(b0)
yi=i* sin(b0)
disp(G01,xi,yi)
end
endfunction
```

13. Code to create G code for modified root profile

```
function [GCODEBCURVE]=gcodebcurve(x0, y0, x1, y1, x2, y2, x3, y3)
for  t = 0: t <= 1: 0.1
xt = ((1-t) * (1-t) * (1-t) * x0) + (3 * t * (1-t) * (1-t) * x1) + (3 * t * t * (1-t) * x2) + (t * t *
t * x3)
yt = ((1-t) * (1-t) * (1-t) * y0) + (3 * t * (1-t) * (1-t) * y1) + (3 * t * t * (1-t) * y2) + (t * t *
t * y3)
disp(G01,xt,yt)
end
endfunction
```